ADDIS ABABA UNIVERSITY

SCHOOL OF GRADUATE STUDIES

SCHOOL OF EARTH SCIENCES

CHARACTERIZATION OF THE GENESIS OF BELESSA KAOLIN OCCURRENCES, HOSAINA AREA, CENTRAL MAIN ETHIOPIAN RIFT

BY

GEMECHU BEDASSA TEFERI

A thesis submitted to the School of Graduate Studies of Addis Ababa University in partial fulfillment of the requirements for the degree of Master of Science in Resource Geology (Mineral Deposits)

June, 2017

Addis Ababa, Ethiopia

ADDIS ABABA UNIVERSITY

SCHOOL OF GRADUATE STUDIES

SCHOOL OF EARTH SCIENCES

CHARACTERIZATION OF THE GENESIS OF BELESSA KAOLIN OCCURRENCES, HOSAINA AREA, CENTRAL MAIN ETHIOPIAN RIFT

BY

GEMECHU BEDASSA TEFERI

ADVISORS: WORASH GETANEH (Dr.)

BINYAM TESFAW (Dr.)

A thesis submitted to the School of Graduate Studies of Addis Ababa University in partial fulfillment of the requirements for the degree of Master of Science in Resource Geology (Mineral Deposits)

June, 2017

Addis Ababa, Ethiopia

ADDIS ABABA UNIVERSITY

SCHOOL OF GRADUATE STUDIES

SCHOOL OF EARTH SCIENCES

CHARACTERIZATION OF THE GENESIS OF BELESSA KAOLIN OCCURRENCES, HOSAINA AREA, CENTRAL MAIN ETHIOPIAN RIFT

BY

GEMECHU BEDASSA TEFERI

Approved by the Examining Committee

Dr. Balemwal Atnafu	_____	_____
Head, School of Earth Sciences	Signature	Date
Dr. Worash Getaneh	_____	_____
Advisor	Signature	Date
Dr. Binyam Tesfaw	_____	_____
Co-Advisor	Signature	Date
Dr. Mulugeta Feseha	_____	_____
Examiner	Signature	Date
Dr. Zerihun Desta	_____	_____
Examiner	Signature	Date

Statement of originality

With this statement I hereby confirm that this MSc thesis work is my own original work under the supervision of Dr. Worash Getaneh and Dr. Binyam Tesfaw, Addis Ababa University, School of Earth Sciences, in the year 2017. I also declare that this work has not been submitted in any form for another degree or diploma at any university or other institution. Data used from the published and unpublished work of others has been appropriately acknowledged.

Gemechu Bedassa Teferi _____ _____

Signature Date

To the best of our knowledge, we recognized that the above statement made by the MSc candidate is correct.

Dr. Worash Getaneh (Advisor) _____ _____

Signature Date

Dr. Binyam Tesfaw (Co-advisor) _____ _____

Signature Date

Abstract

Belessa kaolin occurrence is situated in the Western margin of Central Main Ethiopian Rift (CMER) near Hosaina town which is about 230 km from Addis Ababa. Geology of the kaolin district is composed of Miocene to Quaternary age acidic igneous rocks consisting of pyroclastic tuff, ignimbrite and rhyolite. Based on petrographic study, the main minerals identified in these volcanic rocks include quartz, k-feldspar and plagioclase. The kaolin occurrence is located in the central part of the study area and it is associated with rhyolite. The host rock has been partly and completely transformed to kaolinite. The main aim of the present study is to characterize the genesis of this kaolin occurrence. An integrated study combining geological, mineralogical and geochemical data were carried out in order to characterize the genesis of alteration (supergene or hypogene). Data obtained from morphological study and available physical property tests were also examined to see the possible industrial applications. Moreover, Landsat 8 OLI and ASTER images were enhanced using two techniques (band ratio and band composites) to discriminate lithological units, host rock and vegetation. Spectral signature curves of Belessa kaolin are also compared with other kaolinite spectral curves to produce preliminary model of spectral curves for kaolin occurrences associated with volcanic rocks in the MER. Results from geological, mineralogical and geochemical studies indicate that supergene alteration has played a great role to the formation of Belessa kaolin. The absence of quartz veining and alteration zones with high temperature minerals implies the lack of significant hypogene alteration process. The Chemical Index of Alteration (CIA) and Chemical Index of Weathering (CIW) result also showed that the host rock has experienced a strong alteration and weathering process that resulted in the formation of kaolinite. Furthermore, the higher Ce + Y + La values correspond to the supergene type alteration. The low P and high Cr + Nb concentrations also support supergene origin. From digital image processing, ASTER RGB band combinations of (7, 2, 1), (7, 3, 1) and band ratios of 9/4 showed better contrast on geologic units, vegetation and kaolinite host rock respectively. Moreover, the comparison of kaolinite spectral reflectance curves shows that the spectral curve of Belessa kaolinite can be used as a preliminary model to the kaolin occurrences in the MER. Studies from technological properties like physical tests, chemistry, mineralogy and crystal morphology indicate that Belessa kaolin could have potential applications in paper coating, filler (in paper, rubber, plastic and paint), ceramics, pharmaceuticals and cosmetics.

Key words: Applications, Belessa, genesis, kaolin, supergene, technological property.

Acknowledgement

First and foremost, I would like to express my deepest gratitude to my advisors Dr. Worash Getaneh and Dr. Binyam Tesfaw for their close guidance, suggestion, comment and support.

I take this opportunity to thank Prof. Samson Tesfaye and Tadesse Birhanu (PhD candidate) for providing me Landsat 8 OLI and ASTER image data. The XRD and SEM laboratory analysis is performed in Switzerland, university of Fribourg. For this, I would like to express my uttermost gratitude to Prof. Bernard Grobety and Mr. Ermias Filfilu for their collaboration and support. I would also want to thank Mrs. Liya Tadesse and Ms. Selamawit Tadesse for the physical tests. Also, my sincere thanks to Mr. Angesom Resom, Mr. Misgan Molla and Mr. Wendwossen Sisay for their generous support during sample preparation and thin section laboratory analysis.

I am especially indebted to Mr. Mesfin Kidane Mariyam, Mr. Misgana Wolde, Mr. Abayneh Silassie and Mr. Fantu Zeleke for their presence, encouragement and tireless support during field work.

I acknowledge with grateful thanks the contributions of Mrs. Woinshet Fikadu, Mr. Tolera Shula (Tol), Mr. Samuel Getachew and Ms. Wubanchi Fikadu for their critical support during my studies. I am grateful to Mr. Amdemickael Zafu, Mr. Million Alemayew, Mr. Abate Assen and Mr. Bahiru Zinaye for their comment and technical support. For their presence and encouragement, I would like to thank my lovely friends Bezayit Mitiku, Abdi Chali, Amenti Chali (Amen), Oliyad Efrem (Oly), Lemessa Kumerra (Leme) and Sura Dereje. I also appreciate Rev. Jijo Minase (J) for his prayer and encouragement.

My special thanks go to my dad Bedassa Teferi and my mom Askale Alemu for their prayer, patience, encouragement, presence and financial support during my studies.

Finally, I would like to thank the government officials in Hadiya zone mining Bureau and the local peoples for their collaboration during field work.

Table of contents

List of Figures

List of tables

List of acronyms

a.s.l	above sea level
ASTER	Advanced Space borne Thermal Emission and Reflection Radiometer
CIA	Chemical Index of Alteration
CIW	Chemical Index of Weathering
DEM	Digital Elevation Model
EARS	East African Rift System
EIGS	Ethiopian Institute of Geological Surveys
ENVI	Environment for Visualizing Images
ETM+	Enhanced Thematic Mapper
GCP	Ground Control Points
GIS	Geographic Information System
GPS	Global Positioning System
GSE	Geological Survey of Ethiopia
HI	Hinckley Index
ICP-AES	Inductively Coupled Plasma Atomic Emission Spectroscopy
ICP-MS	Inductively Coupled Plasma Mass Spectroscopy
LOI	Loss on Ignition
MER	Main Ethiopian Rift
MOME	Ministry of Mine and Energy
OLI TIRS	Operational Land Manager Thermal Infrared Sensor
PPL	Plane Polarized Light
SEM	Scanning Electron Microscope
TSA	Total Alkali Silca
WFB	Wonji Fault Belt
XPL	Cross Polarized Light
XRD	X-ray Diffractometer
YTVL	Yerer-Tullu Wellel Volcano-tectonic Lineament

CHAPTER ONE

1. Introduction

1.1. Background

The Main Ethiopian Rift (MER) belongs to the northern most branch of the East Africa Rift System (EARS) (Kurz et al., 2007) and it has been the interest of many researchers for many decades in different aspects of geosciences. These researchers are highly interested to this region because, it is a key sector of the East African Rift System that connects the Afar depression, at the Red Sea–Gulf of Aden junction, with the Turkana depression and Kenya Rift to the south **(**Mohr, 1983; Rosendahl, 1987; Braile et al., 1995; Boccaletti and Peccerillo, 1999; Chorowicz, 2005 cited in Corti, 2009). It also represents and records all the different stages of rift evolution from rift initiation to break-up and incipient oceanic spreading (Ebinger, 2005). The Main Ethiopian Rift is composed of three main different segments (Northern, Central and Southern), characterized by the occurrence of a typical bimodal magmatic activity and two distinct systems of extensional structures: a system of NE-SW- to N-S- trending border faults and a system of NNE-SSW- to N-S-trending Wonji Fault Belt, which is an enechelon arranged faults obliquely affecting the rift floor (e.g. Mohr, 1962 and Gibson, 1969).

As far as mineral commodities are concerned, MER has been targeted at this time mainly for geothermal resources. According to Solomon Tadesse et al. (2003), the region has also a potential for some metallic minerals like Au, Fe and Mg and for many industrial minerals including potash, salt, trona, gypsum, limestone, bentonite, diatomite, pumice and clay (including kaolin). Among the widest range of industrial mineral resources kaolin is one of the most important industrial mineral resources in the rift. This thesis work tries to study one of the kaolin occurrences in the rift called Belessa kaolin.

1.2. Geographic setting of the study area

1.2.1. Location and accessibility

The study area is found in Southern Nations, Nationalities and Peoples Regional Government (SNNP), Hadiya Zone, near Hosaina town. It is more specifically located in the Hosaina map sheet, 0737 B4 according to the Ethiopian Mapping Agency. Hosaina is about 230 km south west of Addis Ababa (see Fig. 1.1). The UTM (Universal Transverse Mercator) coordinates shows that the area is bounded by 380000 to 390000 m E and 830000 to 850000 m N.

From Hosaina town the study area is accessed by the main asphalt road that runs to the small town called Belessa situated in the NE of Hosaina. This asphalt road passes through the study area and helps to access the North, North-East and West part using vehicle. The South, East and Central portions of the study area which are far from the asphalt road, can be accessed by all-weather gravel roads.

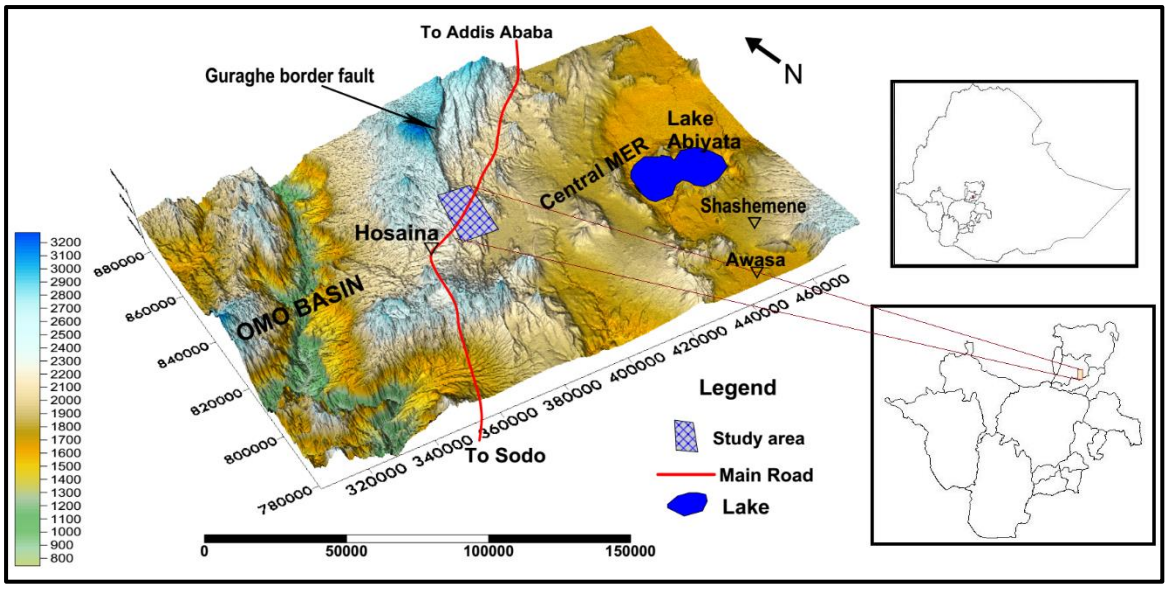

Figure 1.1: *Location map of the study area.*

1.2.2. Physiography and drainage

The study area is located in the western margin of the Central MER where N25°E–N35°E-trending and ESE-dipping Fonko and Guraghe faults are prominent (Corti, 2009). The area can be divided into two main physiographic features; those ridges and cliff blocks rising up to 2600 m above sea level and those which are less than 2200m a.s.l. The first subdivision consists of the southernmost part of Guraghe faults (in NW part) and Fonko faults (in NE, Central and Eastern portion). The second one is found in Northern, SW and SE part of the area forming relatively lower elevation with flat topography.

The simple drainage system of the area is attributed to the existing condition of physiography and vegetation cover. Because the area is relatively elevated topography and densely vegetated with different species of trees and cultivation, there is no way for the drainage system to develop. The drainage system found in the southern most part plays a

role to the formation of the fluvio-lacustrine sediments and it has also a contribution to the Boyo Lake found south of the study area (Fig. 1.2).

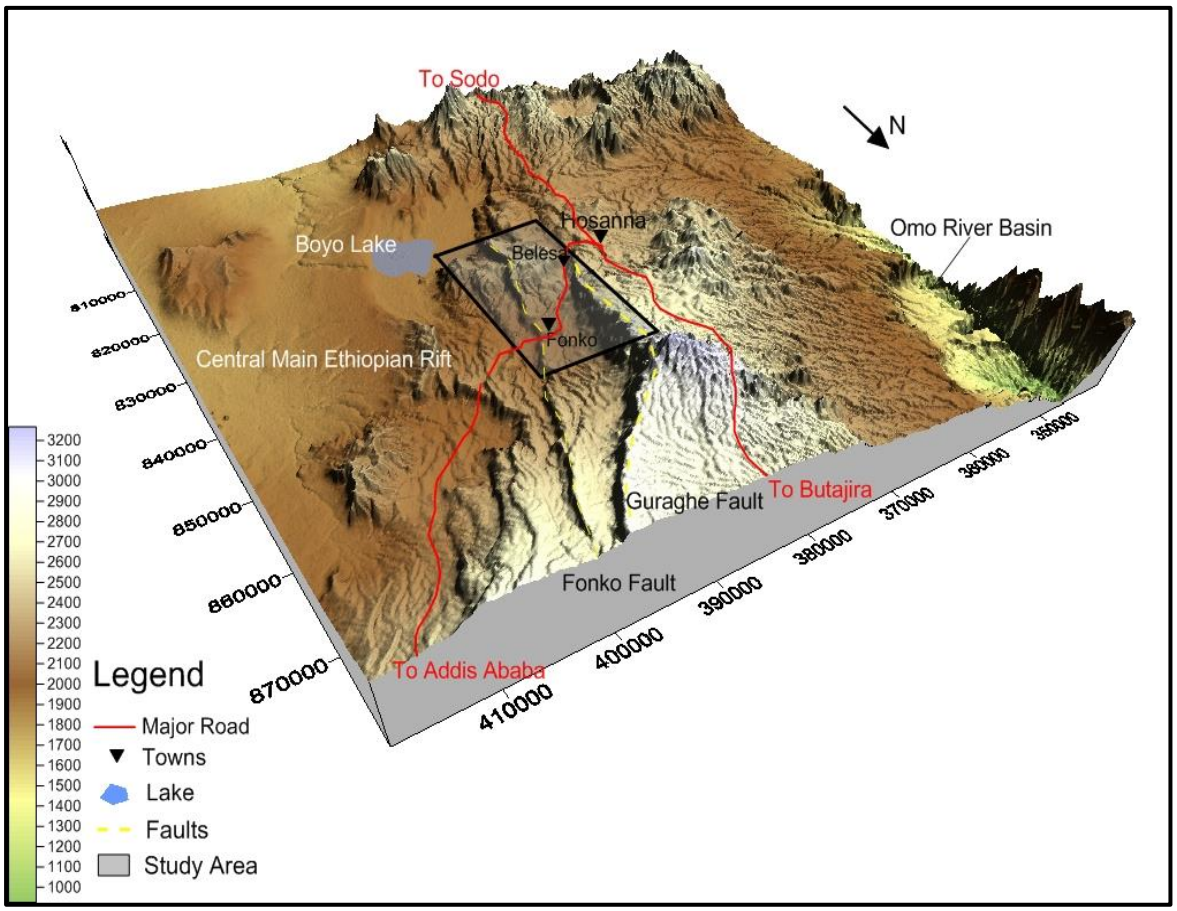

Figure 1.2: *3D DEM map showing physiography of the study area.*

1.2.3. Climatic condition and vegetation

According to climate-data.org in https://en.climate-data.org/location/3664/**,** the area is characterized by a warm and temperate climate. Uniquely, the study area gets significant rainfall even during the driest season. Here the climate condition is explained by taking the average temperature and precipitation of two main towns (Fonko and Belessa) in the study area (see Fig.1.3). Accordingly, the area records highest average temperature of 18.6 ^{0}C in March. While, the lowest average temperature measured in August is about 15.8 ^{0}C. The wettest month (August) measures the highest precipitation (167 mm) while the lowest precipitation is recorded in December (17.5 mm).

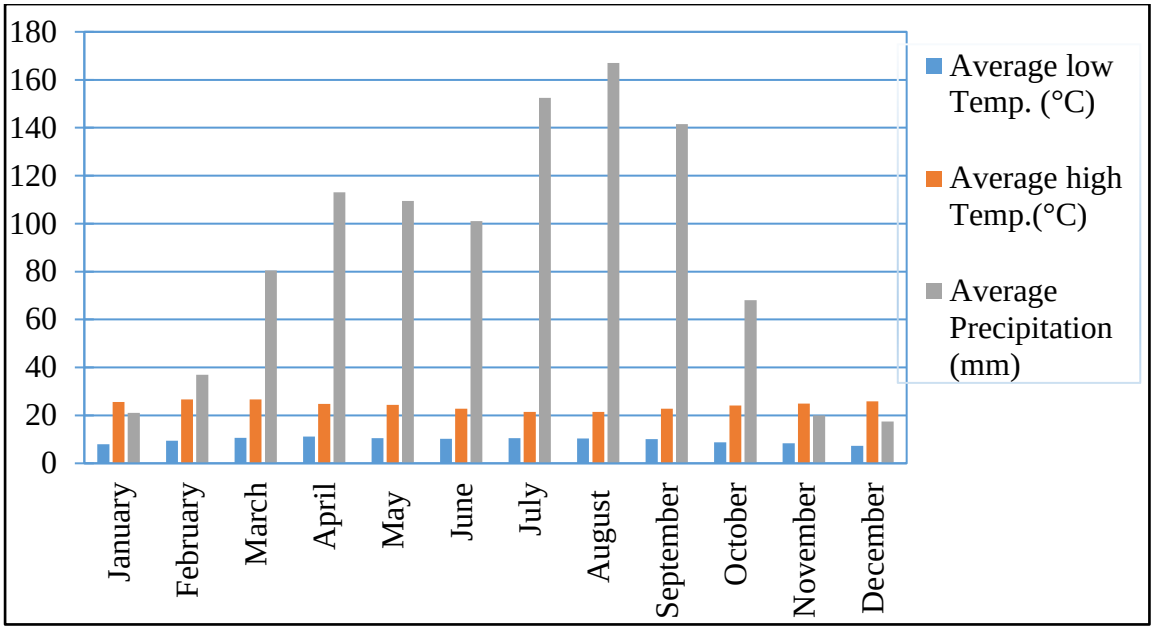

Figure 1.3: *A bar chart showing climatic condition of Hosaina area (https://en.climate-data.org/location/3664/,).*

It is obvious that the distribution of vegetation is highly dependent on the climate of the area. The thick eluvium sediment also creates a favorable condition for the dense vegetation of the area. The vegetation related to the existing climatic conditions include Eucalyptus trees, Junipers, Hagenia abyssinica,Podacarpus grcilior (zigiba),and Vernonia amygdalina (bisana). In addition the area is extensively cultivated and the local people produces crops like Sorghum, Barley, Wheat, Teff, Enset and Khat. These crops are harvested during the driest months (December and January).

1.2.4. Population and settlement

Significant population density is ascribed to the study area. The settlement pattern in the study area is in such a way that villages are densely concentrated along all-weather roads and the main asphalt road. Belessa, Fonko and Lisana are the three densely populated villages' situated in the east, northeast and southeast of Hosaina town respectively.

The Hosaina area including the study region has an estimated total population of 90,000 inhabitants. Among these people Hadiyas are the main ethnic groups in origin, followed by Kembata, Gurage, Silte and Amhara. Majority of the inhabitants speak Hadiyissa. While some people speak Kembatissa, Guragegna, Amharic and Siltigna. As far as religion is concerned, Protestant is the predominant belief followed by Orthodox, Muslim and Catholic. The rural in habitants are mainly engaged in subsistence farming and pastoral farm (http://www.bestbridge.org/communities/hadiya-zone-hossana/).

1.3. Problem statement

Southern parts of Ethiopia has been area of interest for different industrial minerals mainly kaolin for decades. The commercial Kaolin resources investigated so far and used as a source for the consuming industry are mainly restricted to in situ weathering products of granitic intrusive rocks and associated pegmatite (Tibebu Mengistu and Haile Mickael Fentaw, 1993). For example Sabove et al (1985) investigated Bombowoha I and II kaolin deposits from kaolinized pegmatite and granite respectively (Said Mohammed and Sentayew Zewdie, 2000). According to Haile Mickael Fentaw (1995), these deposits are restricted to only some industrial applications due to further beneficiation requirement. Whereas the kaolin resources associated with rift volcanic rocks are important for the kaolinite formations of improved quality.

The kaolin occurrences especially those which are associated with acidic volcanic rocks found in the Main Ethiopian Rift are still not well known and studied. In the same way, there are limited information on the geological, mineralogical, geochemical and morphological studies and interpretations of Belessa kaolin occurrences. For instance, geological maps that are useful for initial follow-up are unavailable. As a result, these gaps obstructs to elucidate the genesis and industrial applications of Belessa kaolin. Moreover, the gaps (trace element study, geological map and morphology) which are remarked during the evaluation of Belessa kaolin by Haile Mickael are also considered in designing this research project.

1.4. Objectives

1.4.1. General objective

The main aim of this research project is to characterize the genesis of Belessa Kaolin and acquire a better understanding on the possible fields of industrial applications.

1.4.2. Specific objectives

- To understand the genesis of Belessa kaolin by examining the geological setting, field characteristics of the deposit, mineralogy and geochemical signatures.
- To produce geological map of the area at a scale of 1:25,000 that will be used for follow-up works.
- To estimate the kaolin resource based on field data and geological map of the study area.

- Determining the physical and chemical properties of kaolin samples to suggest the possible fields of applications.
- Characterizing Belessa kaolin using remote sensing to locate other kaolin occurrences

1.5. Methodology

The general frameworks; Pre-field work, field work and post-field work activities are employed in achieving the complete research project. The pre-field work is commenced by assessing study related literatures, reports and by important discussions with advisors and other peoples. During fieldwork collecting primary data were the main tasks. To come up with the conclusions, those data collected and studied thoroughly at the time of pre-field work and field work are passed through analysis, synthesis, interpretation and presentation during post field work time.

In the preliminary stage of this project, relevant literatures that are closely related with the study are reviewed to know the methodologies that would be followed for this study. Moreover, the literatures were helpful in understanding the regional geological settings and structures. Study specific published and unpublished geological reports are also studied to acquire more information on the study area. In addition, geological structures (faults) are delineated and simple lithological units are discriminated using ASTER images and Landsat 8 OLI TIRS of 2015 and 2016.

1.5.1. Field work and geological mapping

This activity was commenced from October 25 to November 10. During this time, representative sampling of encountered lithological units and transferring of these units and other geological structures into the existing base map were the main tasks. In doing these**,** geological exposures were surveyed including sections along roads, mining excavations and in river banks. Along recording these geological information on the base map, important descriptions of the units and structures were taken using field note book. The rock samples are collected considering lithological variations and kaolin host rock. While Kaolin ore samples are collected based on the lateral and vertical variations (in color, grain size, etc) observed in kaolin exposures. Transferring lithological units and geological structures are done by taking GPS control points (GCP) and locating them on the base map. The information from GCP finally helped in producing geological map at a scale of

1:25,000. All these activities were accomplished by selecting traverses across the strike of geological units and structures.

1.5.2. Analytical methods and data analysis

After finishing the field work, the collected samples are submitted to laboratory for different analysis. The purpose of these analyses is to get vital information for characterizing Belessa kaolin occurrences from genesis and quality points of view. These different analyses include; mineralogical, geochemical, physical tests, petrography, scanning electron microscopy (SEM) and remote sensing and GIS.

a) Mineralogical analysis

This analysis is performed to unveil the minerals present in the kaolin samples and to know how much percent of each mineral is found. These qualitative and quantitative information of the minerals found in kaolin samples are determined by X-ray Diffractometer (XRD). Five representative kaolin samples are selected for this analysis. The samples are collected based on the observed vertical and lateral feature (color, grain size and so on) variations. The Sample preparation is done in Geological Survey of Ethiopia. The preparation passes through three principal steps. First, the kaolin sample is dried by air. Then the sample is milled using mortar. Finally, it is allowed to pass through a 63μm size sieve until we get the desired amount of powdered kaolin (i.e. 10gm). This under size powdered kaolin is the required amount to be used for XRD. To minimize contamination, the caution was always there during preparation by washing all the materials (Mortar and sieve) after milling and sieving individual sample.

The powdered samples are then sent to a laboratory in the University of Frieburg, Switzerland for qualitative and quantitative mineralogical identifications. The diffractograms were recorded with a Rigaku Ultima IV diffractometer equipped with a copper tube, operated at 40kV and 40nA, and a Position Sensitive Detector (PSD) D-tex. Qualitative phase determination was performed with the Rigaku Software PDXL-2 and the ICDD database. Quantitative Mineralogy was determined by Rietveld refinement using the software TOPAS by Bruker. Data presentation and interpretation is done using graphs and some figurative explanations.

b) Geochemical analysis

Samples are collected during field work from both kaolin occurrence sites and associated host rocks. A total of eight samples; 3 rock samples and 5 kaolin samples are selected for

this analysis. Sample preparation is done in Addis Ababa University School of Earth Sciences mill room and ALS Geochemistry, Addis Ababa. Removing of the weathered surfaces and breaking to desirable size is done for the three rock samples in School of Earth Sciences mill room. The jaw crusher is washed and cleaned carefully after breaking each samples to be safe from contamination. Then the three broken rock samples and five kaolin samples are taken to ALS Geochemistry for final preparation. In this laboratory, all the samples are powdered following two basic steps; drying of wet samples in drying ovens (mainly for kaolin samples) and then pulverize the samples using "flying disk" or "ring and puck" style low-chrome steel grinding mills.

The powdered rock and kaolin samples are sent to ALS Geochemistry laboratory found in Ireland to quantify the major and trace elements using Inductively Coupled Plasma Atomic Emission Spectroscopy (ICP-AES) and Inductively Coupled Plasma Mass Spectroscopy (ICP-MS).

c) Physical tests

This test is aimed at seeing the suitability of kaolin in different industrial applications. The performed tests are specific gravity, bulk density and pH. For this purpose five kaolin samples are selected. Whereas, the grain size distribution data are taken from previous work of Haile Mickael Fentaw (2003). All the tests are done in Addis Ababa University School of Earth Sciences engineering geological laboratory and Geological Survey of Ethiopia.

d) Petrographic analysis

Six rock samples representing the study area are selected based on their variability and association with the kaolin occurrences of the area. The thin section preparation is done in Geological Survey of Ethiopia. While the microscopic examination of thin sections is carried out in Addis Ababa University School of Earth Sciences thin section laboratory. The thin section of parent rock is examined to identify the primary minerals of the host rock.

e) Scanning Electron Microscopy (SEM)

This method is employed to describe textural and morphological features of selected kaolin samples. The same five kaolin samples used in mineralogical analysis are given for SEM. The samples are sent for analysis to a laboratory found in University of Frieburg, Switzerland.

f) Remote sensing and GIS

This method has been used thoroughly throughout the course of this research project activities. Because kaolin is an alteration product, remote sensing played a paramount significance for its identification. For this purpose, data like Landsat 8 OLI TIRS of 2015 and 2016 and Advanced Space borne Thermal Emission and Reflection Radiometer (ASTER) images were used. The main aim of using this method is to detect the alteration zones and key alteration mineral (kaolinite) found in the study area. Moreover, these images were used to discriminate features like lithologies, structures and vegetation. This is done by employing image processing techniques like RGB band composite and band rationing.

During the study, data analysis were carried out using Envi 4.7 and Arc GIS 10.2.1 by juxtaposing the imageries with geological map (1:25,000) of the study area and a 90 m resolution digital elevation model (DEM) data. The analysis is also aided by software like Global mapper and Google earth.

1.6. Significance of the research

Belessa kaolin has not so far been studied in the aspects of genesis. A few is also known on its suitability for different industrial applications. Therefore, this research study will have the following contributions and outcomes.

- Interpretation of the Chemical Index of Alteration (CIA) of the host rocks, trace element data from geochemical analysis, mineralogical and morphological data to understand the genesis and alteration phenomena.
- The suitability of kaolin for some industrial applications will be indicated based on available laboratory tests.
- Spectral signature curves and band combinations used to locate other kaolin occurrences will be suggested.

1.7. Thesis overview

This thesis work is organized by dividing in to seven chapters. The first chapter gives a general introduction to the study and methodologies employed. Chapter two is a review of the previous research papers relevant to the genesis, application and other important issues on kaolin deposit. Chapter three deals with the regional geological settings and local geology. In chapter four the mineralogical, geochemical, SEM and satellite data analysis results are presented. Chapter five is devoted to technological properties and possible applications of Belessa kaolin. Discussions on the alteration phenomena, genesis and

quality of Belessa kaolin are addressed in chapter six. The final part, chapter seven consists of the conclusion and recommendation part. Finally, some study related issues are incorporated in the index part.

CHAPTER TWO

2. Literature review

2.1. Kaolin

Kaolin is both a rock term and a mineral term. From the rock point of view, kaolin means that the rock is comprised predominantly of kaolinite and or one of the other kaolin minerals. Mineral wise, it represents the group name for the minerals kaolinite, dickite, nacrite, and halloysite (Dill, 2016; Murray, H.H., 2007 vol. 2). According to Ross and Kerr (1931) kaolin is also defined as a rock mass containing principally kaolinitic clays that are low in iron, and usually white or nearly white in color comprising naturally occurring kaolin group minerals. It can be contained in a variety of kaolinitic rock types. The primary kaolin explains a kaolin which is altered from an igneous or metamorphic rock that was kaolinized in situ by hydrothermal or weathering processes. Secondary kaolin is sedimentary kaolin comprising transported mineral particles. Kaolin is among the major industrial clays including Smectites, and Palygorskite–Sepiolite (Murray, 2007). The main Kaolin minerals include kaolinite, dickite, nacrite, and halloysite. These minerals are dioctahedral 1:1 phyllosilicates having a sheet of silicon atoms in tetrahedral coordination with four oxygen atoms and a sheet of aluminum atoms in octahedral coordination with two oxygen atoms and four hydroxide molecules (see Fig. 2.1). In general, the basic kaolin mineral structure constitute a layer of a single tetrahedral sheet and a single octahedral sheet. Among the kaolin minerals, Kaolinite ($Al_2Si_2O_5$ (OH) $_4$) is the most common mineral and has great industrial importance.

Primarily, kaolin is used as (1) a pigment to improve the appearance and functionality of paper and paint, (2) a functional filler for rubber and plastic, (3) a ceramic raw material, and (4) a component for refractory, brick, and fiberglass products. Other less significant uses for kaolin include chemical manufacture, civil engineering, agricultural applications, and some pharmaceuticals.

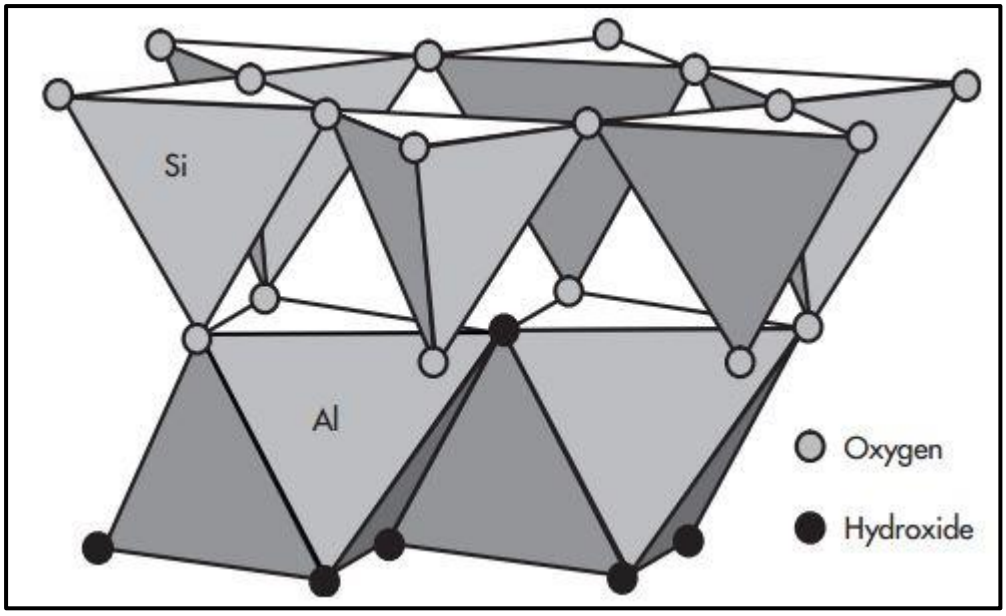

Figure 2.1: *Kaolinite crystal structure (adapted from Grim, 1953).*

2.1.1. Mechanisms of kaolinite formation

Stock and Sikora (1976) confirms the direct formation of kaolinite from biotite by the transformation of the mica structure. This is evident from the textures observed in Argentina, Cerro Rubio and La Esperanza kaolins. Here the growth of kaolinite crystals perpendicular to the biotite surface is indicated through petrographic study (Cravero F., 2001). There is also evidence that, with time, halloysite transforms to kaolinite. Jeong Gi (1998) studied a weathering profile in Korea and demonstrated that as weathering progress the halloysite grains coalesce and convert in to stacked kaolinite plates. This is not in agreement with the idea of Salter and Murray (1993), where they found no evidence of halloysite converting to kaolinite. Moreover, previous researchers (e.g. Bottrill, 1998; Hemley and Jones, 1964 cited in Yuan et. al., 2014) deduced a number of commonly used reactions by which the host rock is altered to give the kaolinite mineral. According to the authors, the feldspars (k-feldspars and plagioclase) in the host rock could be altered to sericite and then to kaolinite based on the following reactions:

$$3K\,[AlSi_3O_8] + 2H^+ \Longrightarrow KAl_2\,[AlSi_3O_{10}]\,(OH)_2 + 6SiO_2 + 2H^+$$

K-feldspar Sericite

$$3(Na, Ca)\,[AlSi_3O_8] + K^+ + 2H^+ \Longrightarrow KAl_2\,[AlSi_3O_{10}]\,(OH)_2 + 6SiO_2 + 3(Na^+, Ca^{+2})$$

Plagioclase Sericite

$$2\,KAl_2\,[AlSi_3O_{10}]\,(OH)_2 + 2H^+ + 3H_2O \Longrightarrow 3Al_2Si_2O_5\,(OH)_4 + 2K^+$$

Sericite Kaolinite

In other way kaolinite could be formed directly from feldspar and with increasing temperature it could be also transformed into pyrophyllite as it is illustrated by the following two reactions.

$$2NaAlSi_3O_8 + H_2O + 2H^+ \Longrightarrow Al_2Si_2O_5\,(OH)_4 + 4SiO_2 + 2Na^+$$

Plagioclase Kaolinite

$$Al_2Si_2O_5\,(OH)_4 + 2SiO_2 \Longrightarrow Al_2Si_4O_{10}\,(OH)_2 + H_2O$$

Kaolinite Pyrophylite

2.1.2. Genesis of kaolin deposits

Many authors (e.g. Dill, 2016; Pruett, 2016; Murray, 1988) classified kaolin deposits as primary or secondary based on their origin. Primary deposits originates in situ by alteration and can be resulted due to weathering activity (supergene kaolin), hydrothermal activity (hypogene kaolin) or in some cases by a combinations of the two processes (Murray, 1988; Murray and Keller, 1993). Whereas, secondary deposits are of sedimentary origin (Gilg et.al., 1999 Cited in Ismail et. al., 2014). Studying the genesis of kaolin have a paramount importance and it has a direct bearing on its industrial applications (Ekosse, 2000). This is because the mode of formation of the kaolin may have considerable influence on its mineralogy, chemistry and morphology of the kaolin (Bloodworth et al., 1993 Cited in Ismail et. al., 2014). Numerous studies have been devoted to understand the genesis of different kaolin deposits in the world. In the following paragraphs critical review on the theoretical concepts and methodologies that surround the genesis (origin) of kaolin deposits will be discussed.

Different authors investigated kaolin deposits of the world geologically, petrographically, mineralogically, geochemically, physically and morphologically to characterize the genesis and indicate the possible industrial applications of kaolin.

Geologically from field observations, Tibebu Mengistu and Haile Mickael Fentaw (1993) suggests a residual origin for the kaolin deposits found near Kombolcha town, Eastern Hararghe. These authors considered four feature in suggesting the residual origins; 1) the extensive surficial coverage of the kaolin; 2) the complete absence of the usual constituents of hydrothermal kaolin deposits like sulphides, alunite, gypsum, mineral zonation and other known hydrothermal manifestations; 3) the gradual transition from partly altered rocks to kaolinized zones and 4) the significant presence of discrete illite and mixed layer illite-smectite, which are considered intermediate phases in the formation of kaolinite. Moreover, the authors also tried to point out the means to identify the hydrothermal origin kaolin deposits; as the presence of vein lets of kaolin, following micro-fractures raises the suspicion of introduction of hydrothermal solutions.

Based on the petrographic studies in thin sections of the host rock; textures and primary mineral assemblages can be identified (Caliani et al., 2010). Kitagawa and Koster (1991) studied the weathering origin Tirschenreuth kaolin deposit and they showed that, in the kaolinite zone plagioclase and biotite of the host rock have been completely decomposed, whereas quartz and most of the K-feldspars are unaltered. In addition, kaolin samples from Amazon region, Brazil showed that the unaltered host rock consists of the mica framework (muscovite and biotite) and the kaolin samples do not show any remains of mica textures (da Costa and Moraes, 1998).

Many authors take the major element chemistry of host rock and kaolin ore to determine the degree of alteration. In the kaolinite formed under weathering process, Cravero et al. (2001) noticed high SiO_2 content in a sample with lower degree of alteration. The authors also observed that a sample with the lowest SiO_2 and highest Al_2O_3 content is due to a higher degree of alteration. Njoya et al. (2006) uses major element geochemistry to characterize the kaolin deposits of western Cameroon by two facies; sandy kaolin and sand poor kaolin. Sandy kaolin generally shows above 60% SiO_2 with Al_2O_3 ranging between 20% and 25%. This is correlated with high quartz content. On the other hand sand poor kaolin is characterized by lower SiO_2 (45-49 %) and higher Al_2O_3 due to higher kaolinite content. Moreover, both types of kaolin facies show a complete loss of MgO, MnO, CaO and Na_2O. This is attributed to their mobility during the kaolinization process and some

authors (e.g. Meyer and Hemley, 1967; Meunier et al., 1983 cited in Njoya et al., 2006) relate this with an advance argillic alteration system close to hydrothermal kaolin deposits. In addition, the small Fe2O3 and TiO2 contents corresponded to the hydrothermal alteration since alteration generally enhances the presence of the ferric oxides and hydroxides in tropical climate (Meunier et al., 1983; Santos et al., 2004 cited in Njoya et al., 2006).

Studying the trace element concentration behavior of host rock and kaolin ore helps also to evaluate chemical mobility during weathering (Grant, 1986). According to Fernández-Caliani (2010), losses of Na, Ca, Mn, Sr, P and U relates to early stages of weathering. With increasing in stages of weathering, partial breakdown of K-feldspar and mica result in significant amount of K, Rb, Cs and Ba to be released. On the other hand Al, Ti, Zr, Hf, Th and REE were immobile elements which are remained during the alteration process and accumulated residually in the kaolin. Dominguez et al. (2008, 2010) also used trace elements to distinguish hypogene and supergene kaolinization processes. These authors propose the contents of Ba, Sr and SO_3 as an indicator of hydrothermal activities. Furthermore, hypogene deposits are known to contain high levels of Ba+Sr, while high levels of Ce+Y+La are attributed to that of supergene kaolin deposits. As far as rare earth elements (REE) are concerned, there exists no agreement among authors on the mobility of REEs. Four different REE behaviors proposed by different authors are summarized by Prudencio et al. (1995); REE are immobile, REE are slightly mobilized, REE are mobilized without fractionation and REE are mobilized and fractionated during weathering. Authors like Nesbitt (1979) and Duddy (1980) explained that REE are fractionated during weathering processes. According to these authors, the weathered residual products are enriched in light REE and depleted in heavy REE.

Nesbit and Young (1996) propose a helpful index used to determine the extent of weathering. This index is called Chemical Index of Alteration (CIA) and is evaluated using the equation; CIA= $[Al_2O_3/ (Al_2O_3+CaO+Na_2O+K_2O)] \times 100$. McLennan and Taylor (1991) indicated 85 to 100 % CIA values for residual soils. High amounts of this index relates to the high amounts of clay minerals and small amounts of residual feldspars in the region. On the other hand, low weathering process is correlated with small amounts of Al_2O_3 (Ghadimian & Khodami, 2015).

Distinction between hydrothermal type and residual type kaolin deposits can be also done based on mineralogical assemblages. Keller (1969) and Dill et al. (1997) put kaolin deposits

containing high temperature alteration minerals like illite, illite-smectite, mixed layer mineral, dickite , nacrite , topaz , pyrophyllite are genetically associated with hydrothermal activities. In other way Nakagawa et al. (2006) classify kaolin deposits containing only kaolinite and quartz minerals as residual type origin.

Table 2.1: *Comparison between supergene (weathering) and hypogene (hydrothermal) kaolinites.*

Properties	**Type of kaolinite**	
	Supergene	**Hypogene**
[A] Geological settings	• gradual transition from partly altered rocks to kaolinized zones	• high temperature and high pressure shear zone environment • Sharp transition to the kaolinized zones. • Quartz veining is common
[B] Mineralogical assemblage	• Monotonous and oxidized minerals. [Contain mainly kaolinite and quartz. Gibbsite is also typical].	• Variegated mineralogy with reducing minerals [High temperature alter-ation minerals (illite, illite-smectite, mixed layer mineral, dickite, nacrite, topaz, pyrophyllite)].
[C] Geochemistry	• Low P and high Cr + Nb.	• Low Ce + La + Y and low Ti
[D] Morphology	• Presence of books of kaolinite particles with angular edges.	• Very fine grained, tightly packed and kaolinite plates occur as singles, sheaves or thin packets. • There are no large kaolinite booklets.

[(A)] Tibebu Mengistu and Haile Mickael Fentaw (1993); [(B)] Keller (1969), Dill et al. (1997) and Dill (2016); [(C)] Dominguez et al. (2008, 2010); [(D)] Ismail et al. (2014)

The morphology of kaolinite crystals is highly related with its genetic environment and parent material (Keller, 1989). The SEM result obtained from Keller (1976a) and Ismail et al. (2014) identified that, kaolinites originating from weathering processes (residual origin) consists a feature of many stacks or books of kaolinite flakes with angular edges and lack of hexagonal booklets. Conversely, kaolin of hydrothermal origin are typically hexagonal booklet and tightly packed (Keller, 1976a, 1978). But it should be noted that morphology is not unambiguous means to differentiate between hydrothermal and weathering kaolin deposits.

Furthermore, Ismail et al (2014) used one of the physical test result (bulk densities) of kaolin in order to reflect their mode of genesis. Accordingly, those kaolin originated from chemical weathering possess relatively low bulk densities (< 2.0). Whereas the hydrothermal origins show higher bulk densities (> 2.0).

2.2. Exploration, mining and processing of kaolin

To bring kaolin resource to a production level, a thorough exploration work that goes from searching to mine closure should be employed by following the main respective phases as explained by Kogel (2014). The first phase is devoted to searching of a deposit on the surface. Here, a geologist from his or her experience tries to see signs of kaolin mineralization during fieldwork. To get information on the subsurface geology, prospectors will depend on outcrops, stream beds and rod cuts. Stratigraphic position, geomorphologic features and topographic elevation are also important searching tools. In addition other prospecting tools like geophysical surveys and remote sensing can be used as a more sophisticated approaches. Lohva and Lehtimaki (2005) suggest a geophysical exploration for kaolin. This is because kaolin has a petro-physical contrast with the overburden and unaltered rock. The second phase involves direct sampling and testing of the deposit. This is usually done by using rotary core drilling and auger drilling methods, which have become standards for sampling of kaolin and other industrial clay. Small number and widely spaced test holes will be drilled randomly to check the discovery. The next step is given for resource development. This step is a gear in bringing the deposit in to production and involves drilling the discovered deposit on a dense grid pattern. Such closely spaced drilling is essential for mineral resource estimations. The three important information used to estimate the resource potential of kaolin deposit include; tonnage, grade and economic viability. Economic viability depends on factors like overburden thickness, kaolin thickness, vertical/horizontal continuity, quality, distance to the processing plant and

so on. Grade and tonnage are estimated from drill hole data. There are two known methods used for grade and tonnage estimations. The one with conventional approaches is based on maps, cross sections and spread sheets. The other one develops 2D and 3D computer driven geostatistical modelling techniques. Then based on increasing geological knowledge and confidence, the resource is classified as inferred, indicated and measured. The fourth step shows a concern on feasibility studies and reserve development. Here, a detailed engineering and economic analysis are considered. Moreover, for a kaolin resource to be converted to economically minable kaolin reserve, it must pass through some factors that include mining, processing, metallurgical/quality, economic, environmental, legal, social, marketing and governmental factors. After passing these factors, the mine design, construction and production (extraction) are the final steps commenced before the mine closure. This step is much concerned with determining size of the mine, mining method, production requirements and required equipment. Closure and restoration is the final important step in kaolin exploration. This involves the process by which the mine site is graded and revegetated. The restoration brings a post mining uses that can give a long term value to the local community.

As far as mining is concerned, the near surface deposit with thin overburden can be mined by simply removing a layer of top soil (Schroeder and Erickson, 2014). Most commonly, kaolin is extracted from small to large scale open pit mines using different equipment including draglines, power shovel, front-end loaders, backhoes, scraper-loaders and shale planers (https://www3.epa.gov/ttnchie1/ap42/ch11/final/c11s25.pdf). In some places, a standard cut and fill mining process is also used (Kogel, 2014). In this mining process, overburden from the first cut is accumulated and the overburden from each subsequent cut is damped in the previously mined-out cut. Moreover, tunneling can be also used as another mining method and it is employed depending on the natural rock strength. In all cases, the mining engineer should consider the geotechnical aspects of the site in order to reduce the risk of wall failure. After kaolin is mined it is usually transported by truck from mine site to processing plant, which is found mostly near the mine area.

Based on end-use applications, kaolin is processed to enhance or control various properties. Kaolin can be processed by mechanical or both chemical and mechanical methods (https://www3.epa.gov/ttnchie1/ap42/ch11/final/c11s25.pdf). Mechanical methods are used for most applications and they involve crushing, grinding and screening. However, chemical and mechanical processes include drying, calcining, bleaching, blunging and

extruding. According to Kogel (2014) processing of kaolin can be classified in to dry, wet and thermal processing. Compared to wet processing, the dry one is less expensive, simple and produces lower quality product (see figure 2.2). It is low level of processing and it results a less refined product. In this process, raw kaolin is crushed to the desired size, dried, pulverized and air-floated to remove the coarse grit. Dry processed kaolin is mainly used in rubber industry and to some extent in paper filling, fiberglass and sanitary ware. In wet processing, the raw kaolin passes through steps including blunging to produce slurry and then fractionated as coarse and fine fractions using centrifuges, hydro-cyclones or hydro-separators. In order to refine the raw kaolin, various chemical methods (bleaching) and physical and magnetic methods are used. Also chemical processing involves leaching with sulfuric acid and then addition of strong reducing agent like hydrosulfite. For use as refractory and filler material, the kaolin has to be calcined after the drying step. Wet processed kaolin is relatively a higher quality product and it is extensively used in paper manufacturing. In other case, thermal processing (calcination) involves a higher temperature firing of the wet or dry processed kaolin. Firing at lower temperature produces meta-kaolin, which is useful in the application of paint, paper, PVC cable and pozzolanic additive. While, firing at much higher temperature result in mullite formation, a product used in rubber compounds. In general, it should be noted that however the basic processing steps remain the same, small advances will underway as new applications discovered. A process flow diagram for dry and wet processing of kaolin is illustrated in figure 2.2.

2.3. Quality and major markets

Kaolin, because of its crystal shapes, sizes and layer structures, it is highly versatile industrial mineral used for various industrial applications Kogel (2014). Commercially, kaolin is more valued for its whiteness and fine particle size. In addition, Brightness, abrasiveness, glossiness and viscosity are also common physical properties that have direct bearing on commercial utility of kaolin (Bloodworth et al., 1993). Such properties result to have a different grade of kaolin. According to Kogel et al (2009) the different grade of raw kaolin are mined and processed for three major area of applications. These include paper (filler and coating), ceramics (sanitary ware and dinner ware) and fiber glass. Other lower volume applications include paint, rubber, adhesive, catalyst, pharmaceuticals, brick and refractory. It is good to note that each of these applications depend on specific properties and processing methods.

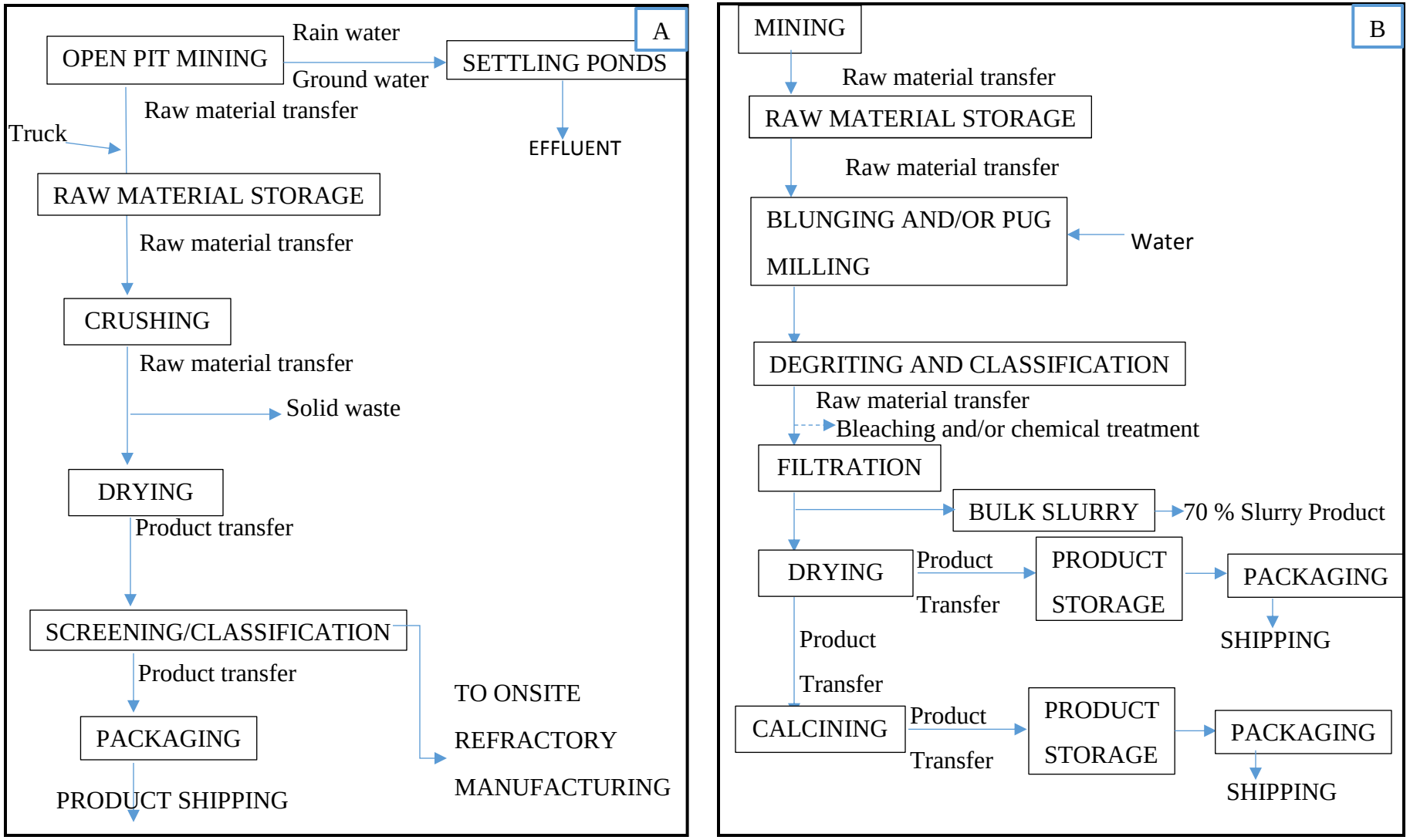

Figure 2.2: *Process flow for kaolin processing. A) Process flow diagram for kaolin mining and dry processing and B) Process flow diagram for wet process kaolin: (https://www3.epa.gov/ttnchie1/ap42/ch11/final/c11s25.pdf).*

2.4. Previous works on kaolin deposits of Ethiopia

Clay deposits as a whole are known to occur in different parts of Ethiopia. According to Solomon Tadesse (2009); Gonder (Chelga), Koka, Shewa (Addis Ababa area), Debre Zeit, Sululta, Ambo, Debre Sina, Debre Berihan, Zega Wodel, Kaffa (Bebeka), Adola (Kibre Mengist area), Wollega (Dilla), Hararghe (Dire Dawa area), Abay River Valley and the Rift Valley Lake regions are the most importat sites known for clay deposits. Those deposits that are entered into the kaolinized realm are found in few places. Bombowoha (Adola) and Kombolcha (Harar) areas are identified for the kaolin deposit with the predominant kaolinite mineral (Tibebu Mengistu and Haile Mickael Fentaw, 2000).

The investigation of kaolin was started in 1970 by Chinese geologists. This group studied the kaolin occurrences of Bombowoha area (Adola greenstone region) and other ten small occurrences found along Addis Ababa- Adola road. Following this, in 1981 geologists from Ethiopian Institute of Geological Surveys (EIGS) Gumerov and Tibebe Mengistu and then Sabov et al in 1985 carried out an extensive exploration on the Bombowoha kaolin deposits. In the respective years, different geologists (Sabov et al, 1986; Said Mohammed and Solomon Engidayehu, 1993 and Said Mohammed and Sentayew Zewdie, 2000) come up with important results that helped in scaling up the information in Bombowoha kaolin deposits. For instance, in the years between 1994 and 1995, the investigation of kaolin was aided by using a geological and a topographic maps at scales of 1:100,000 and 1:50,000 respectively. This is a different scenario as compared to the time before 1994 where there existed insufficient geological knowledge (with only 1:2,000,000 scale geological map) concerning the area surrounding Bombowoha kaolin (Sabov et al., 1985). Therefore, extensive exploration in the area helped to have better knowledge on the quantitative (reserve) and qualitative (quality) information.

The Adola region consists of post-tectonic granitic and quartz diorite intrusions, dominated by leucocratic granites and pegmatites. The pegmatites of various sizes are considered to be associated with the granite intrusions and injections (MOME, 1994). Insitu weathering to a depth of tens of meters results to the kaolinization of both granite and pegmatite.

Three deposits are recognized in Bowbowoha area. Bombowoha I and II are investigated by Sabov et al (1985) and reserves of 120,700 tons and 11,600 tons respectively under C1 category are calculated. Later in 1994 the Bombowoha III kaolin occurrences are discovered. This occurrence were found within kaolinized pegmatite and granite nearby the existing deposits (Said Mohammed and Sentayew Zewdie, 2000).

Haile Mickael Fentaw and Tibebu Mengistu (1998) on their comparison between Kombolcha and Bombowoha kaolins, they tried to see the basic differences of those kaolins in mineralogy, chemistry and morphology. The mineralogical study revealed that kaolinite is the dominant mineral in both kaolins. The deposits also showed traces of illite/muscovite, feldspar and quartz as a common characteristics. The Bombowoha kaolin typically contains Gibbsite and Halloysite as minor constituents. The XRD result curve for Bombowoha kaolin shows a distinctive peaks of kaolinite. The peaks are nearly symmetrical which according to Bramao et al. (1952) suggesting a good crystallinity. The crystallinity index values obtained from the method of Hinckley (1963) also show a moderate crystallinity for Bombowoha. The two deposits also show a difference in their morphology. Kombolcha kaolin consists of a well preserved and expanded books of kaolinite. Elongated with books and plates of kaolinite is the morphology attributed to the Bombowoha deposit.

Chemical analysis results of both kaolin deposits (Bombowoha and Kombolcha) shows a significant differences in total alkali (<3%, 2.54%), Iron (<1%, 2.53%) and alumina (35%, 33.24%). Haile Mickael Fentaw and Tibebu Mengistu (1998) also raise the role of K_2O as an indicator of the degree of alteration of the primary alumina-silicate minerals. Accordingly, relatively higher K_2O values are corresponded to the partly altered material. Genetically, the Kombolcha kaolin is considered as a residual type deposits after comparing it with the chemistry and morphology of known residual deposits. Whereas the Bombowoha kaolin is formed by hydrothermal type and residual type alteration of acidic rocks. Furthermore, authors propose the ceramic industry as a possible industrial application for both deposits, but with some recommendation of beneficiation for Kombolcha kaolin.

More recently, a few studies show those kaolin deposits related with Tertiary volcanic rocks found in the MER. These include, the Ansho kaolin deposits in Hosaina area (Tigistu Melka et al., 2011) and the Koka Kaolin deposits in Koka area (Samuel Getachew et al., 2015). Both are indicated as a byproduct of hydrothermal alteration of trachyte unit and feldspar rich rocks respectively.

2.5. Application of remote sensing in prospecting alteration minerals

Recently, remote sensing technology has been used effectively in mineral deposit and mining areas due to its wide coverage and low cost. Many studies used satellite images for mapping alteration zones, lithological units, structures and vegetation. For these purpose, many authors (Adiri et al., 2016; Mwaniki et al., 2015; Pournamdari et al., 2014) used

Landsat 8 OLI and ASTER images as best discriminators for different geological features. The Landsat 8 OLI data contains a total of 11 spectral bands (see table 2.2): four in the visible (0.43 to 0.67 μm), one in the NIR (0.85 to 0.88 μm), two in the SWIR (1.57 to 2.29 μm), one panchromatic (0.5 to 0.68 μm), one band of cirrus (1.36 to 1.38 μm) and two in the TIRS (10.6 to 12.51 μm). All bands have a spatial resolution of 30 m except that of panchromatic (15 m) and TIRS (100 m). Whereas, the Advanced Spaceborne Thermal Emission and Reflection Radiometer (ASTER) records radiation in 14 bands (see table 2.2): three VNIR (0.52 to 0.86 μm), six SWIR (1.6 to 2.43 μm) and five TIR (8.125 to 11.65 μm) with 15 m, 30 m and 90 m spatial resolution respectively (Adiri et al., 2016).

Various image enhancement techniques are applied to both Landsat 8 OLI and ASTER data. Band rationing and RGB band combinations are among the well-known and effective techniques used to discriminate different geological features (alteration zone, lithological units and geologic structures). In band rationing, one band is divided by another in order to enhance the variability observed in certain features (Pour and Hashim, 2011). That means, to exaggerate a certain feature, the band of a feature that has high reflectance is divided in to the band that show low reflectance. This technique is aimed at emphasizing or standing out the anomaly of target features (Abrahams, 1983). According to Pour and Hashim (2014) band ratios derived from Landsat 8 (4/2, 6/7, 5 and 10 in RGB) are used to discriminate altered rocks, lithological units and vegetation. In this case the altered rocks are shown as yellow and vegetation are shown as red and purple. Also, Rowan and Mars (2002) showed that band 4 over 5 and band 7 over 6 ratios of ASTER image are suitable band ratios to discriminate alunite and kaolinite respectively. For band combinations technique, R, G and B colors are used to display multispectral bands. Then, the spectral response of geologic features (minerals) indicates a maximum in their reflectance (Abhary and Hassani, 2016). These authors used RGB band combinations of 5, 7 and 3 from Landsat 8 OLI to show hydrothermal alteration zone as deep green and blue. They also used the known Abrahams (6/7, 4/3, 5/6) and Chica-Olma (6/7, 6/5, 4/2) ratios from Landsat 8 OLI to see the alteration zones. Abraham's ratio show hydrothermally altered iron oxide as green and clay minerals as red color. Also, Chica-Olma ratio give red color for altered clay minerals, green for iron ions and blue for ferrous oxides. Crosta et al. (2003) used a number of band combinations from ASTER image to discriminate phyllosilicates, which are the main features of alterations. These band combinations include (bands 1, 3, 5 and 7) for alunite, (bands 1, 3, 5 and 6) for illite, (bands 1, 4, 6 and 9) for smectite and kaolinite, and (bands 1, 4, 6 and 7) for kaolinite. Moreover, the RGB band combination of 7, 3 and 1 from ASTER image were

used by Mwaniki et al. (2015) to differentiate lithologic units, structures and morphological features.

Another important concept in the remote sensing method is the spectral reflectance curve analysis. This analysis involves characterizing the shape and wavelength position of strongest absorption and reflectance of features (Suresh et al., 2014). Two methods can be used to produce spectral reflectance curves of different features. One is direct method by which spectral information are collected in the field using an instrument called spectrometer. The other is produced from satellite images using Z-profile spectrum in Envi software. In the curve the vertical axis is represented by an amount of incident light reflected by the features. While wavelength of the energy is represented in the horizontal axis. According to Kalinowski and Oliver (2014) such method is helpful for comparing the validity of spectral curves and field observations. It is also useful to see the distinctive features of the spectrum for a mineral of interest.

Table 2.2: *Characteristics of Landsat 8 OLI (Han and Nelson, 2015).*

Band #	Band name	Wavelength (µm)	Spatial resolution (m)
1	Coastal aerosol	0.43 - 0.45	30
2	Blue	0.45 – 0.51	30
3	Green	0.53 – 0.59	30
4	Red	0.64 – 0.67	30
5	Near Infrared	0.85 - 0.88	30
6	Shortwave infrared (SIWR) 1	1.57 – 1.65	30
7	Shortwave Infrared (SIWR) 2	2.11 – 2.29	30
8	Panchromatic	0.50- 0.68	15
9	Cirrus	1.36 - 1.38	30
10	Thermal Infrared (TIRS) 1	10.60 – 11.19	100
11	Thermal Infrared (TIRS) 2	11.50 – 12.51	100

Table 2.3: *Characteristics of ASTER data (Adiri et al., 2016).*

Band #	Band name	Wavelength (µm)	Spatial resolution (m)
1	VNIR	0.52 – 0.60	15
2		0.63 – 0.69	15
3N		0.78 – 0.86	15
3B		0.78 – 0.86	15
4	SWIR	1.60 – 1.70	30
5		2.145 – 2.185	30
6		2.185 – 2.225	30
7		2.235 – 2.285	30
8		2.295 – 2.365	30
9		2.360 - 2.430	30
10	TIR	8.125 - 8.475	90
11		8.475 – 8.825	90
12		8.925 – 9.275	90
13		10.75 – 10.95	90
14		10.95 – 11.65	90

CHAPTER THREE

3. Geology of the study area

3.1. Regional Geological Settings

3.1.1. East African Rift System and Main Ethiopia Rift

The East African Rift System (EARS) is the classical example of a seismically and volcanically active continental rift, extending several thousands of kilometers and accommodating extension between the Nubian (African) and Somalian plates (Rosendahl, 1987; Braile et al., 1995; Chorowicz, 2005 cited in Mazzarini et al., 2013, Ebinger and Casey, 2001). This grand rift consist of the most important segment, the Ethiopian Rift. In turn the Ethiopian Rift can be divided into two main physiographic segments, namely southern Afar and the Main Ethiopian Rift (MER); the rift morphology is typically developed in this latter segment, where a ~80 km-wide rift valley separates the uplifted western (Ethiopian) and eastern (Somalian) plateaus (Corti, 2009). The MER connects the Afar depression (located at Red Sea–Gulf of Aden junction) with the Turkana depression and Kenya Rift to the south (Hayward and Ebinger, 1996; Corti, 2009 in Mazzarini et al., 2013). It is a magmatic rift that records all the different degrees of rift evolution from rift initiation to break-up and embryonic oceanic spreading (e.g., Ebinger, 2005, Hayward and Ebinger, 1996; Ebinger and Casey, 2001; Corti, 2009; Agostini et al., 2011a). The MER is 700 km long, 80 km wide volcanically active rift situated between the northwestern and southeastern Ethiopian Plateaus (Tesfaye Kidane et al., 2009). Corti (2009) stated that the evolution of rifting in the MER is strictly related to the long term kinematics of the major Nubia and Somalia plates. Field geological and structural data suggested a poly-phase history of rifting in Ethiopia related to a change in Nubia–Somalia motion sometime in the interval 6.6 to 3 Ma (Wolfenden et al., 2004) or at the Pliocene–Quaternary boundary (Bonini et al., 1997; Boccaletti et al., 1998, 1999a; Bonini et al., 2005). The relative Nubia–Somalia motion occurs with a rotation pole located at around 36°S, 35°E and gives rise to a roughly ESE–WNW-directed extension at the latitude of the MER. Different authors put the rate of rift extension almost similarly (e.g.,N108°Eat~ 7 mm/yr, Sella et al., 2002; N 94° E at ~7 mm/yr, Fernandes etal.,2004) and it is generally bounded by discontinuous boundary faults that give rise to major fault-escarpments separating the rift depression from the Ethiopian and Somalian plateaus. The rift floor of the MER is affected by wide spread deformation related to faulting along the Wonji Fault Belt (WFB) (Mohr,1962, 1967; Gibson and Tazieff, 1970; Mohr and Wood, 1976; Mohr, 1983,1987; Chorowicz et al.,

1994; Acocella et al., 2003; Williams et al., 2004; Pizzi et al., 2006; Kurz et al., 2007 cited in Corti, 2009). This faults (WFB) are closely associated with the most recent (Quaternary) volcanic activities in the MER.

3.1.2. MER Segments

According to many authors (e.g. Corti, 2009; Mohr, 1983; Gidey Woldegabriel et al., 1990; Hayward and Ebinger, 1996), the MER can be subdivided into three segments (Northern, Central and Southern). These segments have been interpreted to reflect different stages of the continental extension process, being characterized by different fault architecture, timing of volcanism and deformation, crustal and lithospheric structure (e.g., Hayward and Ebinger, 1996 in Corti, 2009). These different attributes of the three MER segments will be discussed in the following sections separately but giving more emphasis to the central part of MER, which is a sector consisting of the study area.

The **Northern MER** extends from the MER–Afar boundary southwards to the Lake Koka area, where it is separated from the Central MER by the Boru Toru Structural High (Bonini et al., 2005). Different authors (Kazmin et al.,1980; Mohr, 1983; Hayward and Ebinger, 1996; Tadiwos Chernet et al.,1998;Wolfenden et al.,2004) suggested that the main boundary faults in this region show an average $N50^0$ trend and formed since about 10–11 Ma. The same chronology (10–11 Ma) is also attributed to an early syn-rift volcanism in the region by Tadiwos Chernet et al. (1998) and Wolfenden et al. (2004). The southeastern basin margin is marked by the major boundary fault systems of Arboye and Sire, which form a staircase pattern rising to the ~2600-m elevation of the uplifted rift flanks (Wolfenden et al., 2004). In other case, the southwestern margin of this MER sector is characterized by a right-stepping en-echelon pattern (Corti, 2009). Scarce fault-slip data on the rift margins and local structural features indicate a roughly E–W direction of extension (Boccaletti et al., 1992). The evolution of volcanic activity in the Northern MER was explained by Tadiwos Chernet et al. (1998) as early eruption of the flood basalts followed by Mid Miocene eruptions from shield volcanoes along the developing rift shoulders. The subsequent, Quaternary bimodal volcanic activity (lava, pyroclastics and volcanoclastic strata; Wonji Group; is spatially associated with the oblique faults of the Wonji Fault Belt affecting the rift floor (Meyer et al.,1975; Kazmin et al., 1980; Gidey WoldeGabriel et al., 1990).

The **Central MER** is bounded by the Yerer-Tullu-Wellel volcano tectonic lineament to the north and the Goba–Bonga lineament to the south (see Fig. 3.2). It is also bounded to the

east and west by fault escarpments such as the Munesa and Guraghe rift margins (Tsegaye Abebe et al., 2010). According to Corti (2009), in this sector of MER, the rift valley orients between N25° and N45° and is characterized by major rift escarpments on both western and eastern margins; boundary faults show an average trend around N30°E.The western margin is well expressed by the N25°E–N35°E-trending and ESE-dipping Guraghe and Fonko faults (a fault which lies in the study area), whereas the eastern margin is well represented by the N30°E-trending and WNW-dipping Asela–Langano fault system (Fig. 3.1). Both systems are characterized by high-angle (N60°) normal faults, with large cumulative vertical throw. Moreover, the western rift margin is characterized by the presence of roughly N–S trending structural highs like the Boru Toru and Midre Kebd structural highs (Tsegaye Abebe et al., 2005).

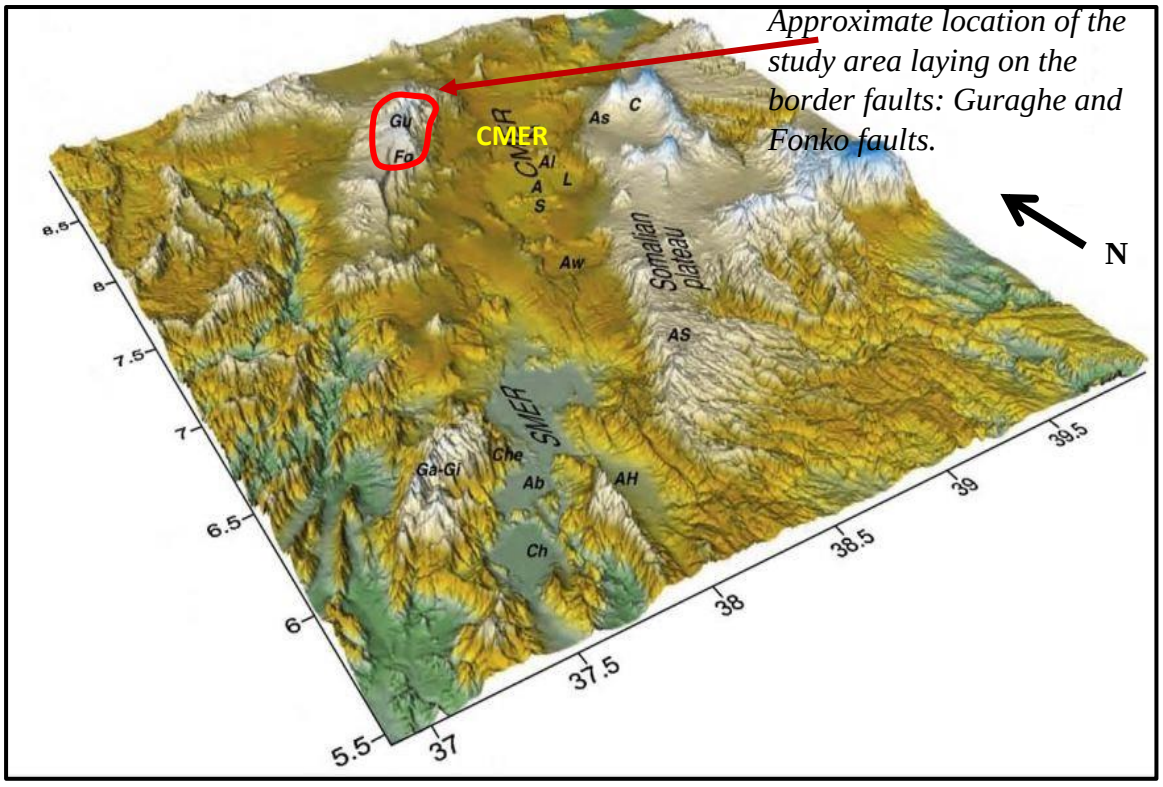

Figure 3.1: *Three-dimensional representation of the rift topography comprising CMER and showing the relative location of the study area (red polygon) and the border faults (Gu: Guraghe and Fo: Fonko) laying in the study area. (After Corti, 2009).*

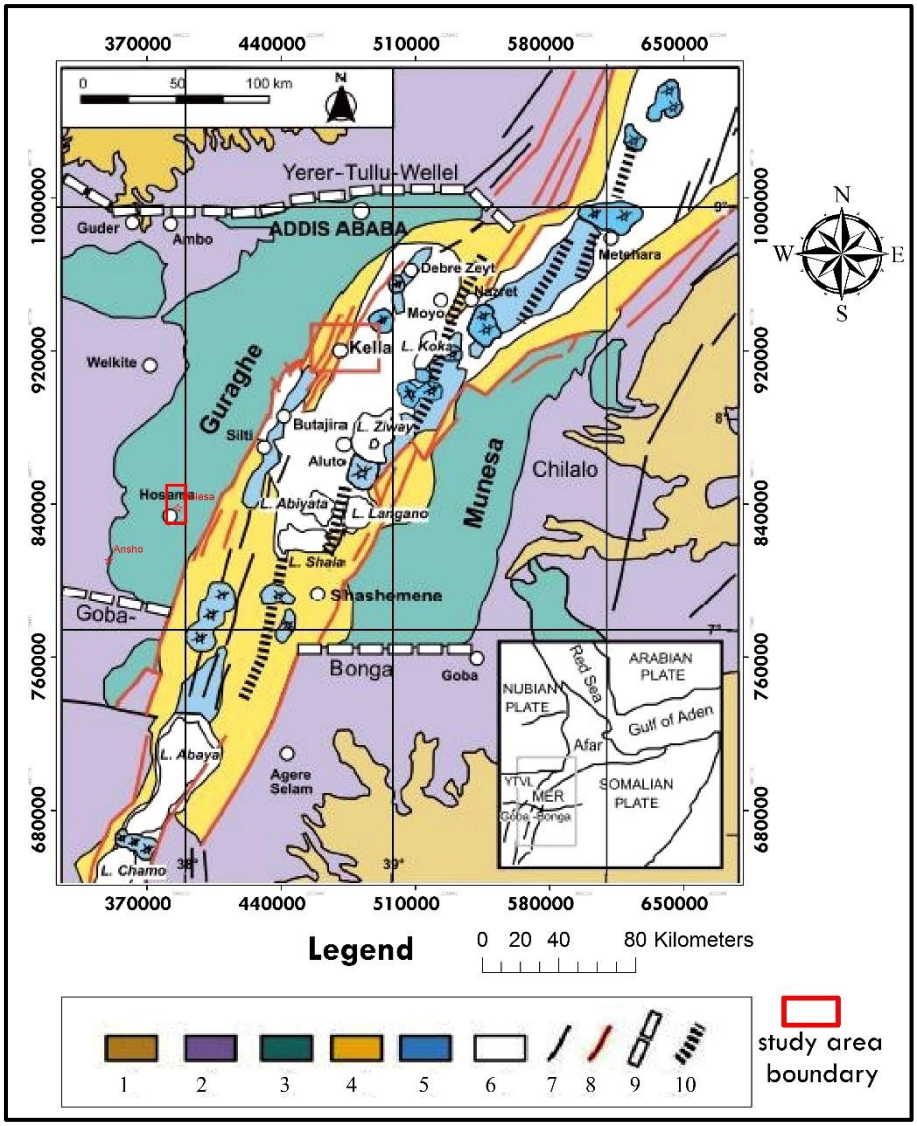

Figure. 3.2: *Simplified geological map of Central Main Ethiopia Rift. Modified after Tsegaye Abebe et al (2010). (1) Pre-Tertiary sediments and crystalline basement, (2) Oligocene(32–29 Ma) and lower Miocene (12–8 Ma) plateau volcanics, (3)Miocene–Pliocene rift-shoulder trachytic–rhyolitic volcanics and pyroclastic layers,(4) Plio-Pleistocene rift floor, (5) Quaternary central volcanics and basaltic lava flows, associated scoria cones and phreato-magmatic deposits, (6) Quaternary lacustrine sediments and interbedded pyroclastics, (7) faults, (8) major rift border faults, (9) major transversal tectonic lineaments in the basement, (10) Wonji Fault Belt segments. Red rectangle: Study area.*

Many authors (e.g. Boccaletti et al., 1992, 1998; Bekele Abebe, 1993; Tesfaye Korme et al., 1997; Acocella and Tesfaye Korme, 2002; Bonini et al., 2005; Pizzi et al., 2006) analyzed fault-slip data on both rift margins in the Central MER and indicated a stress field characterized by an extension direction oriented roughly ESE–WNW, with local variations

between E–W and NW–SE. Bonini et al. (2005) explained these rift margins to be formed in the late Miocene–Pliocene (post ~ 6 Ma). The rift floor in this sector of the rift is affected by dense NNE–SSW-trending faults swarms, with relatively small throws (<100 m), which comprise the Wonji Fault Belt oriented ~N12°E and oblique of ~18° to the roughly N30°-trending boundary faults (Corti, 2009).

Based on geological and geochronological investigations, different authors (e.g. Tsegaye Abebe et al., 2005; Bonini et al., 2005) distinguished four major volcanic episodes in the Central MER. The first volcanic episode (32–29 Ma) covered the main parts of the Ethiopian plateau volcanics consists of the Trap Series (Hofmann, 1997; Pik et al., 1998; Ukstins et al., 2002). The second episode (11–8 Ma) represent a long period of less voluminous and more local volcanic activity related to the development of shield volcanoes, basaltic–trachytic lava flows and associated pyroclastics. Several layers of pyroclastic rocks associated with trachytic and rhyolitic lava domes and flows together with some important central volcanoes were formed in the third (5–3 Ma) episode, and cover the MER shoulders and floor. Finally, in <3 Ma the last volcanic episode consists of uncompact pumiceous fall and flow deposits, rhyolitic–trachytic lava flows forming central volcanic edifices, fissural basaltic lava flows with associated scoria and phreatomagmatic cones,and interbedded lacustrine deposits. (e.g. Di Paola, 1976; Seife Mickael Berhe,1978; Kazmin et al.,1980; Bigazzi et al.,1993). These deposits are generally confined to the MER floor.

A major E–W-trending transverse lineament (Goba–Bonga lineament) marks the boundary between Southern and Central sector of the MER. This transverse lineament results in rotation of the rift valley south of latitude 7°20′. The **Southern MER** (SMER) is characterized by a rotation of the rift valley from N 20-35° to N 5-20°; accordingly, the orientation of the boundary faults is N 0° E to ~ N 20° E in this MER sector (Abbate and Sagri, 1980). The major fault escarpments of Chencha (western margin) and Agere Selam (eastern margin) characterize this sector of the rift (Corti, 2009). According to Levitte et al. (1974) and Ebinger et al. (1993), the end of Southern MER corresponds to a division of the rift valley into two near-parallel grabens, namely the Chamo (or Ganjuli) basin to the west and the Galana basin to the east which are separated by the Amaro Horst. In this rift sector, the Wonji faults are comparatively less developed than in the Central and Northern MER. These faults are oriented around N–S, i.e. roughly parallel to the boundary fault systems. Concerning to the volcanic activity, two main phases of volcanic episodes are attributed to this rift segment. According to different authors, (Ebinger et al., 1993; Gidey Wolde

Gabriel et al., 1990; Ebinger et al., 2000) the Tertiary volcanic activity in the Southern MER started earlier than in the other MER sectors, since the pre-rift flood-basalt event is dated at about 45 Ma. This initial mainly basaltic activity ended around 30 Ma (Zanettin et al., 1978). A second phase of mainly basaltic volcanism started in the Early Miocene with the eruption of stratoid basalts (Levitte et al., 1974 and Zanettin et al., 1978). Authors like Zanettin et al. (1978) and Ebinger et al. (1993) explained that the volcanic activity continued in the SMER during the Miocene up to 11 Ma, with eruption of basalts, trachytes and rhyolites.

3.2. Local geology

3.2.1. Introduction

The thick eluvium sediment, extensive cultivation and dense population makes access to the lithologic units very difficult. However the quarry sites, river cut and road cut exposures were the means to encounter the main rock units. After field traversing, mapping of the rock units is also aided by ASTER and Landsat 8 OLI data (see Fig. 3.3 and section 4.5). The geology of Belessa area is characterized by volcanic rocks of acidic compositions ranging in age from Miocene to Quaternary (Gidey WoldeGabriel et al., 1990). The chronostratigraphic data of the Central Main Ethiopian Rift presented by these authors also indicate that the geology of Belessa area is included in rhyolite, Butajira ignimbrite and Wonji group (pyroclastic rocks and volcaniclastic material).

The rock units in the study area are described based on their actual field association and data obtained from previous works. From oldest to youngest age the main lithologic units identified in the area include;

- Ignimbrite
- Rhyolite
- Pyroclastic tuff and
- Quaternary sediments.

Except the Pumiceous material (not mapped in the current scale of the geological map; 1:25,000), all the above four rock units are included in the geological map (see Fig. 3.8 A). The corresponding geologic cross section is also illustrated to show the sectional view of the kaolin occurrence in its longest dimension (see Fig. 3.8 B). A succinct description for each lithologic units is given below;

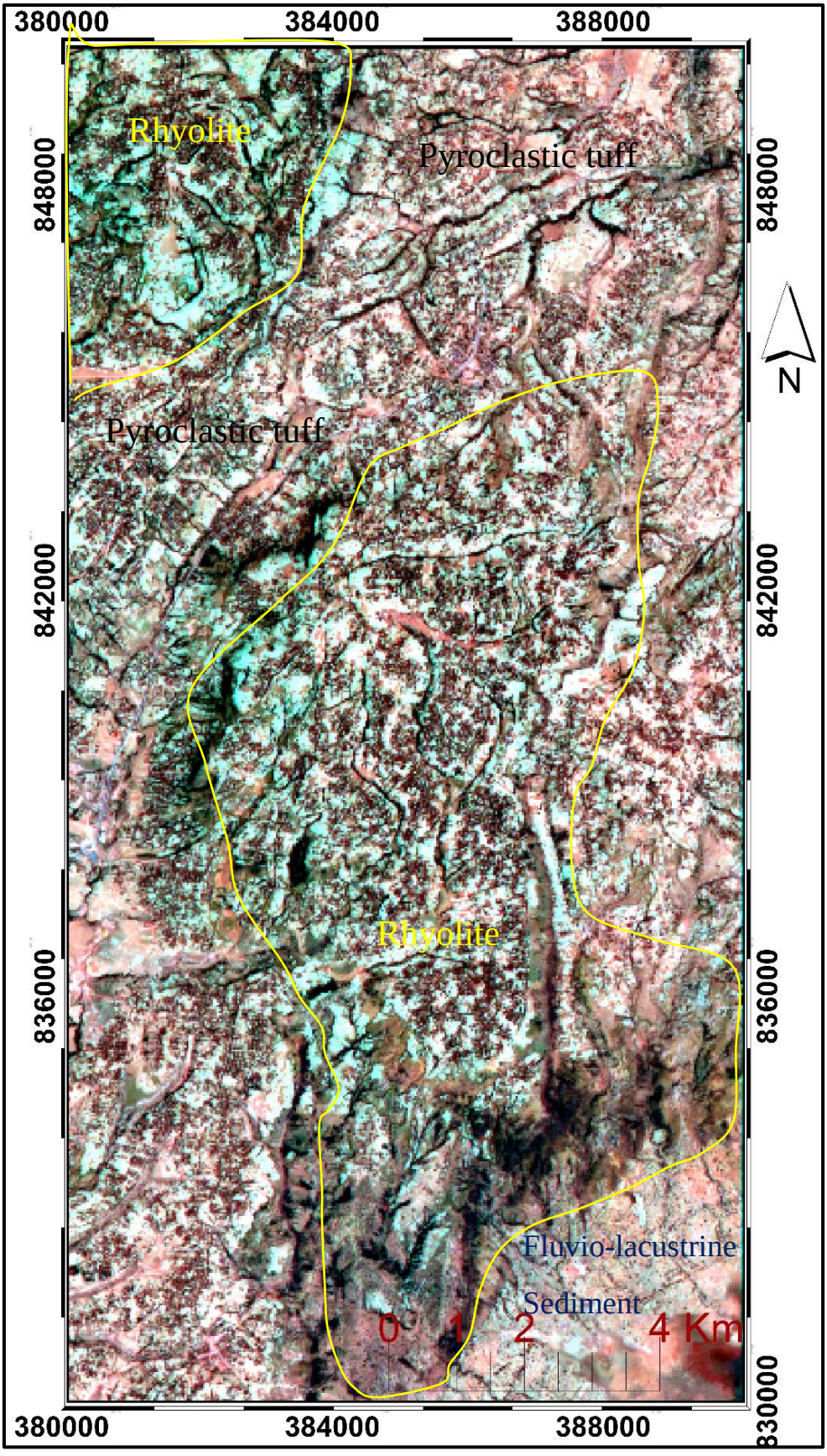

Figure 3.3: *ASTER RGB images of bands 7: R, 2: G, 1: B showing the different lithological units.*

3.2.2. Lithologic and Petrographic Descriptions

3.2.2.1. Ignimbrite

Exposure of this unit is found at three places; Western, North Eastern and Southern parts of the map area (Fig.3.8). In all places it is found associated with quarry site (see Fig. 3.4) and it is exposed by intermittent rivers. It forms rugged and mountainous terrane dissected by rivers. Mostly, this unit is overlain by pyroclastic tuff and a very thick (~50m) eluvium sediments. It has an exposed thickness of 30 meters. In outcrop this unit is massive and hard enough to break it with huge hammer. Also, it is compact and light-gray color. Generally, the ignimbrite is fresh and mainly composed of quartz and rock fragments.

Microscopic study of this rock shows hypo-crystalline textures with quartz (10 %), alkali-feldspar (5 %) and opaque mineral (2 %). Some alkali-feldspar crystals are altered completely and some are partly altered at their twin plane (see Fig.3.5). The opaque mineral also shows equant habit and this is probably magnetite. The remaining modal composition of this rock is constituted by matrix (83 %) composed of alkali-feldspar, quartz and glass shards.

Figure.3.4: *Ignimbrite quarry site exposure in the northern part of the area [a man is 1.70 m].*

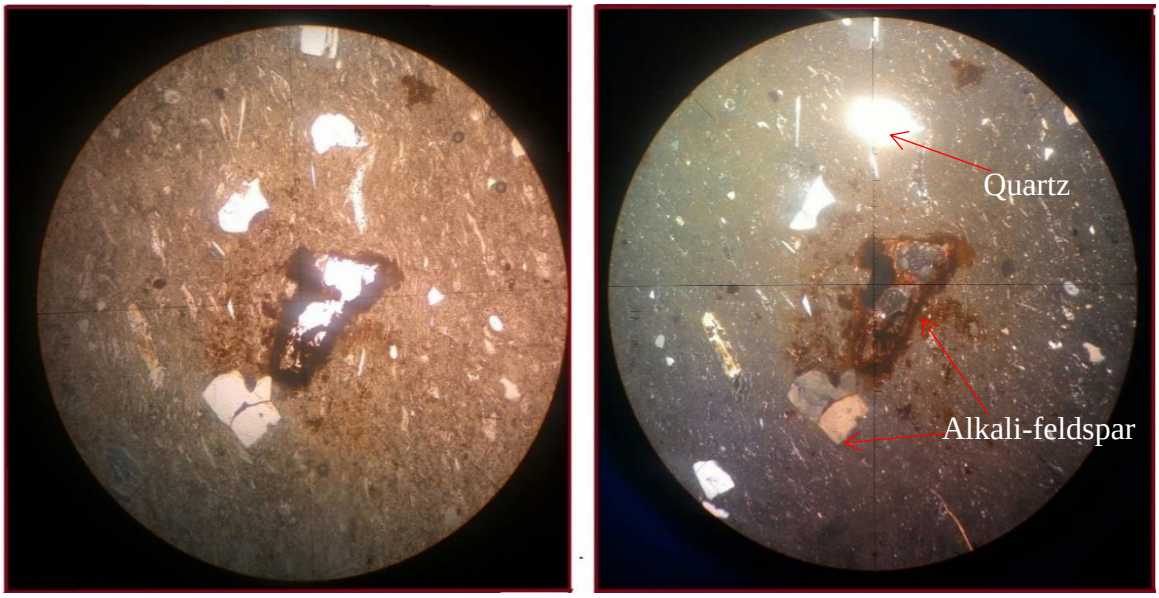

Figure 3.5: *Micro-photo picture of ignimbrite; sample number BHR-0004 in PPL (left) and XPL (right) in 10X magnification.*

3.2.2.2. Rhyolite

This group is the predominant rock type in the area and it covers about 94 km^2. The outcrops of this unit are well exposed in the North Western, Central and South Eastern part (see Fig.3.8). It also extends to some part of the North Eastern part. This unit is exposed mainly by streams and roads forming hills, ridges and mountainous topography. It has a maximum exposed thickness of 150 meters where it forms the fault plane of NE-SW trending huge faults of the area. In places it shows hard, stiff and massive exposure, but it also shows layering (5-15 cm). Exposures of boulder and blocky rhyolite fragments are found in the North Western part of the study area. In the Central part, the weathered part of this unit becomes partly to completely kaolinized, which is an important spot for the occurrences of Belesa kaolin (see Fig. 3.6 E). In most cases this unit overlies the pyroclastic ash flows and ash falls and at places overlain by thick eluvium deposits.

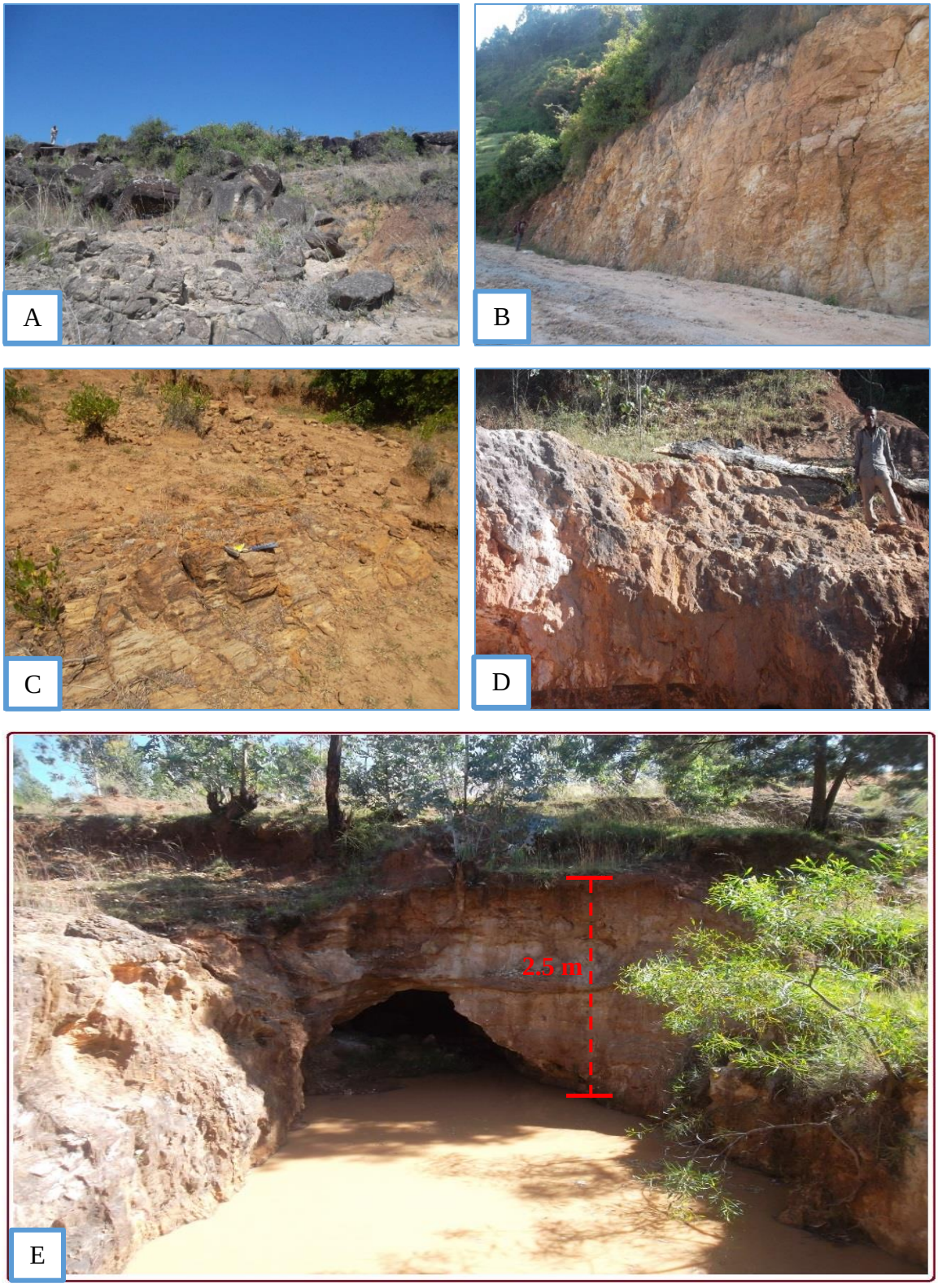

Figure 3.6: *Exposure of rhyolite. (A), (B) and (C) are exposures of unaltered rhyolites, (D) kaolinized rhyolite and (E) Kaolin exposure in central part of Study area.[a man in A & D is 1.7 m, in B 1.78 m and geologic hammer in C is 33 cm].*

The Rhyolite unit is dark gray to reddish brown in fresh samples to light gray and yellowish to white in weathered ones. In most cases this unit is medium to coarse-grained, but fine grained in the vicinities where it is altered into kaolinite. It is also slightly to highly weathered. The deeply weathered exposures show un-welded and loose appearance. Moreover vesicular rhyolite is found in some places. Megascopically, the main phenocryst minerals are quartz and plagioclase. Furthermore, the rock is comprised of glassy rock fragments and fine quartz minerals.

Petrographic study revealed that the rock shows hypo-crystalline and porphyritic texture. It is mainly composed of quartz (12-33 %), alkali-feldspar (6-13 %), and opaque minerals (1-2 %). The remaining (19-52 %) counts for the ground mass which is composed of quartz, alkali-feldspar and plagioclase (see Fig. 3.7). Quartz show subhedral to euhedral grain shape and it is tabular. Also, some quartz grains are zoned, fractured and contains inclusions of opaque minerals. The euhedral to subhedral grain shape alkali feldspar shows Carlsbad twining and prismatic habit. Most importantly, the rims of alkali feldspar are altered to brownish color. The mineral grains in the matrix also show dendritic and a cluster of radial textures. Less amount of pyroxene is found and some part of it is altered to greenish mineral probably epidote or chlorite (see Fig. 3.7 E and F).

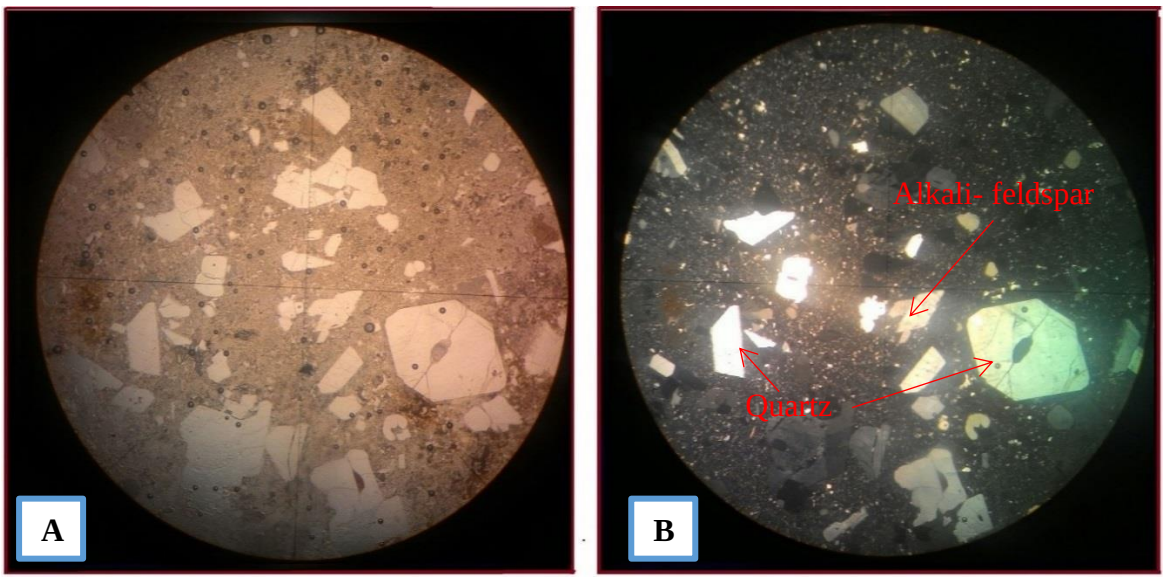

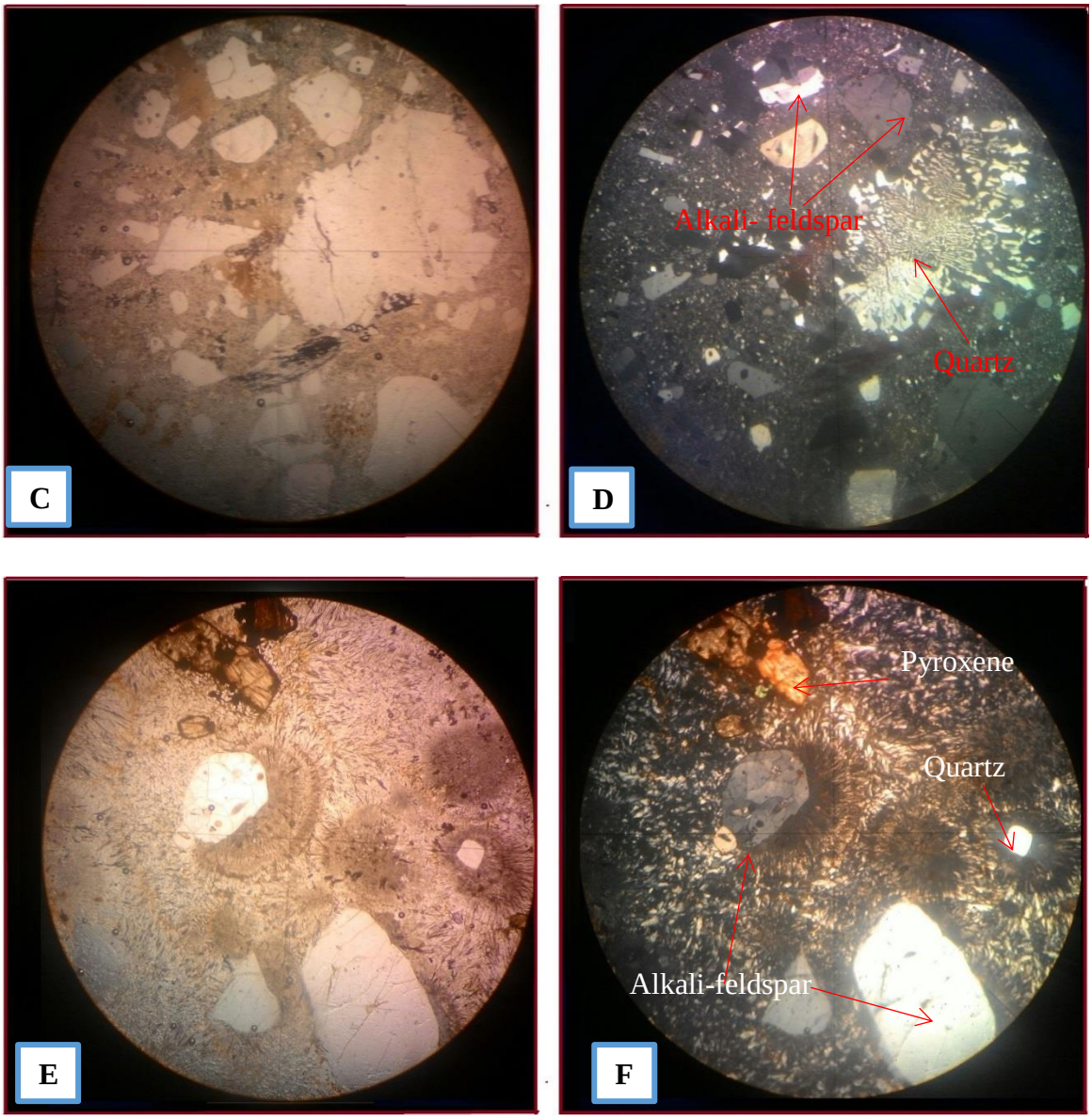

Figure 3.7. *Micro-photo picture of rhyolite; sample number BHR-0015A (A, B, C and D) and BHR-0027 (E and F) in PPL (left) and XPL (right) in 10X magnification.*

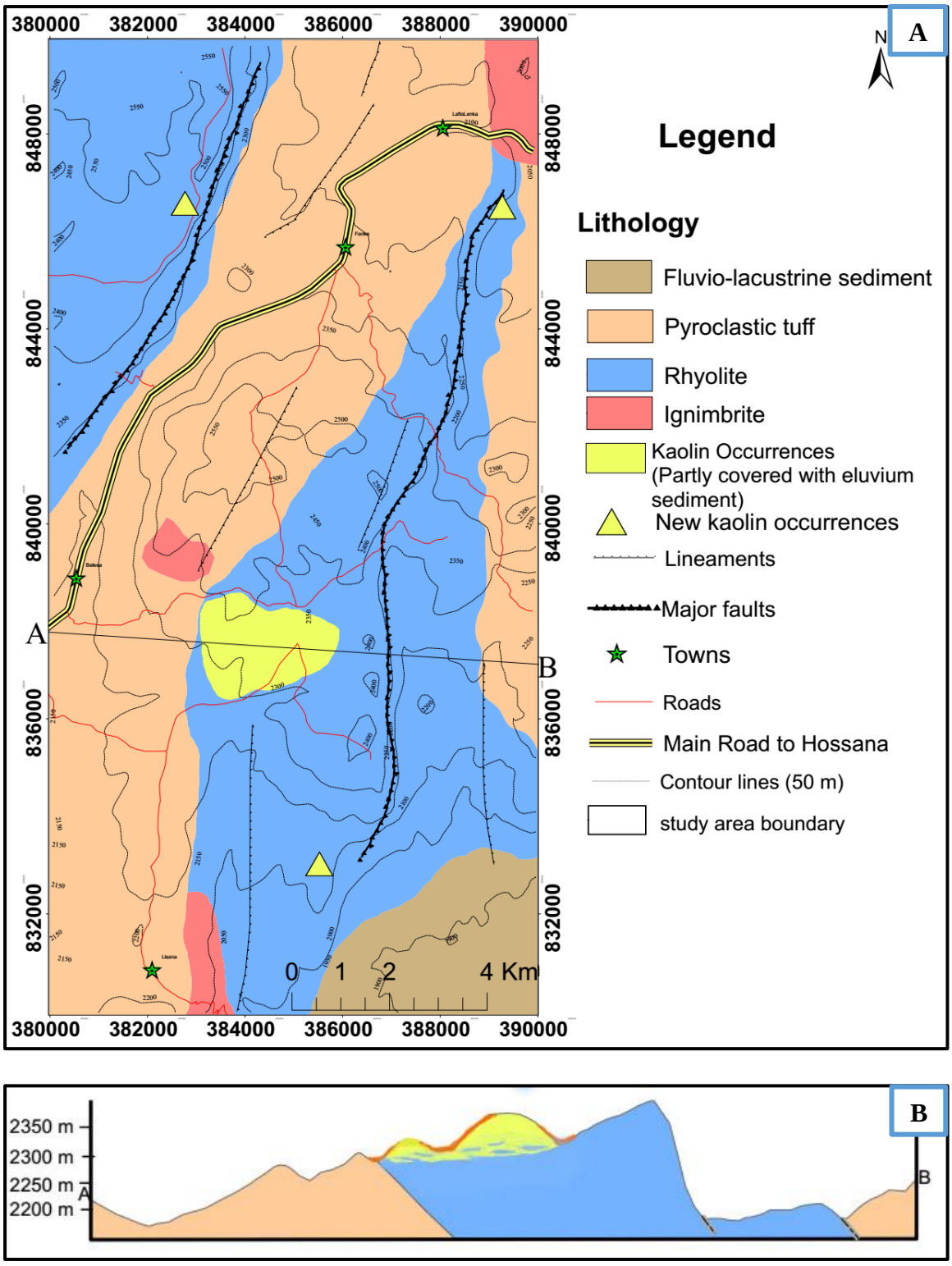

Figure 3.8: *Geological map of the study area (A) and geologic cross section along A-B traverse (B).*

3.2.2.3. Pyroclastic ash tuffs

Next to rhyolite this unit covers a large part of the study area (about 89 km^2). It is extensively exposed in the Northern, Western, Southern and Central part of the map area (see Fig.3.8). At most places it occupies flat lying areas. But, it also forms rugged and hill topography where it is overlain by a thick eluvium sediment (~30 meters). This unit attains an exposed thickness of 15 meters and to some extent altered to kaolin in the Northern part of the map area where it is exposed by rivers (see Fig. 3.9 C). But, horizontally it covers a wider area and from elevation difference it is observed that it could attain a thickness of 98 meters.

Figure. 3.9: *Pyroclastic Ash tuff exposures (A) and (B) ash fall deposits in the NW and Northern (B and C) part [a man is 1.71 m].*

In some places this exposure is massive, of different grain size and laminated toward the bottom part of it. In the Western part in locality called Debub Fonko 4 meters thick ash fall deposit is found underlying 5 meters eluvium deposit and it forms locally constant and

continuous ash layers. Below the ash fall deposit a continuous and massive ash flow layer is also found (Fig. 3.9 A).

Mostly the pyroclastic ash is loose, friable, well-sorted and fine to medium grained. Generally, it is highly weathered and it shows light to dark-gray color. In hand specimen it consists of mainly quartz and dark and fine rock fragments probably basalt. Fine quartz crystals are also identified in the field using hand lens.

3.2.2.4. Pumiceous unit

This unit is found in fewer places in the Northern and North Eastern part of the map area. It is not mapped because of its small size under current scale of the map (1:25,000). Therefore it is mapped together with rhyolite and pyroclastic ash. The exposure in the Northern part is exposed forming hill topography and has a maximum thickness of 15 meters. It is overlain by a 1 meter thick eluvium sediment.

The pumiceous unit is a poorly sorted exposure and it shows a coursing upward textures (see Fig. 3.10). It is highly weathered, loose and friable. Generally, it shows light-gray to brown color and it is composed of pebble to boulder size rock fragments mainly basalt.

Figure 3.10: *Pumiceous unit. (A) Sand size pumiceous unit (B) Upward coarsening Pumiceous unit (geological hammer is 33 cm).*

3.2.2.5. Fluvio-lacustrine and eluvium sediments

Mappable alluvial and lacustrine sediments are exposed in the South-East part of the map area (see Fig.3.8). Most part of the exposures are found forming plain topography. The

fluvial sediment is related to the rivers and streams of the area. It is unconsolidated loose material and it ranges in thickness from 10 to 15 meters. Marshy areas and lacustrine sediments are associated with the lake called Boyo, which is found south of the study area. In both cases, they mainly consist of clay, silt and sand size sediments. The eluvium sediment is the overburden residual soil over most of the lithologies and kaolin occurrences. In some places it is as thick as 20 meters. In all cases the color varies from reddish to brown (Fig. 3.11).

Figure 3.11: Lacustrine and alluvial sediments [a man is 1.73 m].

3.2.3. Geologic structures.

The major faults of the study area include part of the Guraghe border faults and Fonko faults. These faults form parts of the boundary faults in the western margin of the Central MER. They are found associated with the rhyolite unit. Both faults are characterized by having a trend of N 32^0 E and high angle (65^0 to 70^0) normal faults. They are also long with a vertical throw of about ~80 to 150meters (Fig. 3.12).

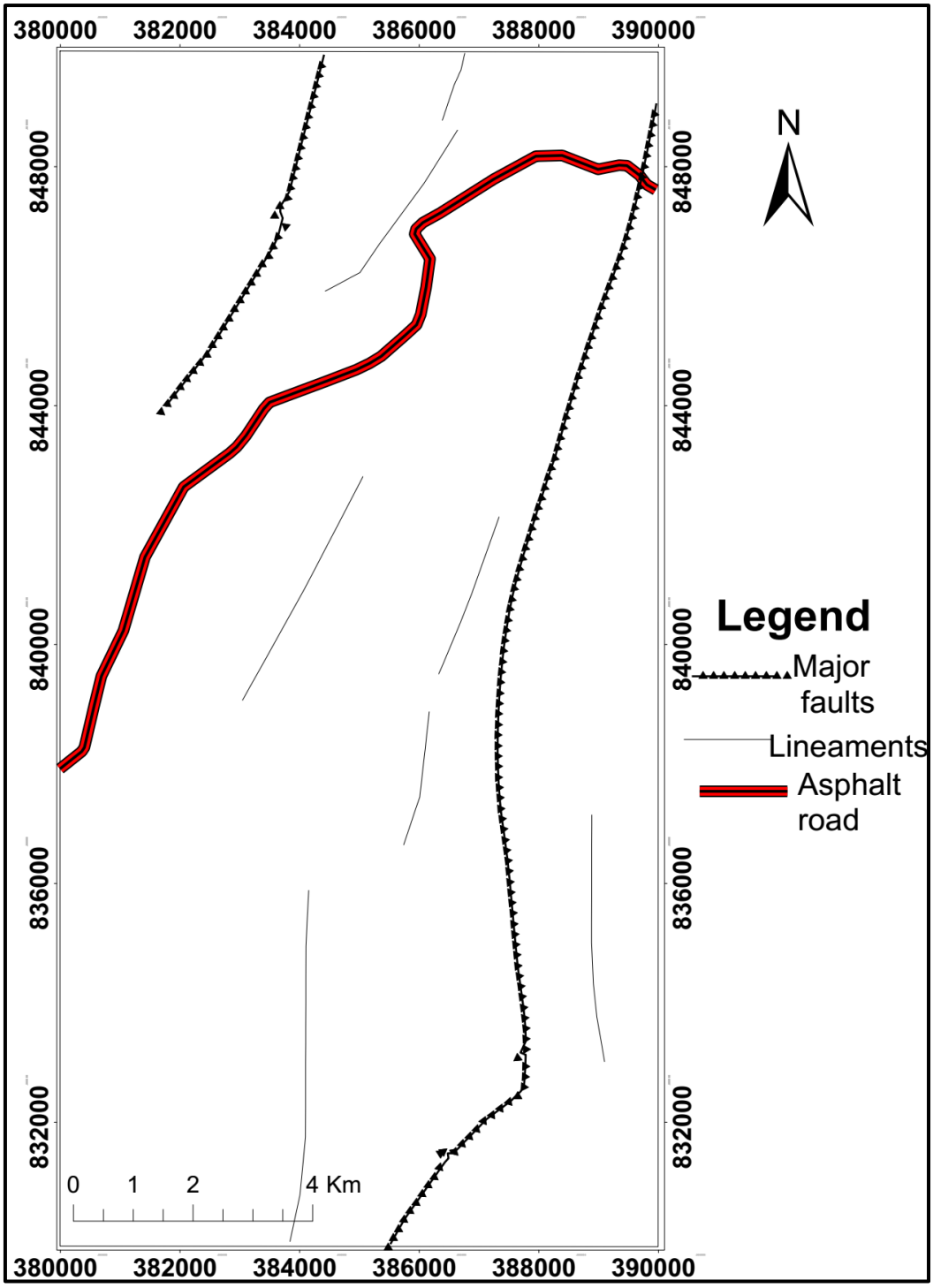

Figure 3.12: *Fault patterns of the study area.*

CHAPTER FOUR

4. Belessa kaolin deposit

4.1. Introduction

In this section, the investigation results of Belessa kaolin from field observations (geological settings) and different analyses techniques like geochemistry, mineralogy, morphology and remote sensing are presented. These analyses are employed in order to examine the evidence for genesis of kaolin in terms of primary (hypogene or supergene), to understand the alteration phenomena and to elucidate the possible industrial applications.

4.2. Geological settings

Belessa kaolin occurrence is located in the central portion of the study area east of Belessa town and it is known as Belessa Kaolin (Haile Mickael Fentaw, 2003). The specific location of this deposit is 384352 E and 837967 N. Presently, it is being exploited by local people and sometimes sold for industries. The deposit is found in the mountainous topography and clearly exposed in the mine site. The mine area is comprised of a low land terrain which is slightly undulating and in parts ascribed to a plateau landforms.

The geology of the study area dominantly consists of pyroclastic tuff and Miocene rhyolite (section 3.2). The kaolin is altered from and is associated with this rhyolite. The host rock (rhyolite) is characterized by moderate to high degrees of alteration. The kaolin is found overlain by overburden that ranges in thickness from 5 to 10 meters. The overburden consists of silt to sand size and reddish brown eluvium sediments. The kaolinization zone is restricted to a limited vicinity and a fresh unaltered rhyolite is encountered after a short traverse from the kaolinized area. That means, the degree of alteration gradually increases towards the exposed deposit as approaching it from all direction. In the freshest rhyolite exposure there is either no or very thin overburden. Three exposed outcrops of kaolin occurrences show variable thicknesses having a maximum of about 8 meters. But, from elevation profile during field traverse the kaolin deposit thickness is inferred to be 70 meters.

Based on area coverage and composition, Belessa kaolin can be classified into two. The first one is exposed in a much localized manner. It has relatively the thickest outcrop reaching up to 8 meters. This exposure is constituted by soft kaolin and it consists of purely kaolinitic layers with some quartz nodules and rock fragments. It is fine grained and appear as white color and slightly compact (see Fig.4.1 C and Fig. 4.2). The second one is found

in closer distance to the vicinity of pure kaolinite and it is exposed in two different places. These exposures consist of quartz bearing kaolinitic layers. These are relatively harder and consolidated. They have an average thickness of 5 meters and show whitish brown and pink colors (see Fig. 4.1 A). Fine quartz minerals are also identified in the field by using hand lens.

In addition to Belessa kaolin, new kaolin occurrences were encountered during traversing. These occurrences are located in the North Western area 'Oda Ido' locality (see Fig. 4.3) and in Southern part in 'Lisana' area. They are exposed by streams up to 1 meter exposed thickness. Both are hosted by rhyolite and they are found underlying 5 to 10 meters thickness eluvium deposits. They show whitish gray color and contains fine quartz crystals. The mineralogical composition from XRD analysis result showed that the occurrence in the southern part consists of halloysite, quartz and sanidine minerals.

Figure 4.1: *Views of Belessa kaolin [a man in (A) is 1.7 m, a man in the left side of (c) and (D) is 1.8 m].*

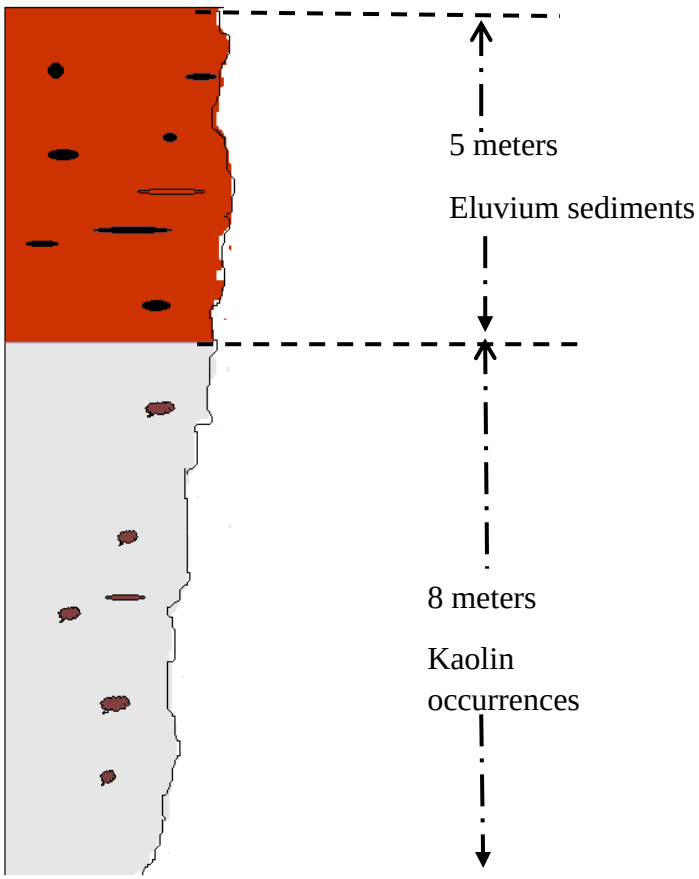

Figure 4.2: *Section showing the exposed part of Belessa kaolin exposure (not to scale).*

Figure 4.3: *A new kaolin occurrences in the North Western area 'Oda Ido' locality (E: 382729 N: 846695). A man is 1.71 m.*

4.2.1. Resource estimations

The resource estimation method adopted here is the conventional approach by using the geological map of study area, field observation and estimated kaolin deposit thickness. Therefore, the parameters involved in the resource calculation are; area (A) from the geological map (see Fig. 3.8), thickness (h) from elevation profile during traversing and bulk density (ρ) from laboratory test.

Thus, Resource (kaolin deposit) = (A) x (h) x (ρ)

$$= (441\ m^2) \times (70\ m) \times (1.4\ g/cm^3)$$

$$= 43{,}218\ tons$$

The above resource estimation considers both pure kaolinite and quartz bearing kaolin. Moreover, it should be noted that this tonnage represents only those kaolin resources found in Belessa area. Based on the level of geological knowledge and confidence, this resource is classified under indicated mineral resource. This is because the study lacks drill hole and it is only based on data from field observations and mineralogy test. But other modifying factors listed by Kogel (2014) (see Fig. 4.4) make the pure kaolinite more feasible. The new kaolin occurrences found in other parts of the study area are only indicated in the map and to estimate the resource, further work has to be done.

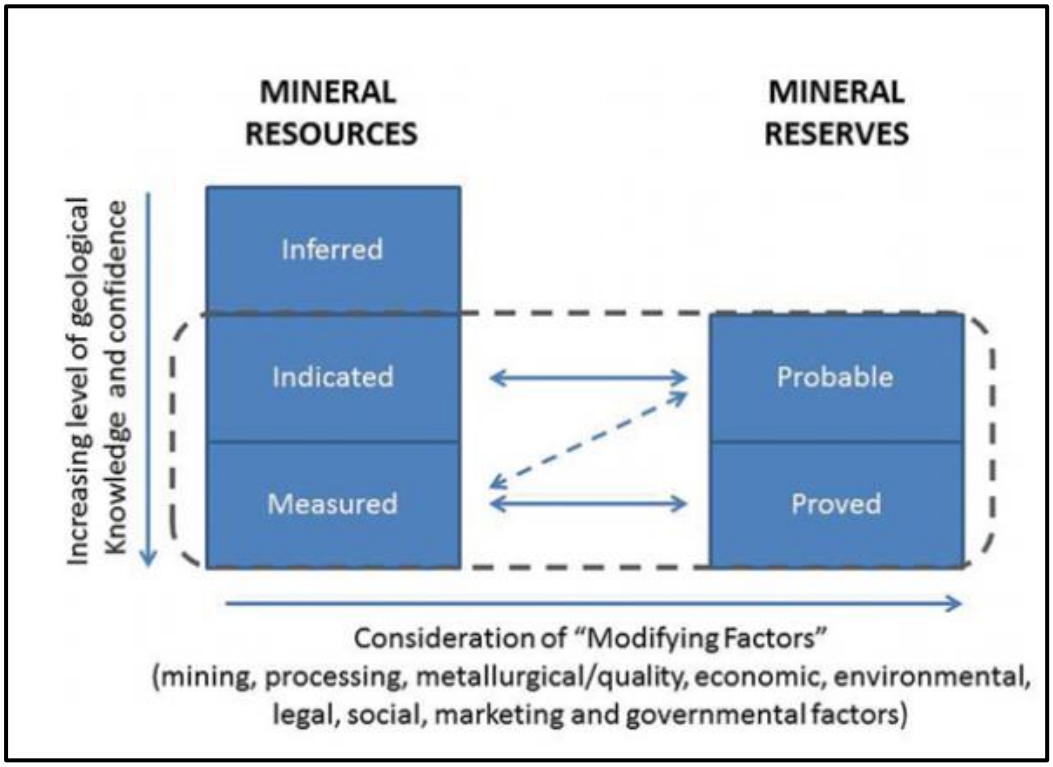

Figure 4.4: *Classification scheme for mineral reserves and resources* (Kogel, 2014).

4.2.2. Crystal morphologies

Scanning electron micrograph technique was employed to study the crystal morphology of Belessa kaolin deposits. All the samples show predominantly kaolinite crystals. Three types of morphologies are recognized. The first type shows platy crystals exhibiting hexagonal outlines and formed many stacks (see Fig 4.6 A and B). These are highly or well crystallized kaolinite particles characterized by smooth surface structures with defined edges and basal planes. Few elongated crystals with well-defined outlines are also found (Fig 4.6 C). The third type forms many hemispherical structures with pimply surfaces (see Fig 4.6 D). The latter two types of morphologies are consisted of medium crystallized kaolinite particles. Among the three types, most of the SEM images in this study show perfect hexagonal plate like shape as the predominant crystal morphology. These crystals consist of stacks and books of kaolinites occur as overlapping separable layers. Especially, the pure kaolinite sample BHR-0054 shows numerous six sided flakes of well crystallized kaolinite crystals (Fig. 4.6 A). The flake surfaces of hexagonal kaolinite crystals show a maximum dimensions from 0.4 to 1.5 μm. For the spherical crystals, the maximum dimension is up to 0.4 μm. The abundance of the three type morphologies (hemispherical, elongated and platy) has been influenced by alteration intensity and time of formation (Fiore, 1995). At the initial stages, the hemispherical type kaolinites were formed. But as time goes, the alteration intensity increases and the amount of elongated and platy form kaolinite increased (see Fig.4.5). The arrangement of crystals also became more orderly. The kaolin sample (BHR-0051) from southern part of the study area which is composed of halloysite, sanidine and quartz shows different morphology (Fig. 4.6 E). The morphology of this sample is elongated tube which is typical for halloysite mineral.

The morphologies can be also related to the crystallinity of kaolinite (Parham, 1976). That means, hexagonal kaolinites with smooth surfaces, defined edges and regular shape corresponds to a well crystallized kaolinite particles. Also, it is observed that there is a correlation between crystallinity and particle diameter. Hence, highly crystalline kaolinite samples show larger particle diameters. Therefore, in this study most of the kaolinite samples are highly crystalline.

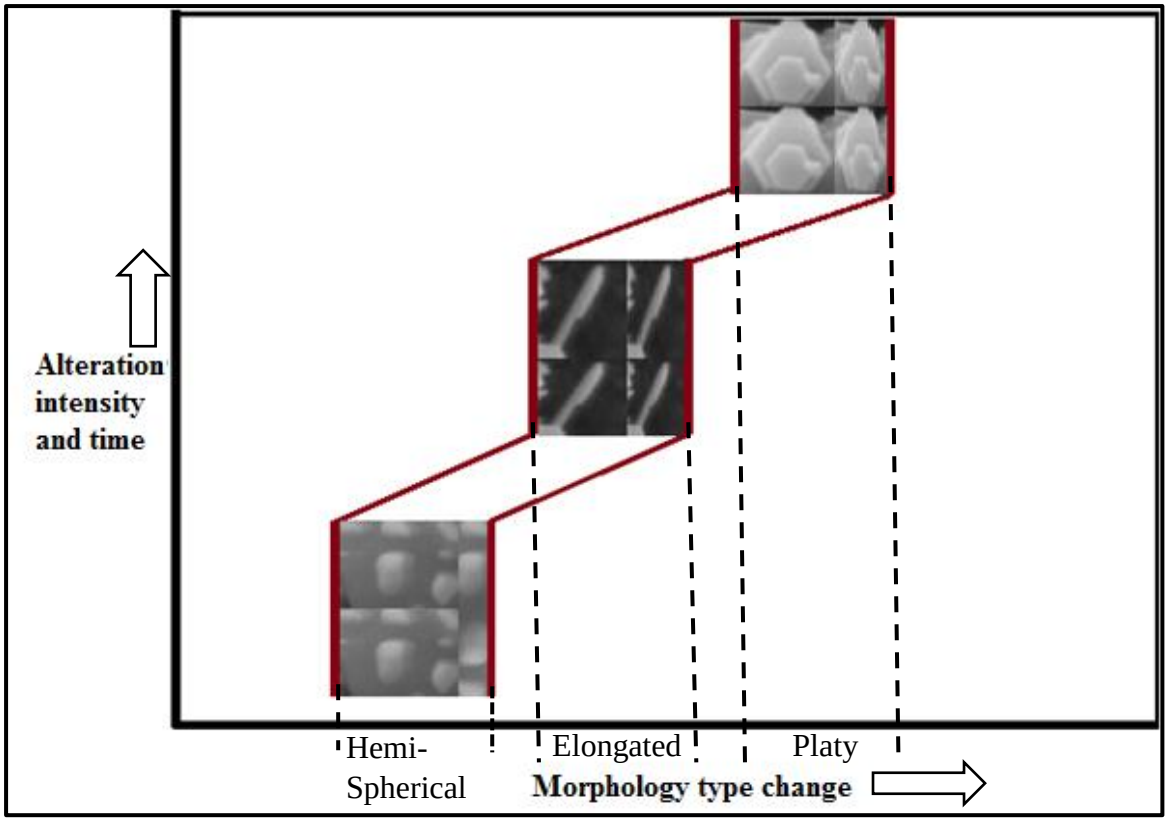

Figure 4.5: *Schematic drawing that shows the morphology change of kaolinite with alteration intensity and time (after Fiore, 1995).*

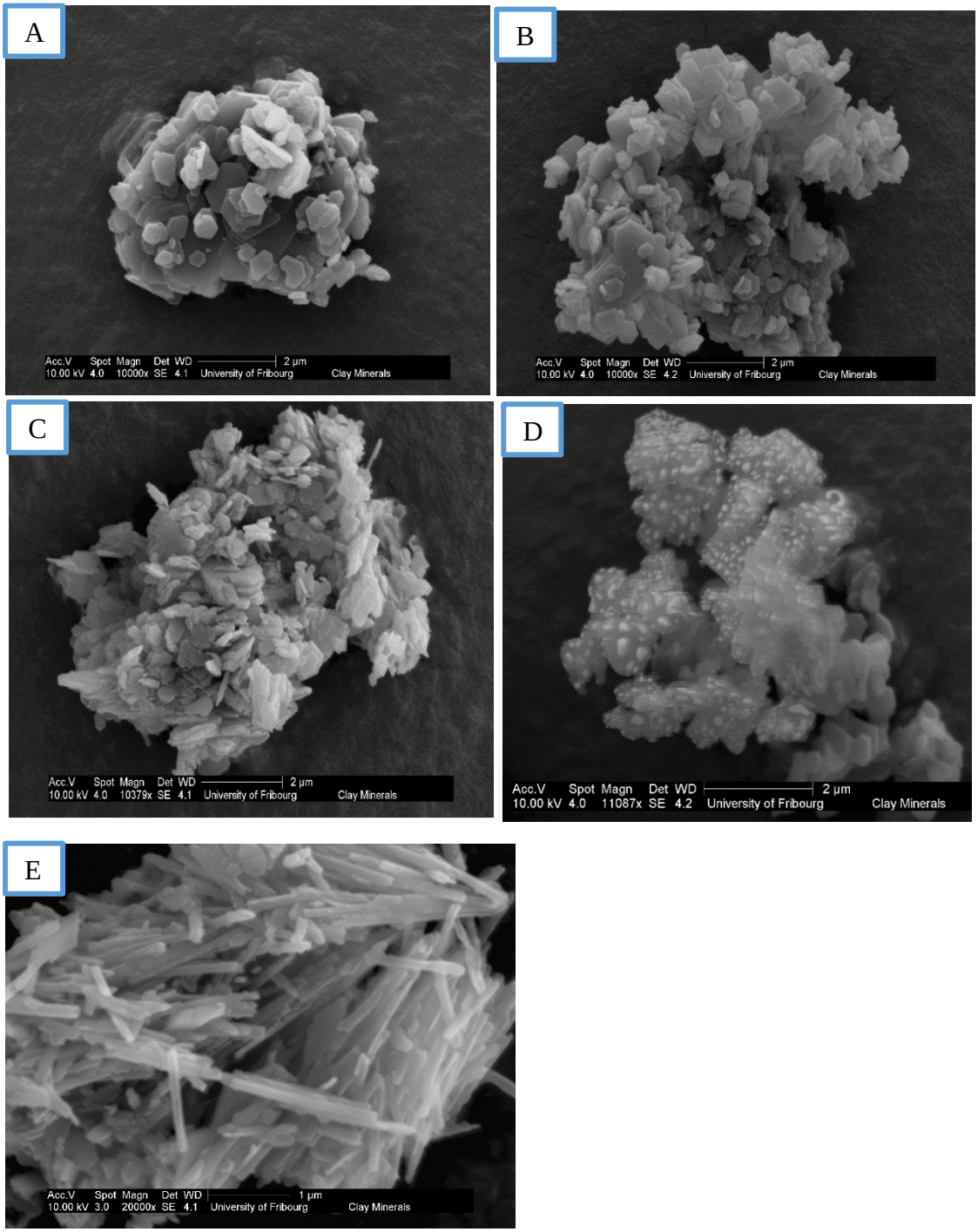

Figure 4.6: *SEM photograph of platy euhedral (A and B), elongated (C) and hemispherical (D) kaolinite crystals and (E) halloysite crystals. [(A) Represent pure kaolinite; (B), (C) and (D) are from quartz bearing kaolin].*

4.3. Mineralogy

The mineralogy of the kaolin samples were determined using X-Ray Powder diffraction. In this section, the qualitative and quantitative mineralogical determination performed for all kaolin samples will be examined. The XRD results (qualitative and quantitative) of samples collected from Belessa kaolin deposits are given in table 4.1 and figure 4.9 A to E. These results showed clear resemblances and differences. Qualitative measurements by XRD revealed that kaolinite is the only clay mineral which occurs in the ores. As a component of "universal impurity" (Chakraborty, 2014), quartz is also found associated with the kaolinites in all kaolin samples (except in pure kaolinite sample BHR-0054). The mineralogical result showing the presence of quartz is also supported by the slightly higher ratio of SiO2/Al2O3 (>1.2) which indicates the presence of other silicate phases beside the kaolinite. The amount of these minerals varies from slightly kaolinized to completely kaolinized samples. Thus, kaolinite and quartz value show a ranges of (53.2 – 100 %) and (0- 46.8 %) respectively (Fig. 4.7).

Table 4.1: *Mineral compositions for Belessa kaolin deposits*

	BHR-0016 B	**BHR-0053 B**	**BHR-0017**	**BHR-0054**
Quartz	46.80%	40.10%	10.90%	0%
Kaolinite	53.20%	59.90%	89.10%	100%

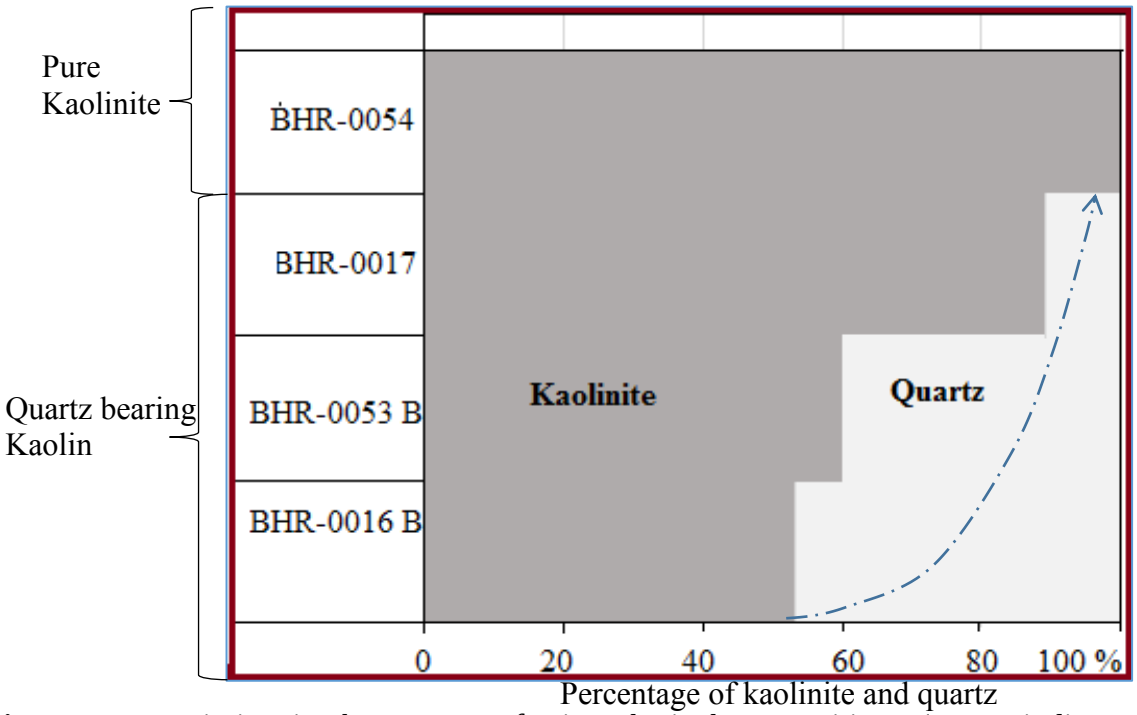

Figure 4.7: *Variation in the amount of mineralogical compositions (arrow indicates increasing alteration); after Da Costa and Moraes (1998).*

Some of the kaolin samples contain slightly disordered kaolinites, which are not perfectly described by the crystalline kaolinite. The kaolin sample from southern part (BHR-0051) of the study area show a slight mineralogical difference from the above samples which consists of halloysite, quartz and sanidine as the main identified phases (see Fig. 4.9 E).

The XRD results in figure 4.9 show differently changing patterns. The differences in the X-ray peaks (sharpness and resolution) are related to the degree of crystallinity of kaolinite (Chakraborty, 2014). It is also observed that some of the peaks are missing and still some other become broad when order of crystallinity changes. These differences result to have a classification of highly crystalline, medium crystalline and poorly crystalline kaolinites. Most of the patterns in this study show a sharp x-ray diffraction peaks indicating that most of the samples are well crystallized. The quartz bearing kaolin samples BHR-0016B (Fig. 4.9 A), BHR-0053 B (Fig. 4.9 B) and BHR-0017 (Fig. 4.9 C) and the pure kaolinite sample BHR-0054 (Fig. 4.9 D) shows medium to high crystalline kaolinites. Moreover, the kaolinites show a series of strong X-ray diffractions peaks mainly at about 7Å (~ 13^0 2θ) and 3.5 Å (~ 26^0 2θ). In figure 4.9 E, the broad peaks, especially on the high theta side, are typical for highly disordered halloysites. The phases with sharp peaks are quartz and sanidine. The quartz in all samples are part of the parent rock. While, sanidine is the high temperature polymorph of K-feldspar, which is typical for rhyolites.

A parameter Hinckley index (HI) suggested by Hinckley (1963), is measured to know the crystallinity of kaolinite crystals (level of defects in kaolinite) more accurately. It is calculated from three XRD patterns of representative kaolin samples using the formula explained by Pruett and Pickering (2006) (see Fig. 4.8). Accordingly, the result shows a higher Hinckley indexes for all selected samples (0.84 to 1.22). These ranges of HI values correspond to a low defect, well ordered or well crystallized kaolin. The results of HI calculations are also consistent with the sharp x-ray diffractions patterns. Most of the XRD patterns from Fig. 4.9 A to D shows highly crystalline kaolinites. These means that, kaolinite has also low defect structure marked by the presence of many rhythmic kaolinite peaks. The X-ray diffraction patterns of Belessa kaolinite are shown in figure 4.9.

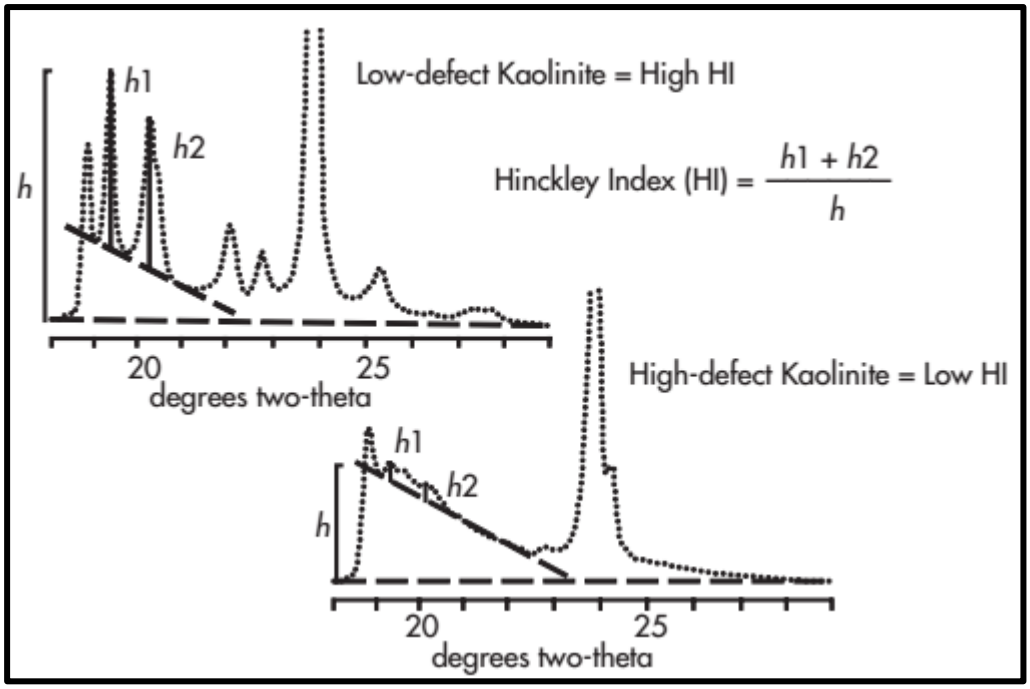

Figure 4.8: *Hinckley index formula with example of high and low defect kaolinite (after* Pruett and Pickering, 2006*).*

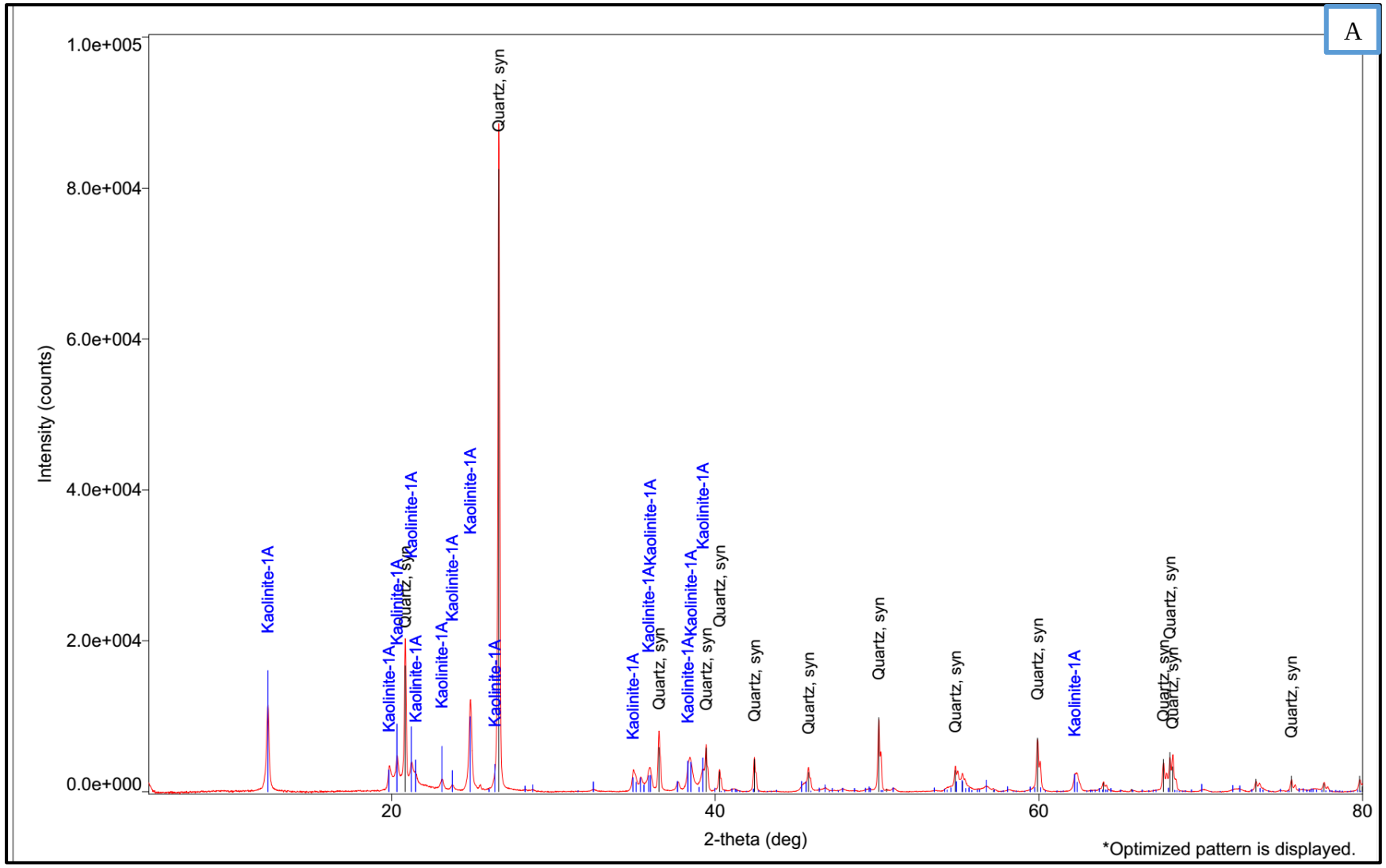
A
1.0e+005
8.0e+004
6.0e+004
4.0e+004
2.0e+004
0.0e+000
Intensity (counts)
20
40
60
80
2-theta (deg)
*Optimized pattern is displayed.
Kaolinite-1A
Quartz, syn

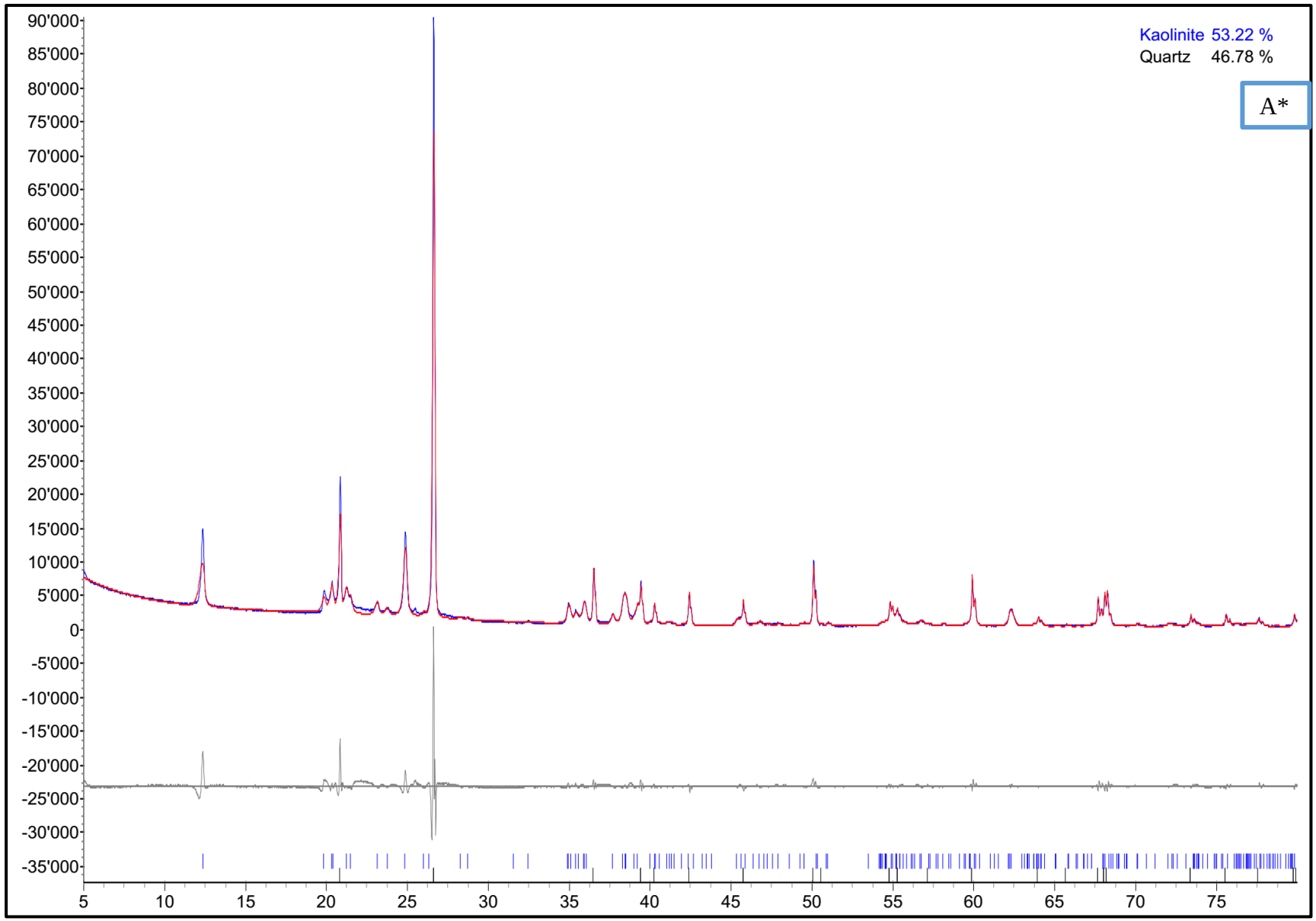
Kaolinite 53.22 %
Quartz 46.78 %
A*
90'000
85'000
80'000
75'000
70'000
65'000
60'000
55'000
50'000
45'000
40'000
35'000
30'000
25'000
20'000
15'000
10'000
5'000
0
-5'000
-10'000
-15'000
-20'000
-25'000
-30'000
-35'000
5
10
15
20
25
30
35
40
45
50
55
60
65
70
75

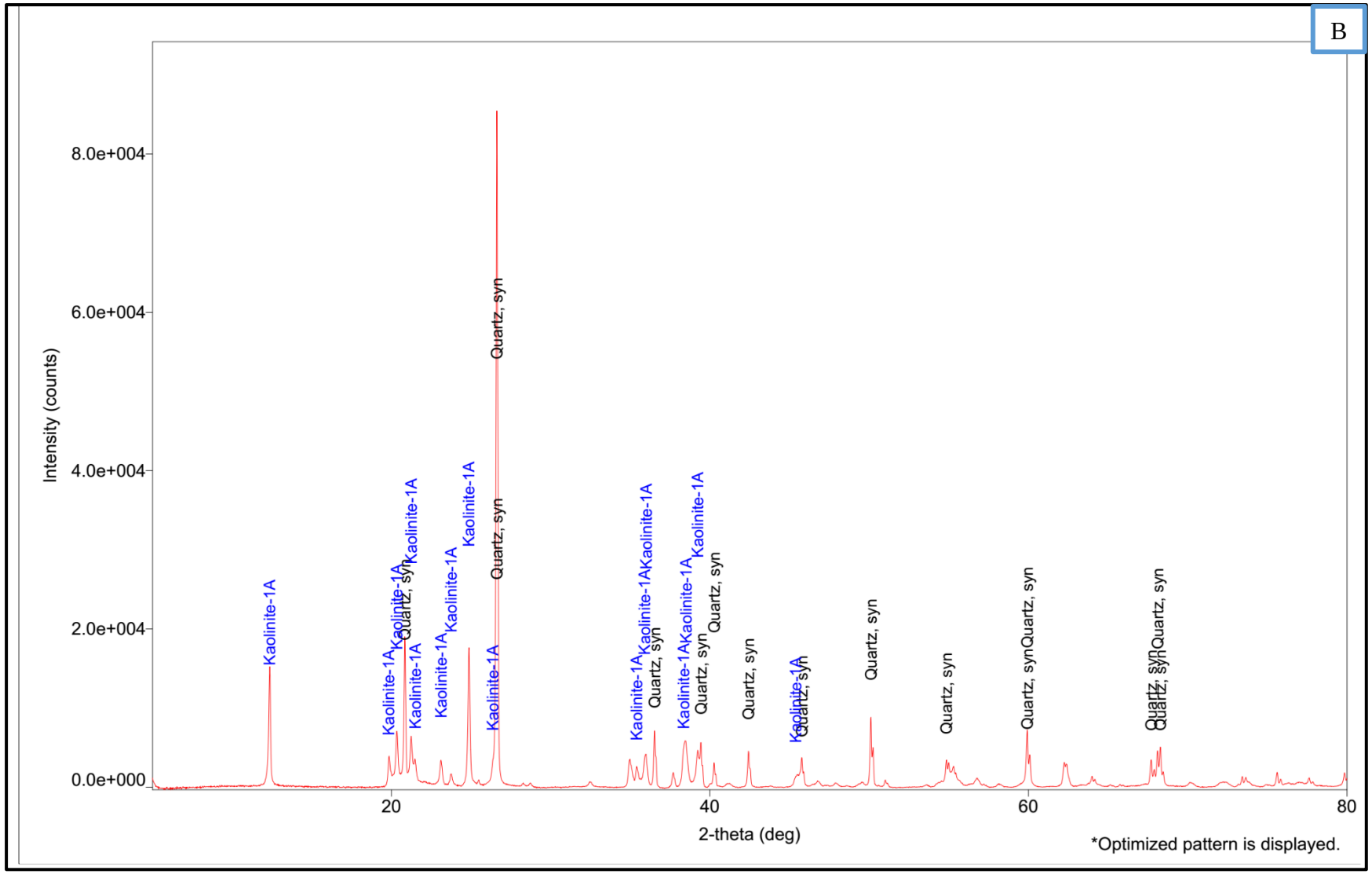
B
Intensity (counts)
8.0e+004
6.0e+004
4.0e+004
2.0e+004
0.0e+000
20
40
60
80
2-theta (deg)
*Optimized pattern is displayed.
Kaolinite-1A
Quartz, syn

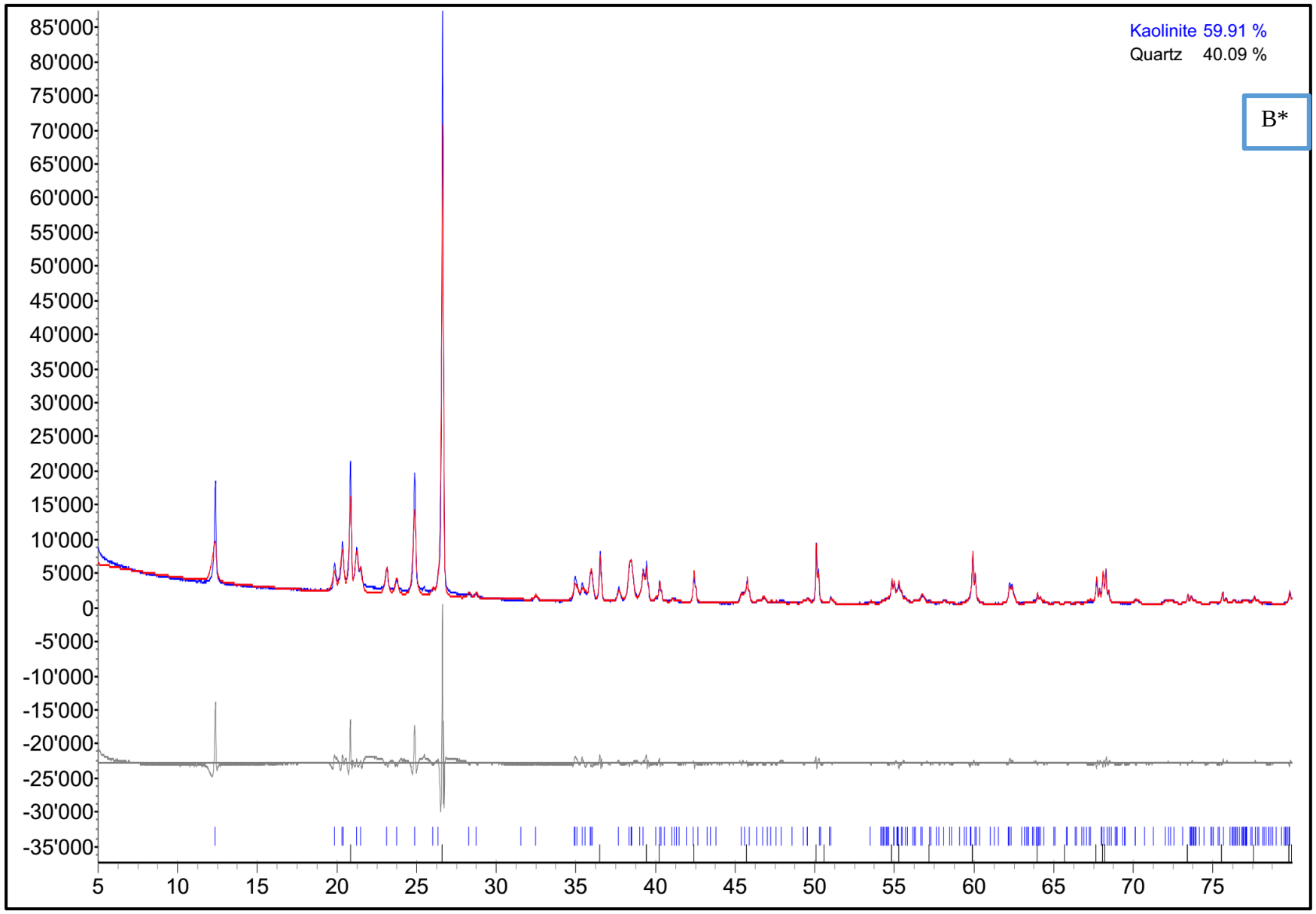
Kaolinite 59.91 %
Quartz 40.09 %
B*
85'000
80'000
75'000
70'000
65'000
60'000
55'000
50'000
45'000
40'000
35'000
30'000
25'000
20'000
15'000
10'000
5'000
0
-5'000
-10'000
-15'000
-20'000
-25'000
-30'000
-35'000
5
10
15
20
25
30
35
40
45
50
55
60
65
70
75

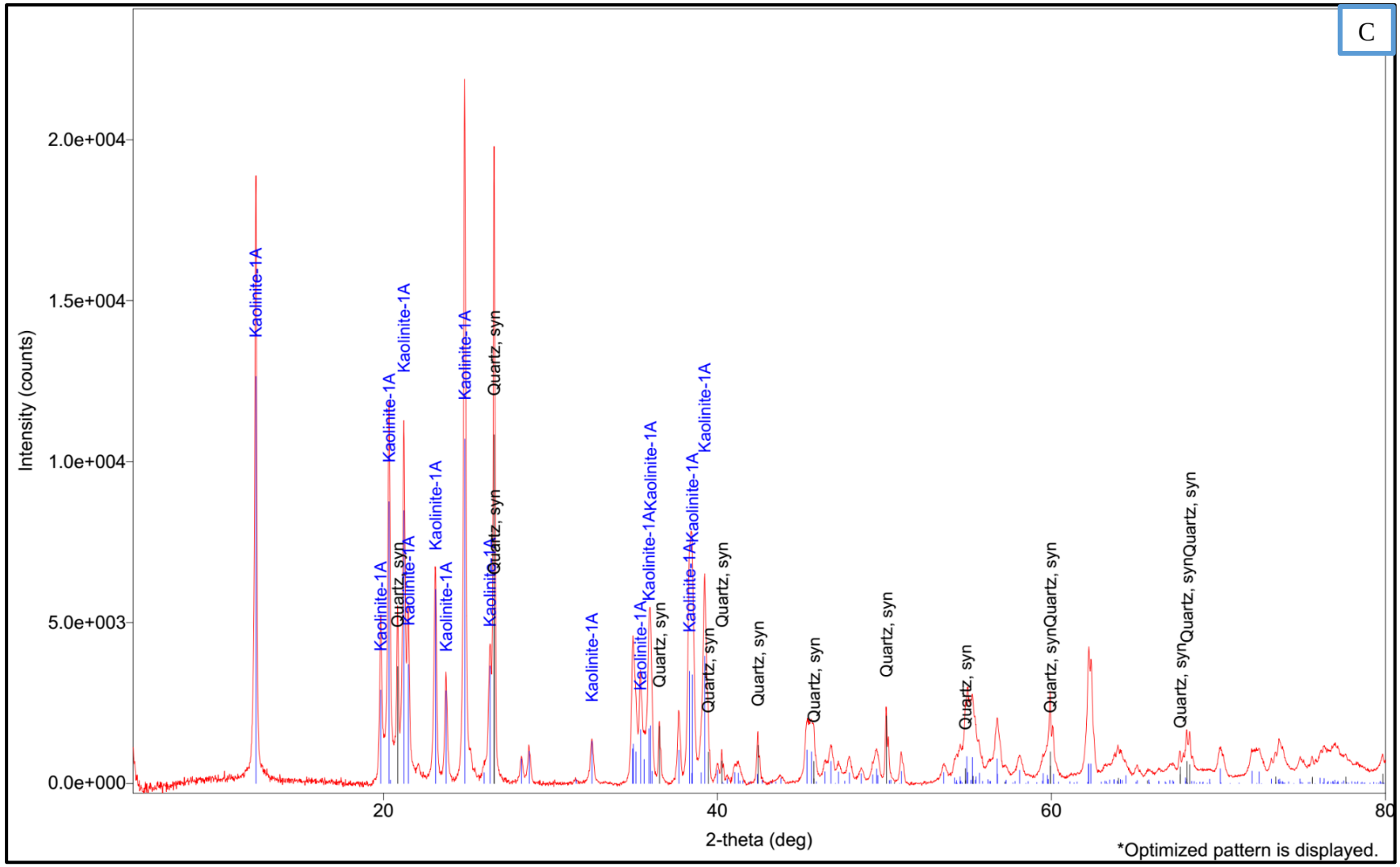
C
Intensity (counts)
2.0e+004
1.5e+004
1.0e+004
5.0e+003
0.0e+000
20
40
60
80
2-theta (deg)
*Optimized pattern is displayed.
Kaolinite-1A
Quartz, syn

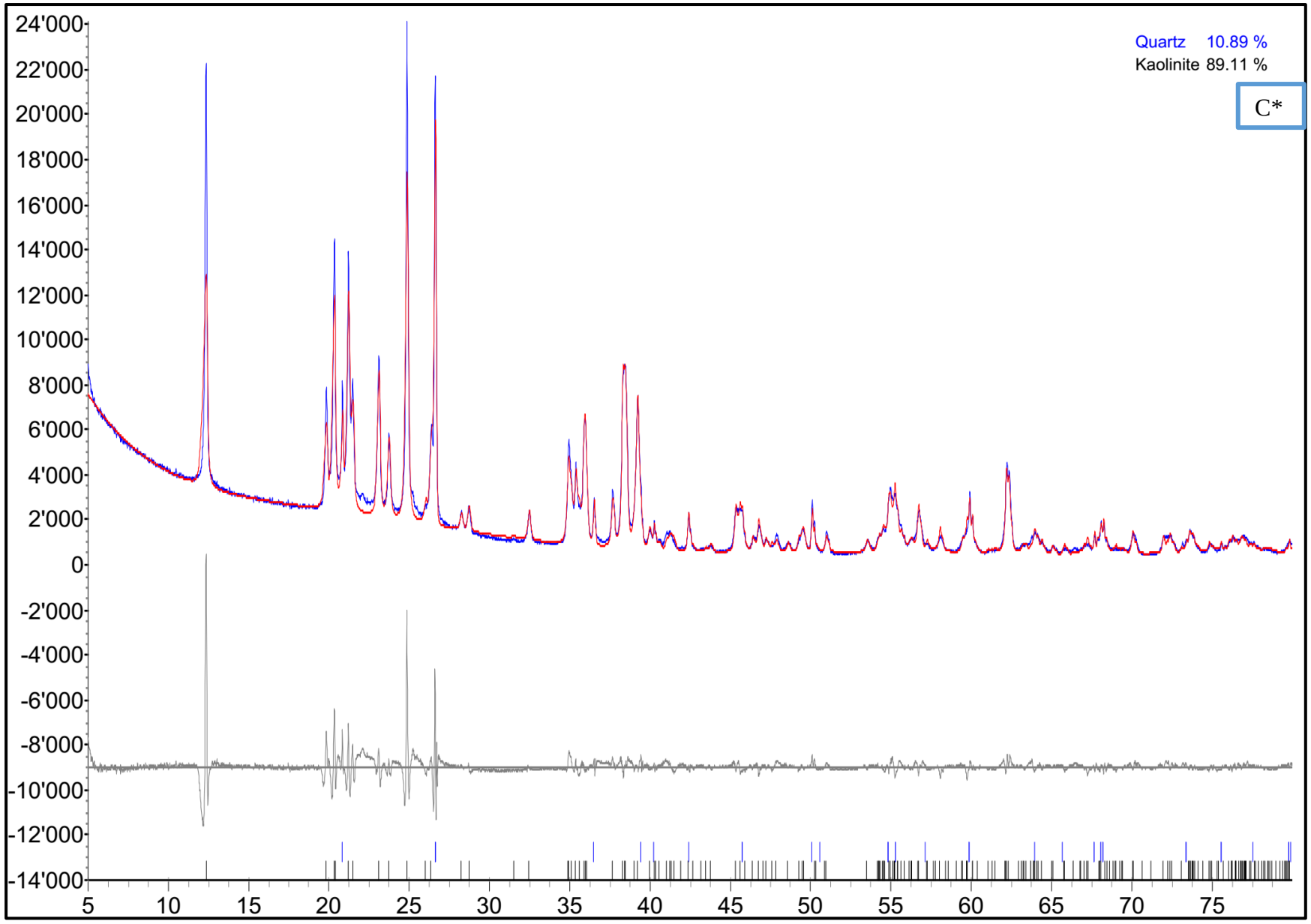
Quartz 10.89 %
Kaolinite 89.11 %
C*
24'000
22'000
20'000
18'000
16'000
14'000
12'000
10'000
8'000
6'000
4'000
2'000
0
-2'000
-4'000
-6'000
-8'000
-10'000
-12'000
-14'000
5
10
15
20
25
30
35
40
45
50
55
60
65
70
75

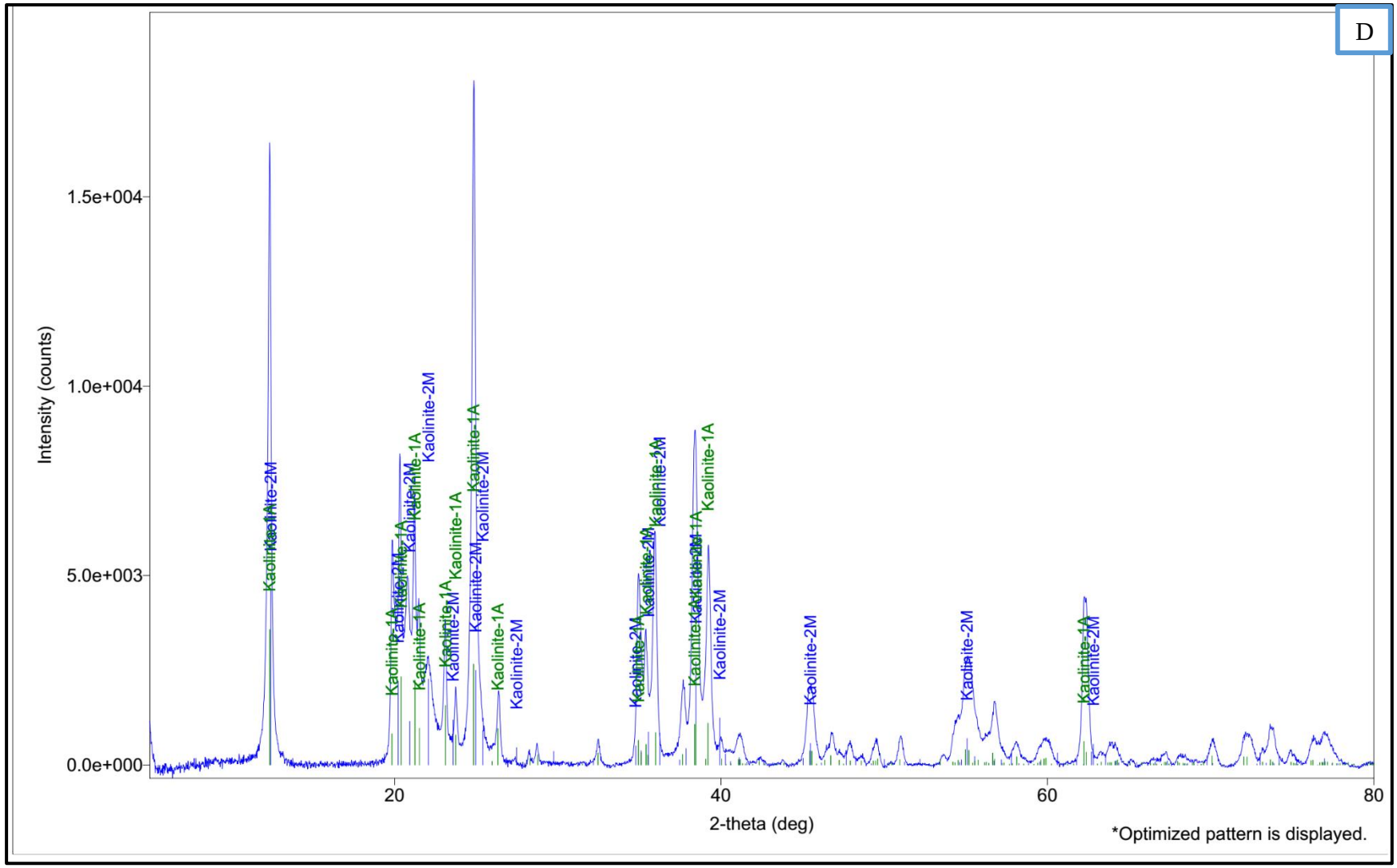
D
Intensity (counts)
1.5e+004
1.0e+004
5.0e+003
0.0e+000
20
40
60
80
2-theta (deg)
*Optimized pattern is displayed.

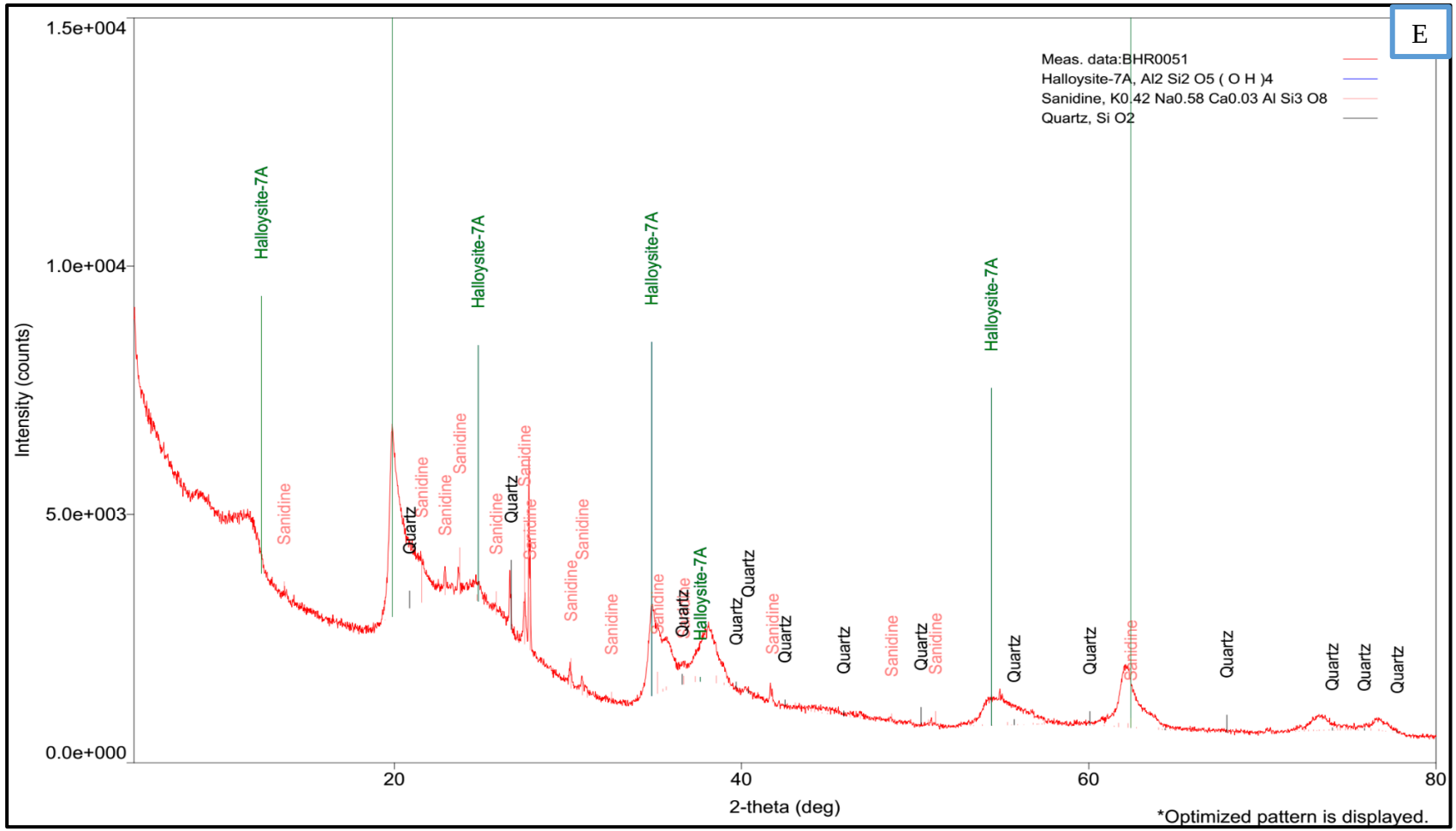

Figure 4.9: *XRD patterns of selected Kaolin samples. (A: BHR-0016B, B: BHR-0053B, C: BHR-0017, D: BHR: 0054, and E: BHR-0051 show the identified phases and those patterns with (*) represent their corresponding quantitative data).*

4.4. Geochemistry

Geochemically characterizing the kaolin deposits and their host rock is an important task for interpreting the alteration phenomena and their genesis. For this purpose, three geochemical data (major element, trace element and LOI) are used. The major element and LOI data are much useful to see the alteration phenomena, while the trace elements are studied to get evidence for the origin of kaolin deposits. The chemistry of kaolin is also important to establish their proper utilization in various industrial applications and to identify undesired impurities like Fe_2O_3 which are going to decrease their industrial value. For geochemical analysis purpose 8 samples (three rhyolite and five kaolin) are sent to ALS Geochemistry laboratory found in Ireland and analyzed for major and trace elements using Inductively Coupled Plasma Atomic Emission Spectroscopy (ICP-AES) and Inductively Coupled Plasma Mass Spectroscopy (ICP-MS). The loss on ignition (LOI) was also attained using WST-SEQ. According to Rollinson (1993), LOI is the total volatile content of the rock obtained after igniting it with a temperature of 1000^0c. Major, trace and REE element concentrations of the analyzed samples are listed in table 4.2. These chemical data give details of the chemistry of parent rocks and their derivative kaolin occurrences showing significant chemical differences between them.

Table 4.2: *Major and trace element composition of rhyolite and kaolin samples. k* and <L.D stands for kaolinized and below detection limit respectively.*

Sample (wt.%)	BHR-0006 Rhyolite 383603 E 837805 N	BHR-0012 Rhyolite 387888 E 842118 N	BHR-0016A Rhyolite (k*) 383521 E 838392 N	BHR-0016B Kaolin 383544 E 838321 N	BHR-0017 Kaolin 383501 E 837558 N	BHR-0051 Kaolin 385548 E 833032 N	BHR-0053B Kaolin 384352 E 837967 N	BHR-0054 Kaolin 384181 E 837800 N
SiO2	69.2	70.5	76.3	71.2	65	53.2	64.2	46.7
Al2O3	15.25	11.45	16.7	19.5	24.1	23.3	24.2	37.5
Fe2O3	4.16	4.5	0.85	0.84	1.84	6.76	0.4	0.14
CaO	0.17	0.21	0.03	0.03	0.05	0.54	0.02	0.09
MgO	0.08	0.08	0.01	0.02	0.03	0.13	< L.D.	0.01
Na2O	1.4	4.15	< L.D.	< L.D.	0.03	2.93	0.04	< L.D.
K2O	1.5	4.73	< L.D.	< L.D.	0.06	2.52	0.03	0.01
TiO2	0.19	0.35	0.18	0.21	0.47	0.63	0.21	0.57
MnO	0.01	0.08	< L.D.	< L.D.	0.03	0.18	< L.D.	< L.D.
P2O5	< L.D.	0.02	0.01	< L.D.	0.02	0.01	0.01	0.01
BaO	< L.D.	0.03	< L.D.	< L.D.	0.01	0.08	< L.D.	< L.D.
Total	91.96	96.1	94.08	91.8	91.64	90.28	89.11	85.03
LOI	7.27	3.66	7	7.74	9.66	9.43	9.29	14.6

Sample (ppm)	BHR-0006 Rhyolite 383603 E 837805 N	BHR-0012 Rhyolite 387888 E 842118 N	BHR-0016A Rhyolite (k*) 383521 E 838392 N	BHR-0016B Kaolin 383544 E 838321 N	BHR-0017 Kaolin 383501 E 837558 N	BHR-0051 Kaolin 385548 E 833032 N	BHR-0053B Kaolin 384352 E 837967 N	BHR-0054 Kaolin 384181 E 837800 N
Li	10	10	10	20	10	< L.D.	80	< L.D.
C	0.03	0.01	0.03	0.03	0.02	0.05	0.02	0.02
S	< L.D.	< L.D.	< L.D.	< L.D.	< L.D.	< L.D.	0.01	0.01
Sc	2	5	3	2	8	8	3	3
V	< L.D.	9	6	7	19	12	8	11
Cr	10	10	10	20	30	10	10	10
Co	< L.D.	< L.D.	< L.D.	< L.D.	2	< L.D.	< L.D.	< L.D.
Ni	6	2	< L.D.	< L.D.	2	2	1	< L.D.
Cu	1	< L.D.	< L.D.	< L.D.	2	2	< L.D.	< L.D.
Zn	254	212	5	9	24	144	15	8
Ga	49.7	32.5	42.9	43.6	49.4	46.9	46.6	59.3
Ge	< L.D.	< L.D.	< L.D.	< L.D.	< L.D.	< L.D.	< L.D.	< L.D.
As	0.8	0.1	0.3	0.1	1	0.8	< L.D.	0.2
Se	5	0.5	1	0.9	0.7	1.4	0.6	0.4
Rb	80.4	129.5	1.9	2.4	5.6	20.5	2.4	0.2
Sr	14.6	16.6	2	3.5	8.7	54	9.7	8.7
Y	405	113	213	175	103	59.2	177	61.6
Zr	3060	1070	3080	2780	1810	1230	2900	1490

Nb	380	139	362	342	229	130.5	350	199.5
Mo	< L.D.	5	< L.D.	< L.D.	3	1	2	5
Ag	0.8	< L.D.	1.1	1.1	0.9	< L.D.	3.4	0.7
Cd	< L.D.	< L.D.	< L.D.	< L.D.	< L.D.	< L.D.	< L.D.	< L.D.
In	0.197	0.088	0.051	0.034	0.022	0.201	0.018	0.014
Sn	25	8	23	23	13	10	20	11
Sb	0.22	< L.D.	< L.D.	0.05	0.1	0.05	< L.D.	< L.D.
Te	0.01	< L.D.	< L.D.	< L.D.	0.01	0.03	< L.D.	0.01
Cs	0.27	1.4	0.06	0.09	0.2	0.14	0.09	0.04
Ba	33.2	330	6.3	12.9	64.6	748	20	12.8
La	138	179.5	4	11	61.6	74.6	45.3	26.3
Hf	76.9	24.6	80.4	73.3	47.9	30.2	77	36.7
Ta	25.3	8.1	25.2	22.1	15	9.2	25.9	10.4
W	2	3	4	1	4	2	1	5
Re	< L.D.	< L.D.	< L.D.	< L.D.	< L.D.	< L.D.	< L.D.	< L.D.
Hg	0.006	< L.D.	0.033	0.276	0.104	< L.D.	0.049	0.054
Tl	0.09	< L.D.	< L.D.	< L.D.	0.03	0.51	< L.D.	< L.D.
Pb	113	20	< L.D.	4	30	27	87	15
Bi	0.02	0.01	0.05	0.01	0.02	0.15	0.02	0.03
Ce	1030	236	44.4	71	79.8	272	85.9	34
Pr	41.4	36.9	3.71	4.72	6.98	16	8.03	5.5
Nd	174	145.5	24.2	27.7	24.7	60.2	37.6	27.5

Sm	48.8	26.5	15.75	14.95	8.15	11.3	15.65	7.1
Eu	3.69	3.85	1.4	1.47	1.19	2.21	1.65	1
Gd	50.2	20.3	22.9	19.6	10.35	10.05	19.15	8.33
Tb	10.05	3.33	5.41	4.6	2.52	1.64	4.61	1.39
Dy	69.2	20.4	39.8	32.8	20	10.9	33.9	8.94
Ho	14.3	4.02	8.54	7.15	4.43	2.11	6.88	1.84
Er	42.9	11.05	27.4	23.2	14.9	6.44	22.2	4.92
Tm	6.34	1.67	4.47	3.81	2.48	0.93	3.57	0.69
Yb	40.8	10.1	30.3	27.1	19.7	5.88	25.2	4.12
Lu	5.97	1.43	4.58	3.94	2.96	0.81	3.71	0.59
Th	60.7	18.55	60.6	52.5	43.4	23.7	60.8	9.52
U	11.4	4.61	9.51	9.14	5.06	1.16	10.45	9.18

In the following sections the analysis results of major and trace elements will be presented. To determine the extent of weathering and alteration, chemical index of weathering (CIW) and chemical index of alteration (CIA) are also calculated from the whole-rock chemical analysis.

4.4.1. Major Element Geochemistry

Major elements are the main constituents of both parent and altered rocks. They include: Si, Ti, Al, Fe, Mn, Mg, Ca, Na, k, P and Ba. In a major element chemical analysis result (table 4.2), they are traditionally listed as oxides. Before the major oxides are directly used, they are normalized to get volatile free value (N_M) using the following formula.

$T_M - LOI = T$

$N_M = M/T*100$

Where, T_M = Total value of the major oxide with LOI

LOI= Loss of ignition

T= Total value without LOI

M= Major Oxide

N_M = Volatile free major oxide

In order to establish the alteration phenomena and genesis of Belessa kaolin, different diagrams were produced using major element data. The resulting diagrams are presented after the data are integrated using processing software like Microsoft excel and Petrograph version 2beta.

On the Total Alkali Silca (TSA) diagram the classification of volcanic rocks is based on the diagram of Le Bas et al. (1986) in which the total alkalis are plotted against silica. The diagram shows that the parent rocks fall in the rhyolite region (see Fig 4.10 A). Furthermore, the classification diagram of silicic volcanic rock from Le Bas et al., (1986) is plotted using Agpaitic index against SiO2 (Fig. 4.10 B). Agpaitic index is calculated by using the following formula.

$$\text{Agpaitic index} = \frac{Al_2O_3}{Na_2O + K_2O}$$

The result showed that the nature of the host rock (rhyolite) is peralkaline.

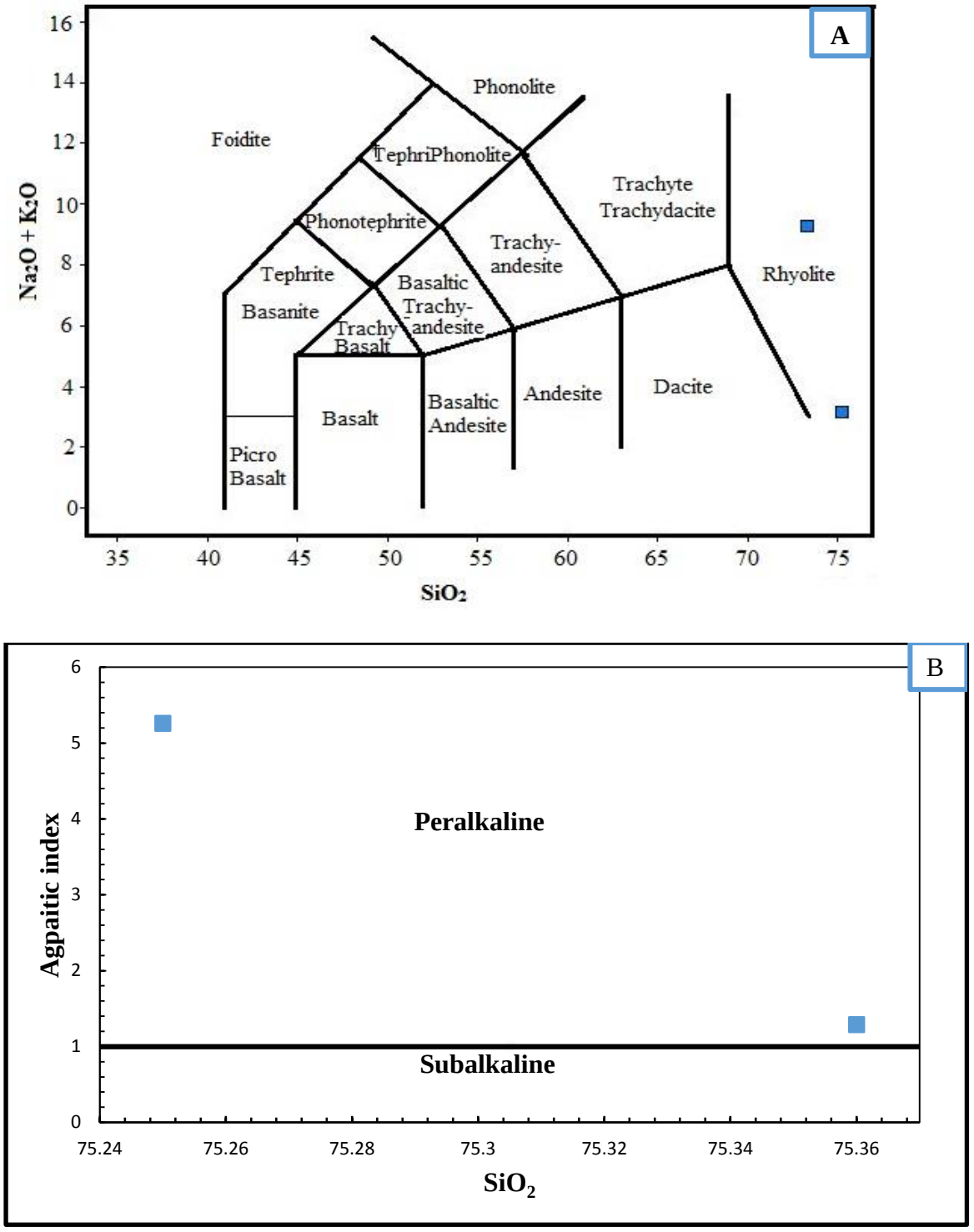

Figure 4.10: *A) TAS diagram .B) Classification of silicic volcanic rocks from Belessa area after Le Bas et al. (1986).*

The major element compositions of parent rock (unaltered) and completely altered rocks (kaolin) show significant differences (see table 4.2). In this study, the parent rock displays a range of concentrations (73.36 -81.1 wt. % SiO_2), (11.91 -17.75 wt. % Al_2O_3), (0.9 - 4.68 wt. % Fe_2O_3) and (3.15 – 9.24 wt. % Na_2O+ K_2O). It also shows relatively the lowest LOI (3.66-

7.27 %). In the same way, the completely altered rocks (kaolin) contains range of values; (54.92 wt. % to 77.56 wt. % SiO_2), (21.24 wt. % to 44.1 wt. % Al_2O_3), (0.16 wt. % to 7.49 wt. % Fe_2O_3) and (0.01 wt. % to 6.04 wt. % Na_2O+ K_2O). All LOI values of the five kaolin samples are high (7.74 wt. % to 14.6 wt. %). The Na_2O, MnO and BaO are completely lost in pure kaolin sample. The pure kaolin is also depleted in K_2O and CaO and it has more or less similar to that of the parent rock in MgO and P_2O_5. On the contrary, the TiO_2 shows minor increment in all samples with advancing of kaolinization. This is due to a strong tendency of TiO_2 to be concentrated in the fine pure kaolinite particle fraction (Bundy and Conley, 1962). Al_2O_3 has a positive correlation with LOI and a negative correlation with that of SiO_2 (Fig. 4.11). Low alumina in some kaolin samples are due to the presence of impurities. The direct relation of LOI with Al2O3 can be used to estimate the kaolinite content (Searle and Grimshaw, 1959). In this case, the higher the LOI is consistent with increase in the amount of kaolinite. In figure 4.12., different triangular diagrams and graphs are plotted to show the amounts and relation of major oxides and LOI in the kaolin and rock samples of the study area. These diagrams are also useful to examine the weathering processes in the region.

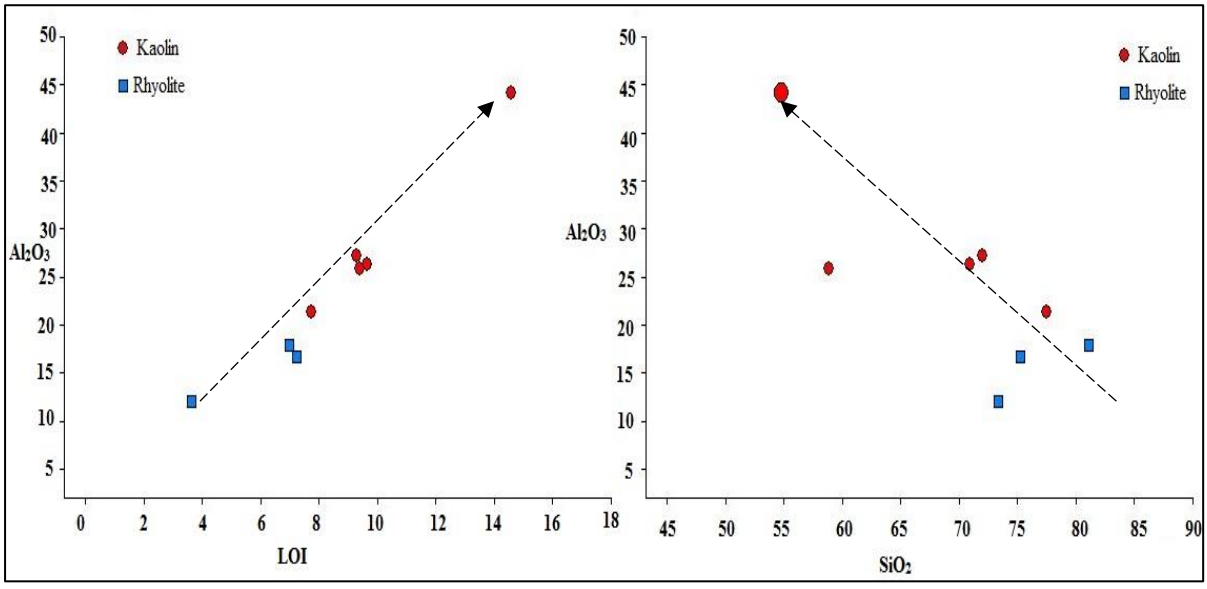

Figure 4.11: *A graph showing the relation of Al2O3 with LOI and SiO2. (Arrows indicate the general alteration trend).*

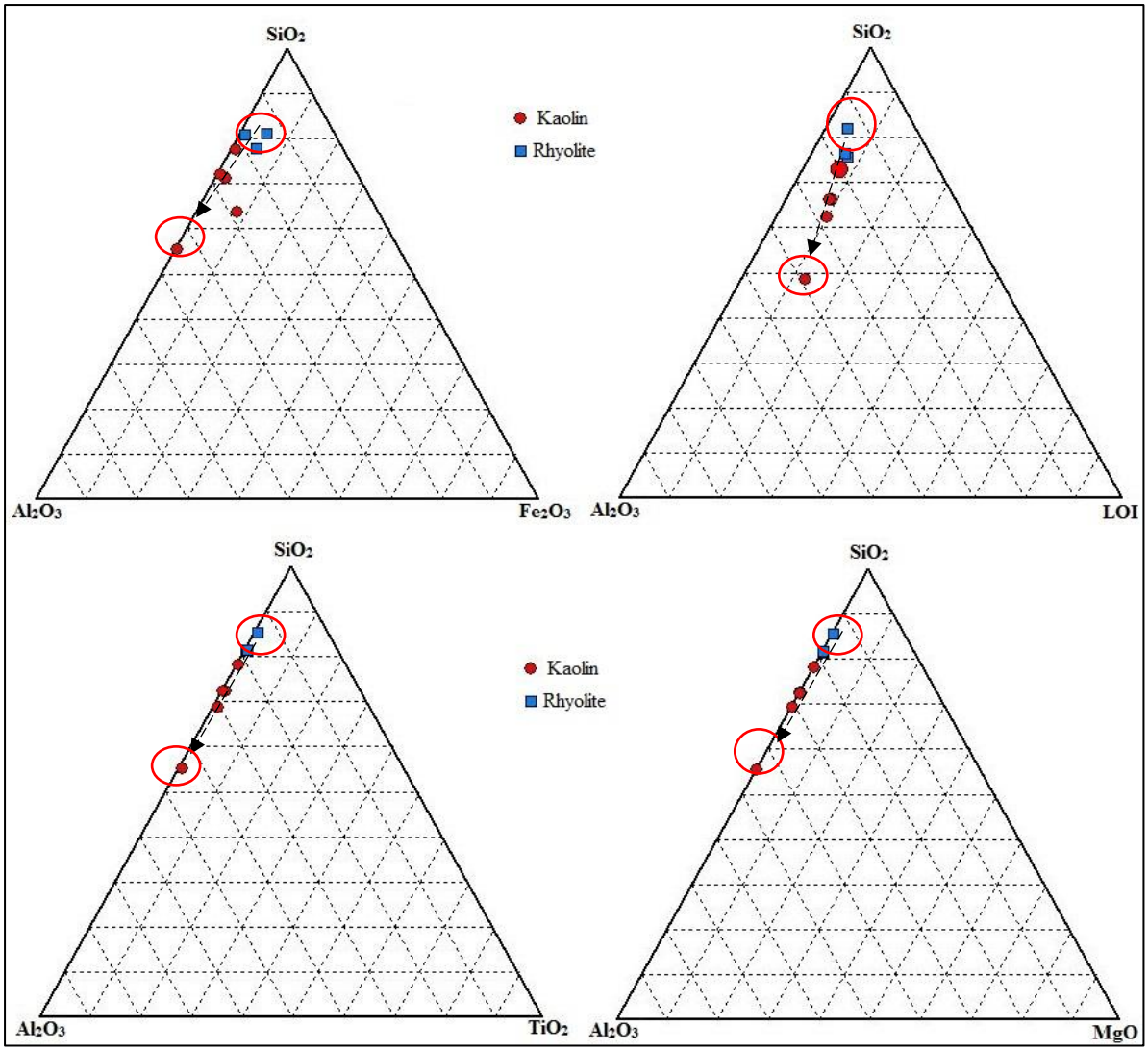

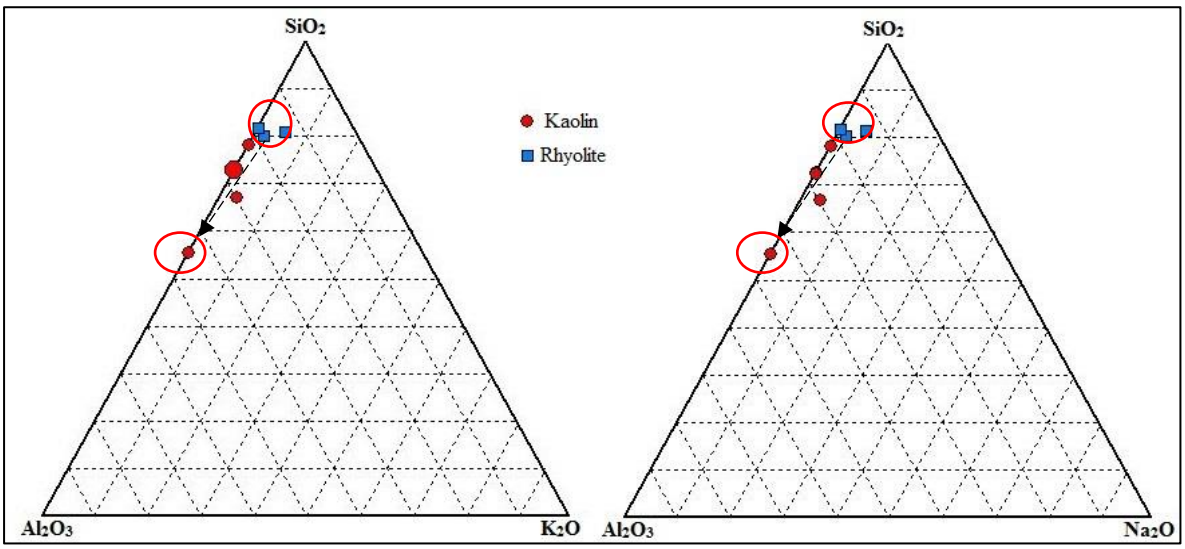

Figure 4.12: *Triangular diagrams between the main oxides [all arrows indicate the increase in alteration].*

Based on whole rock chemical analysis, a variety of chemical indices were used to characterize the intensity of weathering and alteration. In this study, the Chemical Index of Weathering (CIW) and Chemical Index of Alteration (CIA) are used to evaluate the extent of weathering and alterations respectively. The values are calculated using the following mathematical formulas;

CIW= $[Al_2O_3 / (Al_2O_3 + CaO + Na_2O)] \times 100$ (Harnois, 1988)

CIA= $[Al_2O_3 / (Al_2O_3 + CaO + Na_2O + K_2O)] \times 100$ (Nesbitt and Young, 1982).

Result of the above calculation for each samples showed that, both indexes (CIW and CIA) steadily increases going all the way from the fresh parent rock to a highly altered kaolinized rock (see Fig. 4.13 A). Therefore, CIA shows a value that increases from 55.7 % to 99.7 %. While, CIW has a value that increases from 72.4 % to 99.7 %. Figure 4.13 B shows that from intermediate to completely altered kaolin, there is an increase in Al2O3 content which is consistent with an increase in kaolinite content. This shows that with higher degree of alteration the higher Al2O3 content will be. Furthermore, in figure 4.13 C the mobile species Na_2O and K_2O are plotted against Al_2O_3 to see the effect of weathering and alteration. Accordingly, both Na_2O and K_2O show negative correlation with Al_2O_3. The abundances of these mobile elements in kaolinized rock are much smaller than that of parent rock. This indicates they are depleted substantially during weathering.

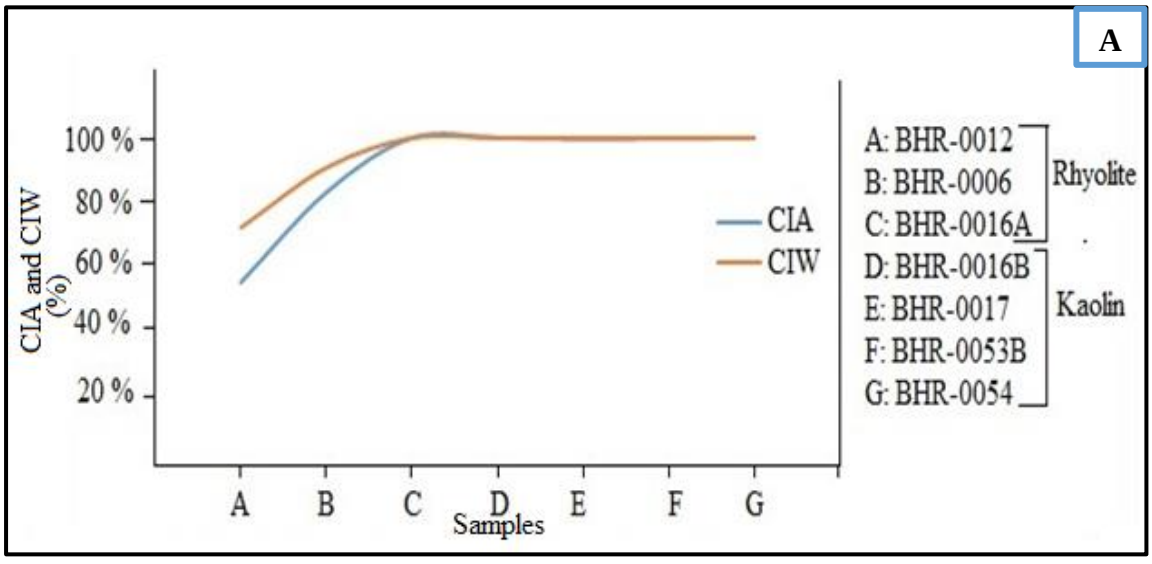

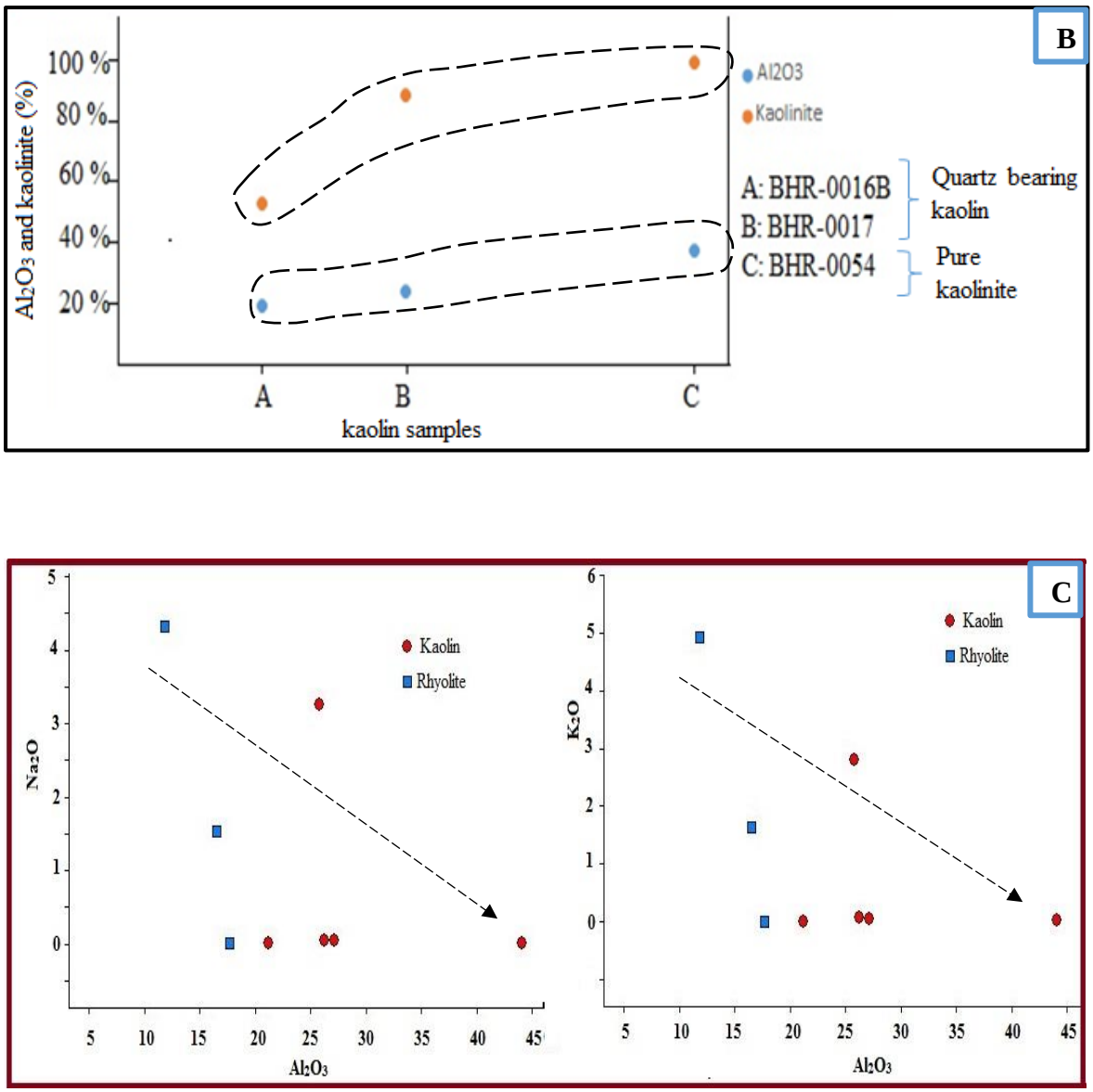

Figure 4.13: *(A) Graph showing CIA and CIW values from parent rock to kaolin, (B) Al2O3 and Kaolinite content from less altered kaolin A to completely altered kaolin C and (C) Major element- Al2O3 variation diagrams (arrows indicate the general trend where alteration and weathering increases).*

The ternary systems A-CN-K [(Al_2O_3-(CaO + Na_2O)-K_2O)] and A-CNK-F [(Al_2O_3-(CaO + Na_2O+ K_2O) - Fe_2O_3] are used to better visualize the weathering and alteration trends in the kaolin deposit (see Fig. 4.14). In A-CN-K diagram, the extensively kaolinized samples are plotted in the top corner showing the predominance of Al-bearing minerals (Kaolinite). The fresh rocks are located in the center of the diagram showing relatively K enrichment (see Fig. 4.14 A). According to Aristizabal et al. (2005) this phenomena corresponds to a presence of more felsic protolith. This is consistent to a K-feldspar rich parent rock of the study area. The A-CNK-F shows that the fresh parent rock is closer to CaO + Na_2O+ K_2O indicating it is

enriched by K, Na and Ca bearing minerals. Whereas, the highly weathered and altered materials are depleted of these elements and are displaced towards the Al_2O_3-Fe_2O_3 edge (Fig. 4.14 B).

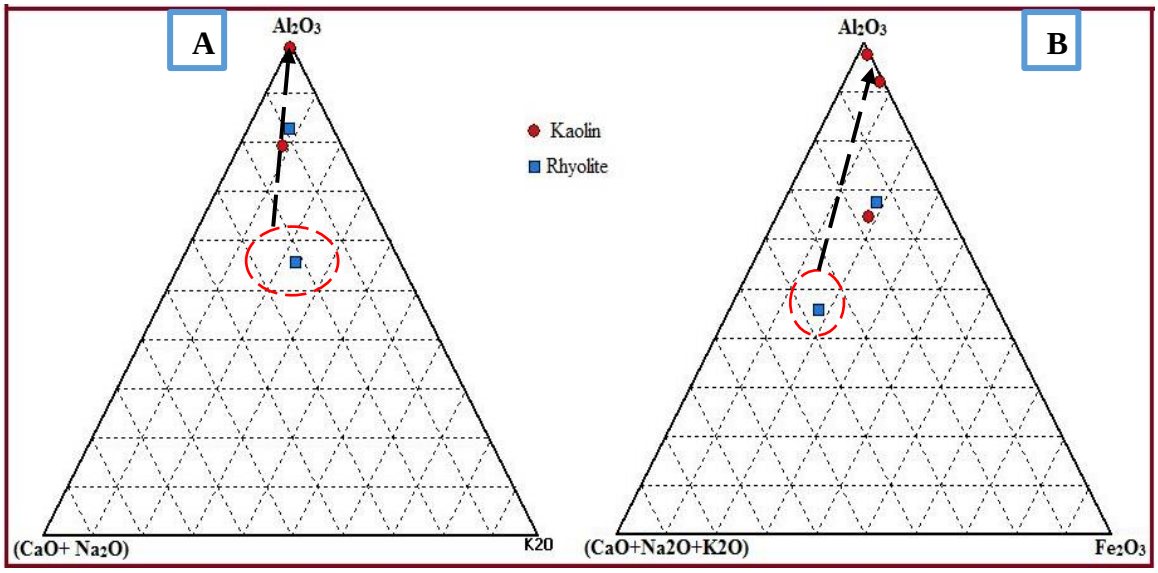

Figure 4.14: *(A) A-CN-K diagram (B) A-CNK-F diagram. In both case the arrow indicates the general alteration trend: (After Nesbitt and Young, 1989).*

4.4.2. Trace Element Geochemistry

Rollinson (1993) explained trace elements as, those commonly substitute for major elements in the rock forming minerals. They are present in a rock in concentrations of less than 0.1 wt. %, that is less than 1000 parts per million (ppm). Trace element distributions of the fresh and kaolinized rocks are shown in table 4.2. According to many authors (Ex. Dominguez et al., 2008; Cravero et al., 2001; Dill et al., 1997), trace elements are efficient in distinguishing the origin of kaolinization as hypogene and supergene. In the same way, in this study trace elements are used in interpreting the origin of kaolinization in Belessa kaolin deposit. For this purpose the trace element data are presented using REE diagrams and a binary diagram.

From the analyzed trace elements only Ni, Li, Sb, Ge, Re, Tl, Cd, Co and Cu are below the detection limits in the kaolinized samples. The studied trace element data also show some clear trend. Both fresh and kaolinized samples show higher contents of Zr (1070- 3080 ppm) and Nb (139-380 ppm) because these elements remained immobile during early and moderate stages of weathering. The REE content for a wholly kaolinized rocks (BHR-0053B and BHR-0054), for slightly kaolinized rock (BHR-0006) and for unaltered rhyolite rock (BHR-0012) were plotted in figure 4.15 normalized to chondrite value determined by Boynton (1984). This diagram shows that the pattern of rhyolite rocks is more or less similar to that of kaolinized

rock. The only difference is observed with the amount of REE concentration they contain. This similarity may indicate inherent connection between the two (Yuan et al., 2014). Both fresh and kaolinized rocks show slightly enriched LREE compared to HREE with distinct Eu anomaly. This may indicate that HREE are more soluble than LREE (Middleburg et al., 1988). The kaolin samples also shows strong negative Eu anomaly compared to that of parent rock. This strong Eu anomaly can be traced to the feldspar in the parent rhyolite (Dill, 2016). Moreover, in fresh rhyolite, slight negative Ce anomaly were detected. A slightly negative Ce anomaly in pure kaolinite (see Fig. 4.15 B) can be related to the oxidation environment (Ghadimian and Khodami, 2015; Dill, 2016). This in turn shows the effect of weathering in the volcanic rocks of the region. In contrast to the fresh host rock, the slightly kaolinized host rocks shows positive Ce anomaly. Such peculiar characteristics of the kaolinized host rock (rhyolite) and some kaolin samples are well-known characteristics in weathering process of soil formation (Njoya et al., 2006). Also, a scenario with a negative Eu and Ce anomalies and a slightly positive Gd anomalies is related to the weathering of acidic host rock for the kaolin deposit (Da costa and Moraes, 1998).

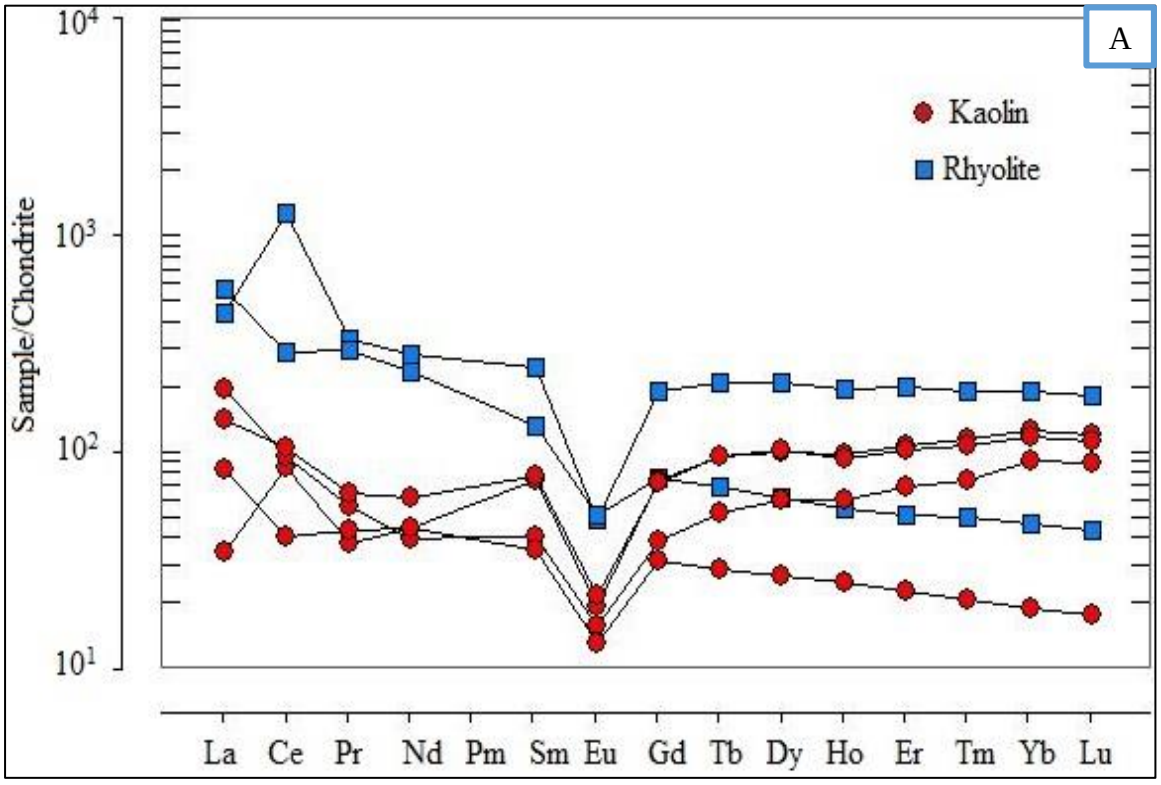

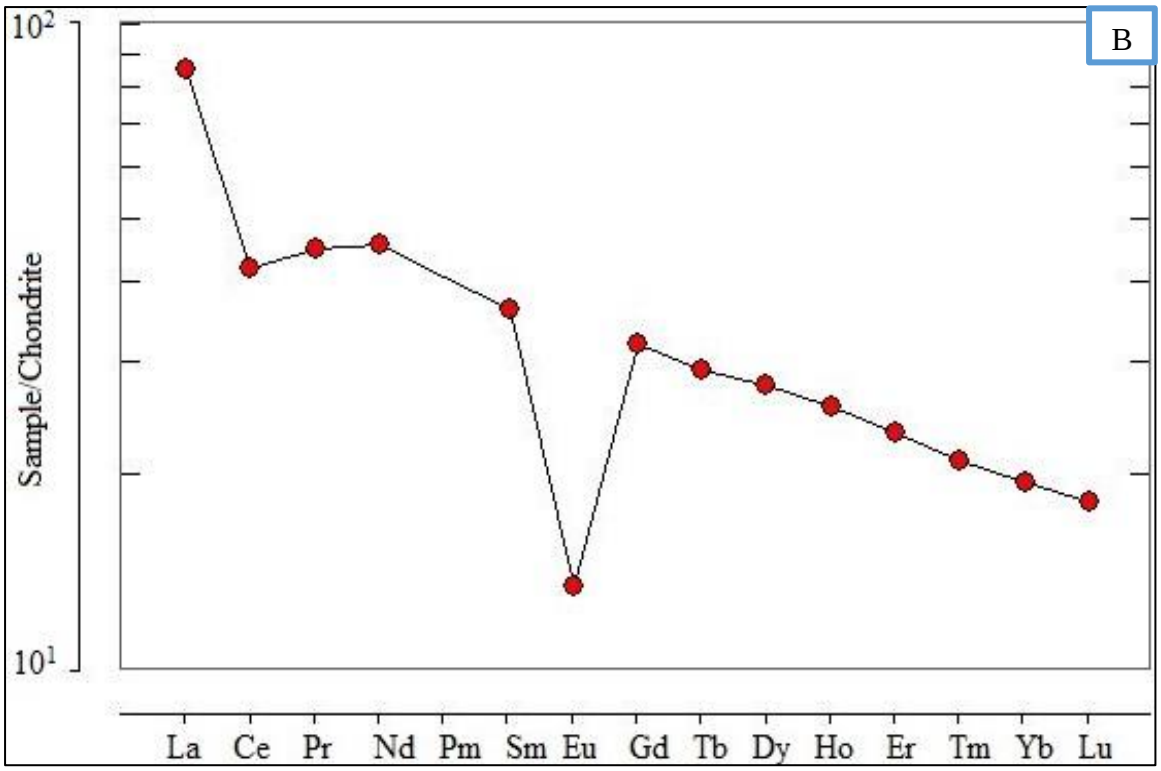

Figure 4.15: *REE variation diagram of kaolin and rhyolite (A) and pure kaolinite (B). Chondrite normalizing values are determined from Boynton (1984).*

The significant mobilization and fractionation of REE occurs during intense weathering and they are not significantly mobilized during initial stage of weathering (Middleburg et al., 1988). To see the behavior of REE all the way from the freshest host rock to the kaolin, the parameter R proposed by Middleburg et al. (1988) is adopted. This parameter is a measure of the degree of feldspar breakdown and the accumulation and formation of clay minerals. The R ratio is calculated by using the major elements and LOI concentrations in the equation R= (CaO + Na2O + K2O)/ (Al2O3 + LOI). Accordingly, R ratio value approaches zero (0) when the intensity of weathering and alteration is strong enough to result kaolinized material. In this case the REE concentrations are highly depleted. In other way, the R values approach 1 for unaltered or less altered rocks and REE shows enrichment. In this work, the freshest host rock and the kaolin samples show R value of 0.61 and 0.004 respectively. These show that R value decreases with kaolinization. It is also observed that the pure kaolinite contains very low concentration of REE. In general, it is observed that LREE have a positive correlation with R ratio value demonstrating the depletion of LREE with kaolinization (Fig 4.16).

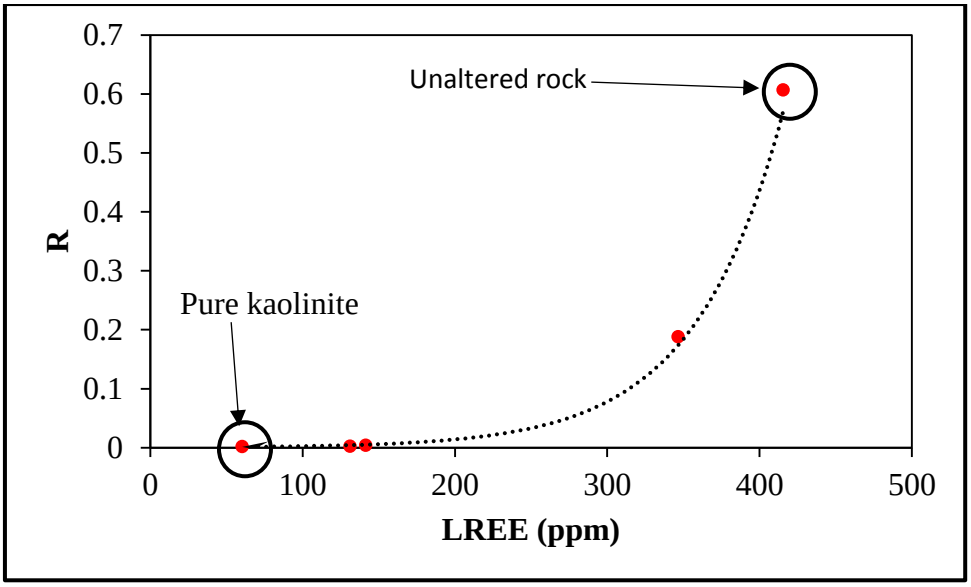

Figure 4.16: *Relation between R and LREE (La + Ce) [dotted line is trend line], (adopted from Al-Ani and Sarapaa, 2009).*

The multi-element variation diagram which is normalized to primordial mantle is plotted based on MacDonough and Sun (1995). This diagram helps to further characterize the alteration phenomena and genesis of Belessa kaolin deposit. Figure 4.17 (A) and (B) shows the multi-element variation diagrams of the host rock and Belessa kaolin deposit. Accordingly, the host rocks contain higher quantities of Rb and K though they show depletion of Sr and Ti. The kaolin ore distinctly shows significant depletion of Rb, K, Sr and Ti. These elements are probably derived from easily leachable minerals like feldspars and they are depleted and selectively leached (except for Ti) from weathering profiles during moderate alteration stage. Unlike to those of Rb, K and Sr, the depletion of Ti is probably due to substitution of Cr (Dill et al., 1997). On the contrary, Zr, Hf, Th and Nb do not show significant change in their concentration because they remained immobile under extreme alteration stage and they accumulated residually in the kaolin.

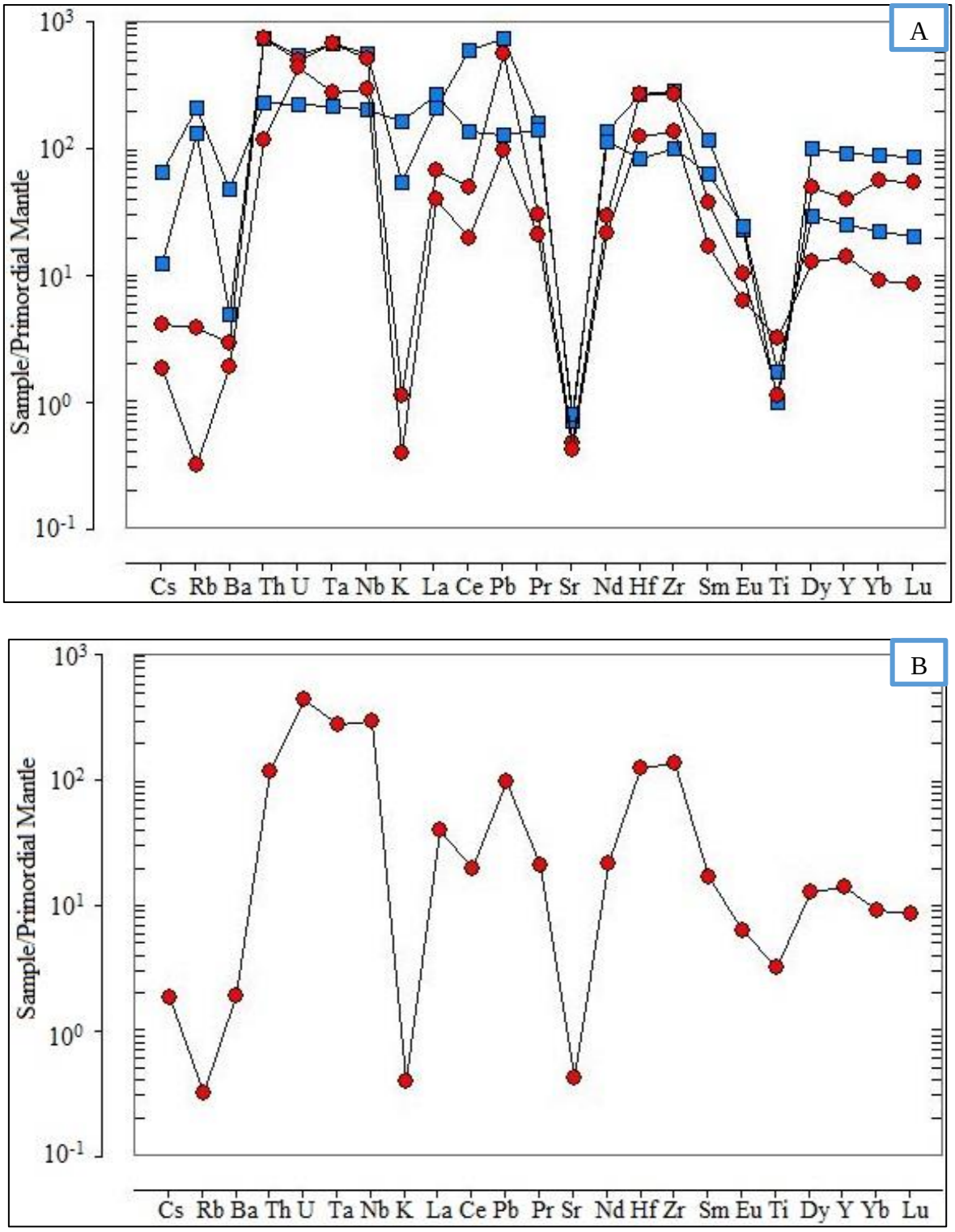

Figure 4.17: *The multi- element variation diagram of kaolin and rhyolite (A) and pure kaolinite (B). Primordial mantle normalizing values are determined from McDonough and Sun (1995).*

4.5. Digital image processing

4.5.1. Introduction

Remote sensing images have been used widely for successful mineral exploration programs. One of the most important mineral commodities identified using these image are clay minerals. In this study, a cloud free Advanced Space borne Thermal Emission and Reflection Radiometer (ASTER) and Landsat 8 Operational Land Imager (OLI) data are used. ASTER consists of 14 bands, namely three visible near infrared (VNIR) bands, six short wave infrared (SWIR) bands and five thermal infrared (TIR) bands. The ASTER image shows higher spectral resolution mainly in the SWIR region. With this spectral resolution identification of specific alteration assemblages becomes possible (Rowan et al., 2005). Such attribute of ASTER makes it efficient to discriminate minerals like clays, carbonates, silica, iron-oxides and other silicates (Kalinowski and Oliver, 2004). However, Landsat 8 consists of eleven spectral bands; five bands in the VNIR, two bands in the SWIR, one band panchromatic and three bands in the TIR.

The study area has considerable vegetation and soil cover which imposes a significant effect up on using remote sensing method. So, this issue is tackled to some extent by using the method in combination with field observations. In order to stand out the different features (lithological units, alteration minerals, geologic structures and vegetation) found in the study area, band ratio and RGB band combination were the two most effective image processing techniques applied to both ASTER and Landsat 8 OLI data. Moreover, spectral reflectance curves of kaolin deposit sites are produced. Finally, the spectral signatures of Belessa kaolin sites are compared with the spectral curve of kaolinite mineral from spectral library and with the kaolin found around Lake Koka, Arsi Zone. All data are processed by using ENVI 4.7 software packages.

4.5.2. Band ratios and their composite images

In this study band ratio method is used to create the RGB band combinations of the image using various efficient band ratio values including Chica-Olma and Abraham's index. These different ratios enable to identify different target features (in this case kaolinite and the host rock). In this section the different types of ratios calculated are also set in RGB color composite in order to improve the discrimination of target features found in the study area. The main features detected by band ratios and band combinations are then simply delineated using colored polygon.

In Landsat 8 OLI**,** combination into red, green and blue channels to produce a false color composite of ratio imageries were obtained using two band ratios; Chica-Olma's and Abraham's ratio. The Chica-Olma index (see Fig. 4.18 A) is represented by RGB values of

6/7:6/5:4/2. Here each observed color depicts different features: red color show clay minerals, green color show Ferrous mineral and iron oxide is represented by blue color. Results from the individual band ratio images display light tones for clay minerals, ferrous mineral and iron oxides in band ratio of 6/7, 6/5 and 4/2 respectively. In figure 4.18 B the order 6/7:4/3:5/6 represents the RGB values of Abraham's index. In this band combination, clay minerals are represented by red color. The green part discriminates vegetation and the blue depicts hydrothermally altered iron oxides (Abhary and Hassani, 2016). In the same way to that of Chica-Olma ratio, the lighter tone in each band ratio represents the corresponding discriminated features. Furthermore, several RGB combinations and band ratios that are related to kaolinite and lithologic units of the study area are also produced using ASTER data.

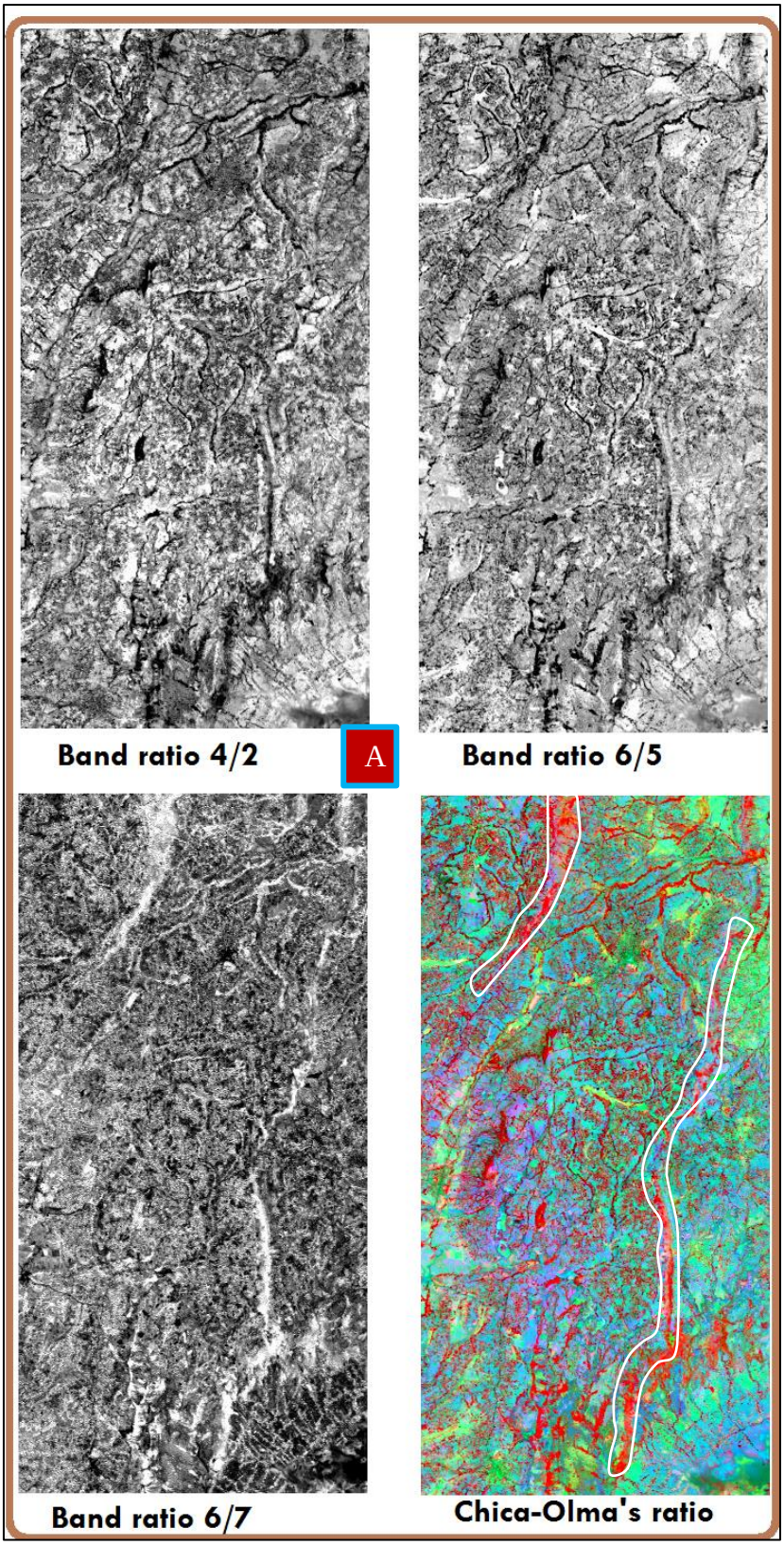
Band ratio 4/2
A
Band ratio 6/5
Band ratio 6/7
Chica-Olma's ratio

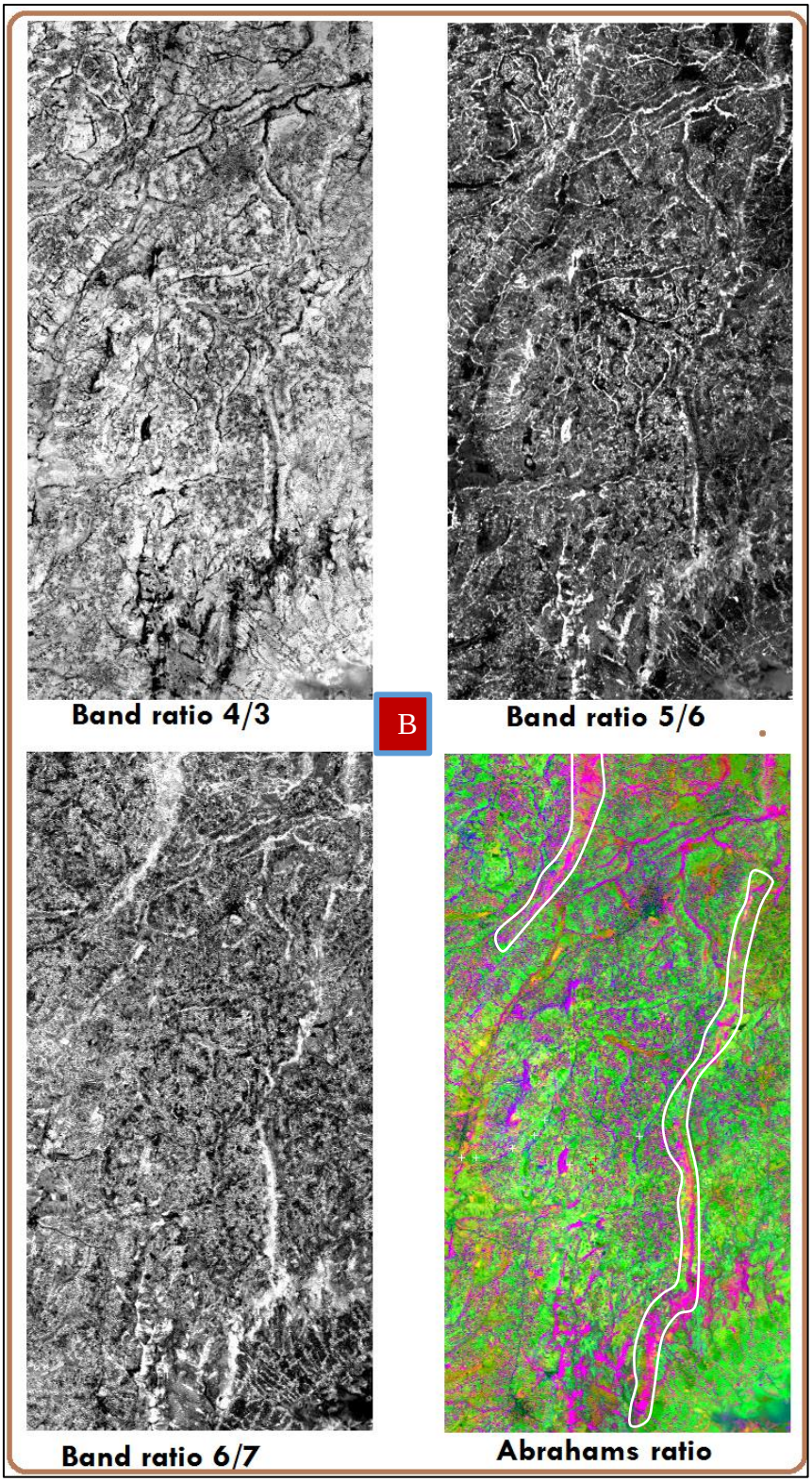

Figure 4.18: *(A). Landsat 8 OLI Images of Band ratios 6/7, 6/5 and 4/2. Chica-Olma ratio image is the RGB color composites of 6/7:6/5:4/2. (B). Landsat 8 OLI Images of Band ratios 6/7, 4/3 and 5/6. Abraham's ratio image is the RGB color composites of 6/7:4/3:5/6.*

ASTER image scenes covering the study area were analyzed to have a general sight on clay mineral alteration and lithological variations. The SWIR ASTER data are especially produced by using band ratios and RGB band composite method to show the altered clay mineral mainly kaolinite and its host rock. For this purpose, highly sensitive band ratios and band combinations are used by juxtaposing the data obtained from field observations. Thus, the host rock (rhyolite) is best discriminated by 9/4 band ratio (see Fig. 4.19 A). The composite RGB images of bands 7, 2, 1 (Fig. 4.19 B) and 7, 3, 1 (Fig. 4.19 C) were also selected for better visual interpretation of the different lithologies and geologic structures found in the study area. The RGB image combination of bands 7, 3, 1 is distinctly most important in standing out the vegetation (shown as green), lithologies, structures and physiography.

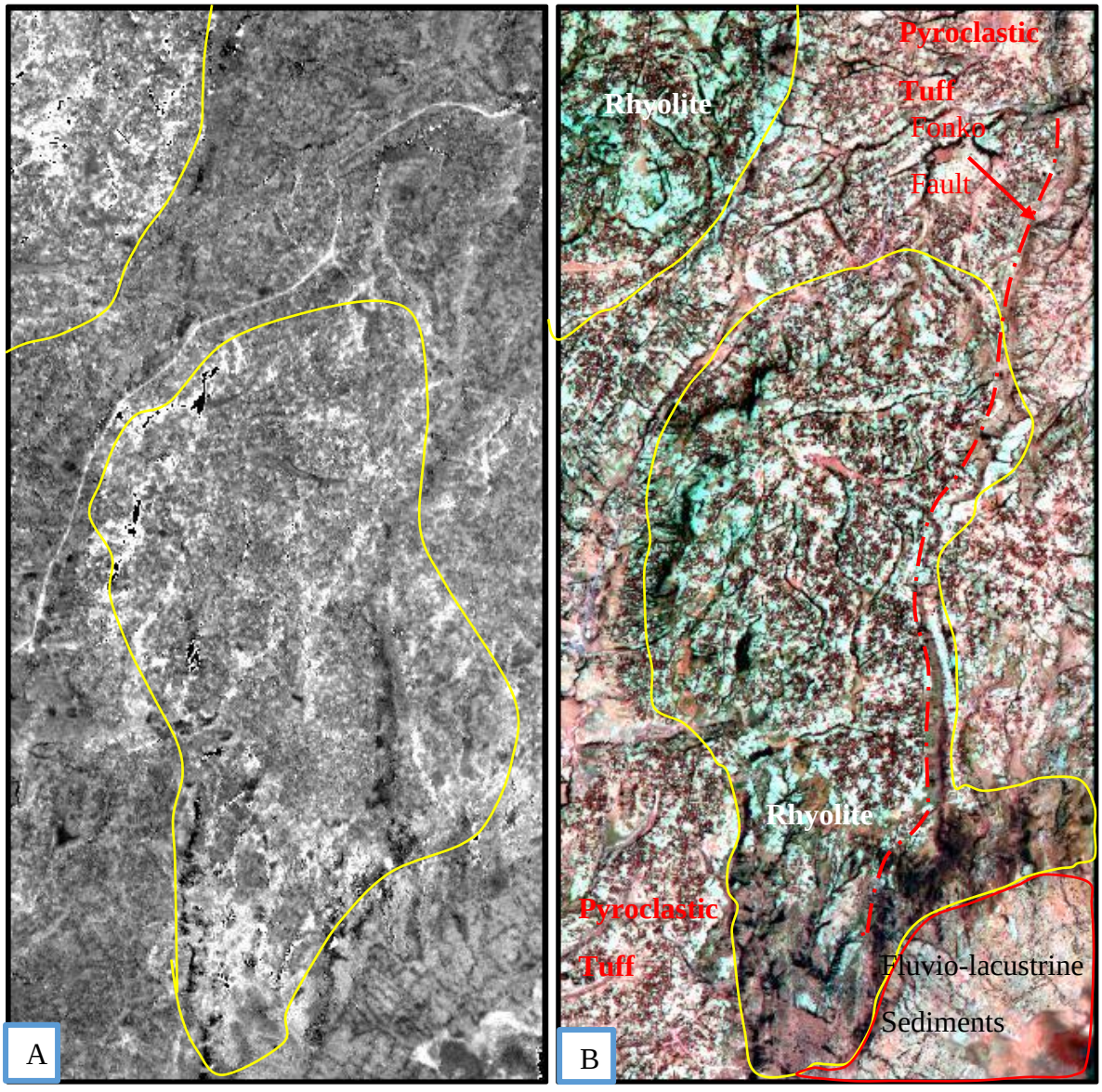

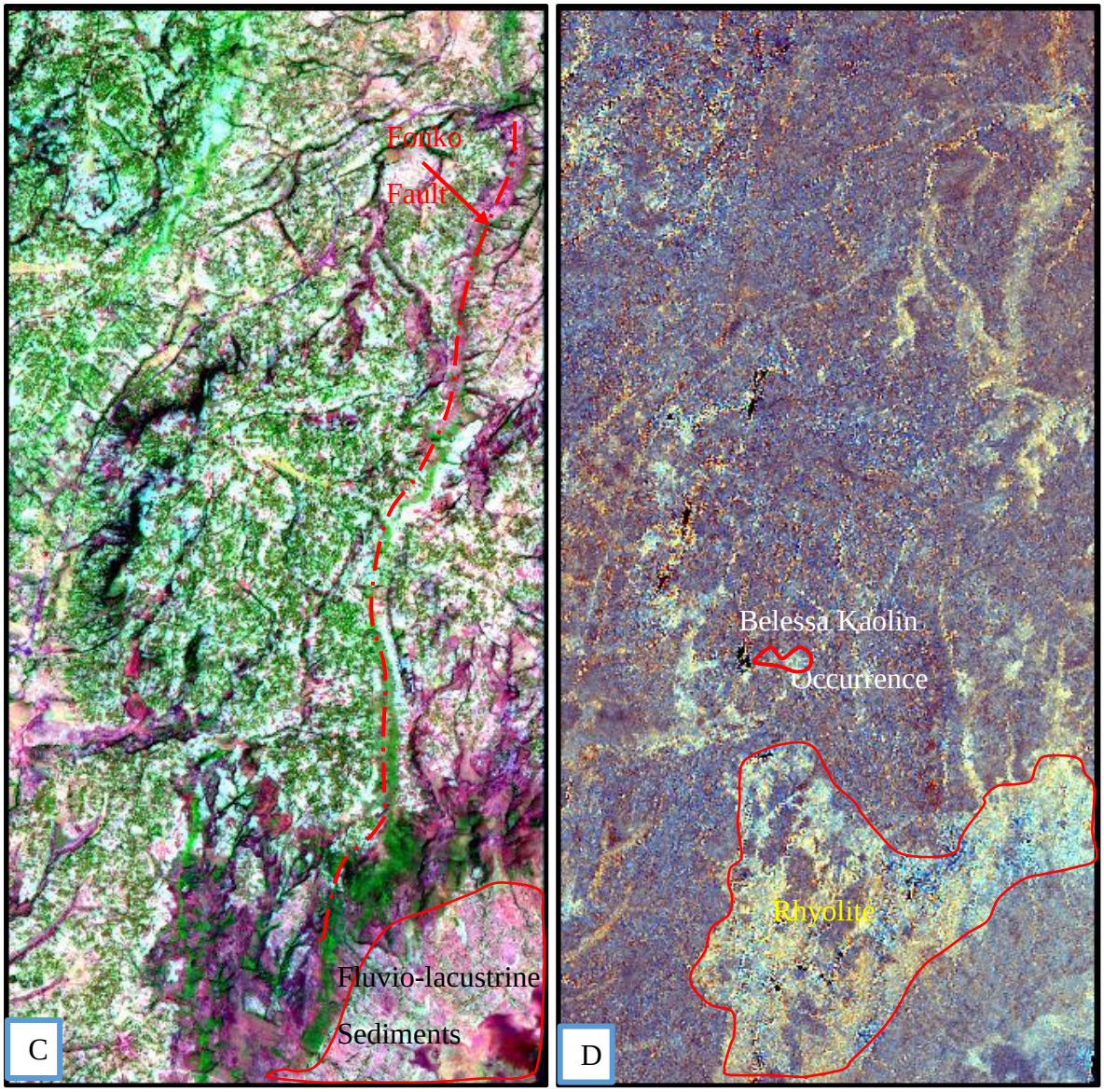

Figure 4.19: *A) ASTER Band ratio of 9/4 ,B) ASTER RGB band combination of 7, 2, 1 C) RGB color combination image of band 7, 3 and 1 in ASTER and D) ASTER Band ratios of 5/6, 7/6, 7/5 in RGB.*

Kaolinite could be discriminated by using the RGB band combinations of R: 5/6, G: 7/6 and B: 7/5 (see Fig. 4.19 D). In this channel, kaolinite is seen as whitish blue color. In other way the kaolinite can also be differentiated using band ratios of (4+6)/5 and 7/5 (see Fig. 20 A and B). Here, kaolinite is identified as white color.

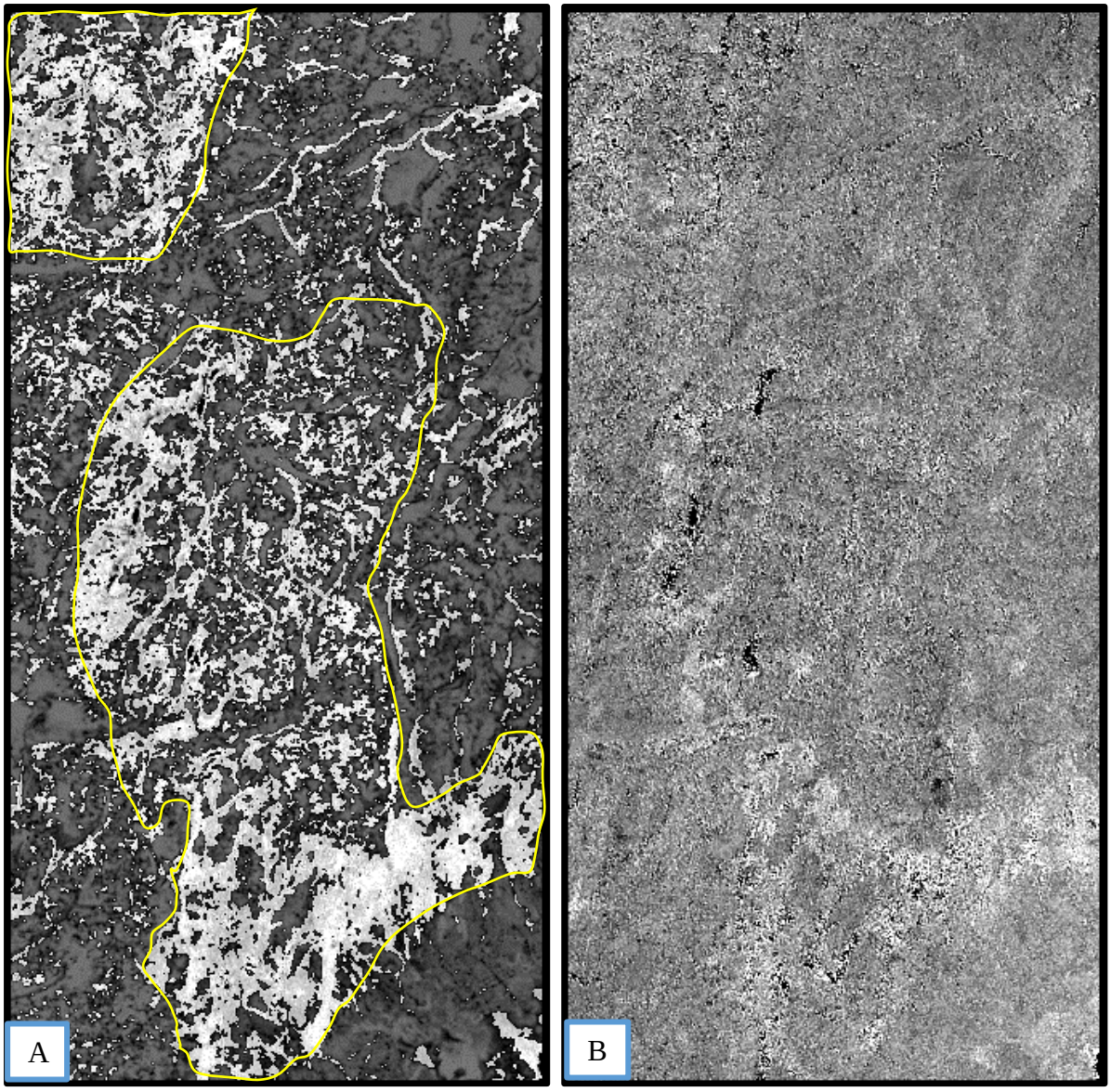

Figure 4.20: *ASTER band ratios (A) (4+6)/5 and (B) 7/5 both depicting kaolinite as white color.*

4.5.3. Comparison of spectral reflectance curves of kaolinites

Using ASTER data spectral reflectance curves of Belessa kaolin taken from two sites are produced (see Fig. 4.21 A and B). Accordingly, the kaolinite shows higher reflectance in the visible-near infrared (VNIR) spectrum and lower reflectance in the short-wave infrared (SWIR) spectrum. To validate the obtained result the spectral curves of Belessa kaolin are also compared with the kaolinite spectral curves (kaolinite CM9 and KL502) taken randomly from spectral library of Envi 4.7 (Fig. 4.21 C and D). Consequently, the spectrums with higher and lower reflectance value showed that the spectral curves of Belessa kaolin are more or less consistent with the spectral curves of kaolinite produced in the laboratory.

Furthermore, the spectral curves of Belessa kaolin are also compared with that of kaolin found around Lake Koka area, Arsi zone, Oromiya regional state. To compare their reflectance values, Landsat 8 OLI and Landsat ETM+ are used for Belessa and Koka kaolins respectively. Such comparison is aimed at producing a preliminary model of spectral signature curves for kaolin occurrences found in the Main Ethiopian Rift. The result in figure 4.22 shows that in all cases the higher reflectance is observed in the short wave infrared band. The lower reflectance is recorded in the visible bands. Therefore, it is noted that the spectrums of highest and lowest reflectance values of Belessa kaolin signature curves are almost consistent with the spectral signature curves of kaolin around Lake Koka.

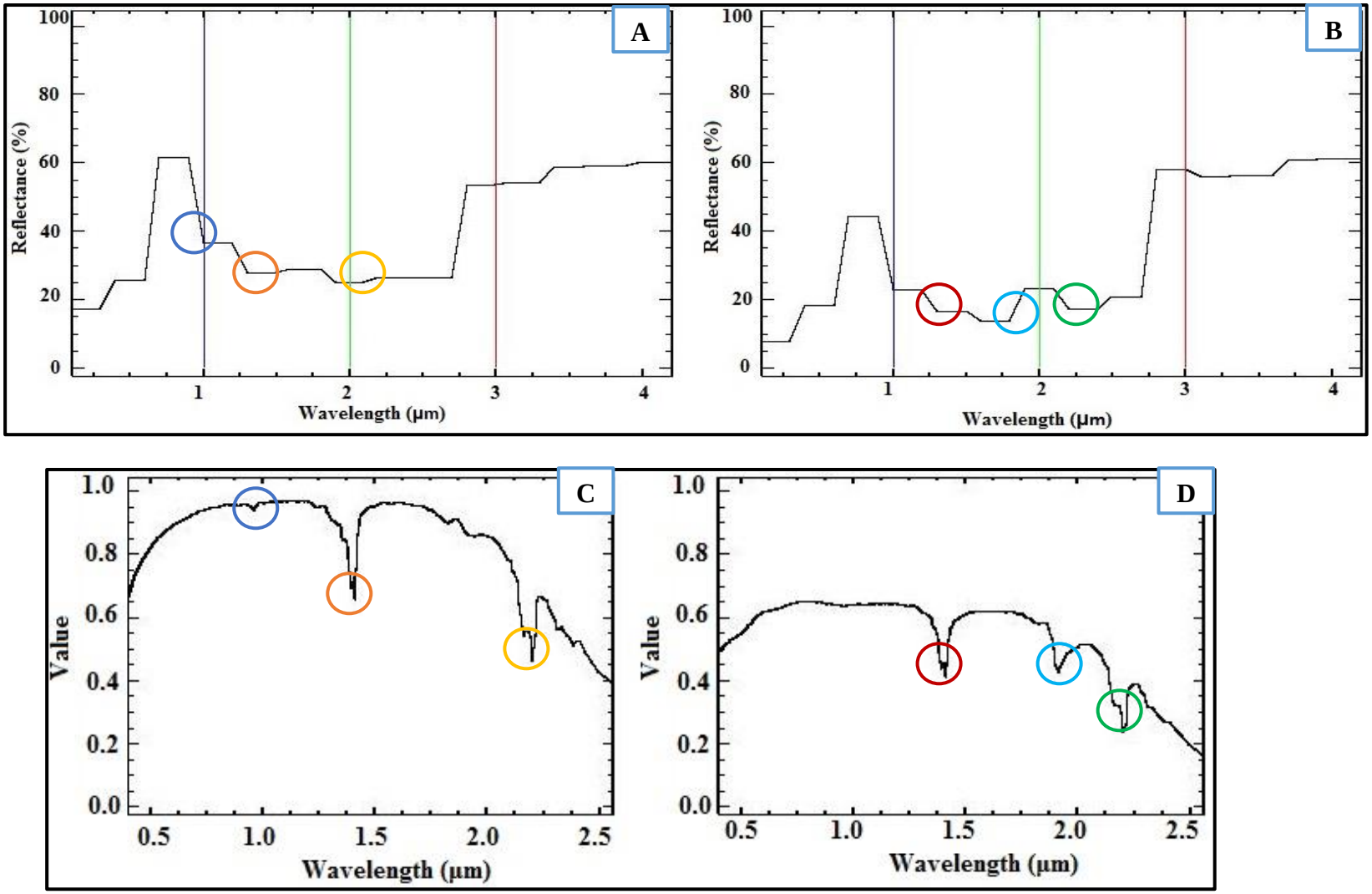

Figure 4.21: *A & B are spectral signature curves of Belessa kaolin produced from ASTER image and C & D are the corresponding kaolinite spectral curves taken from spectral library of Envi 4.7 software [all circles represent low reflectance values].*

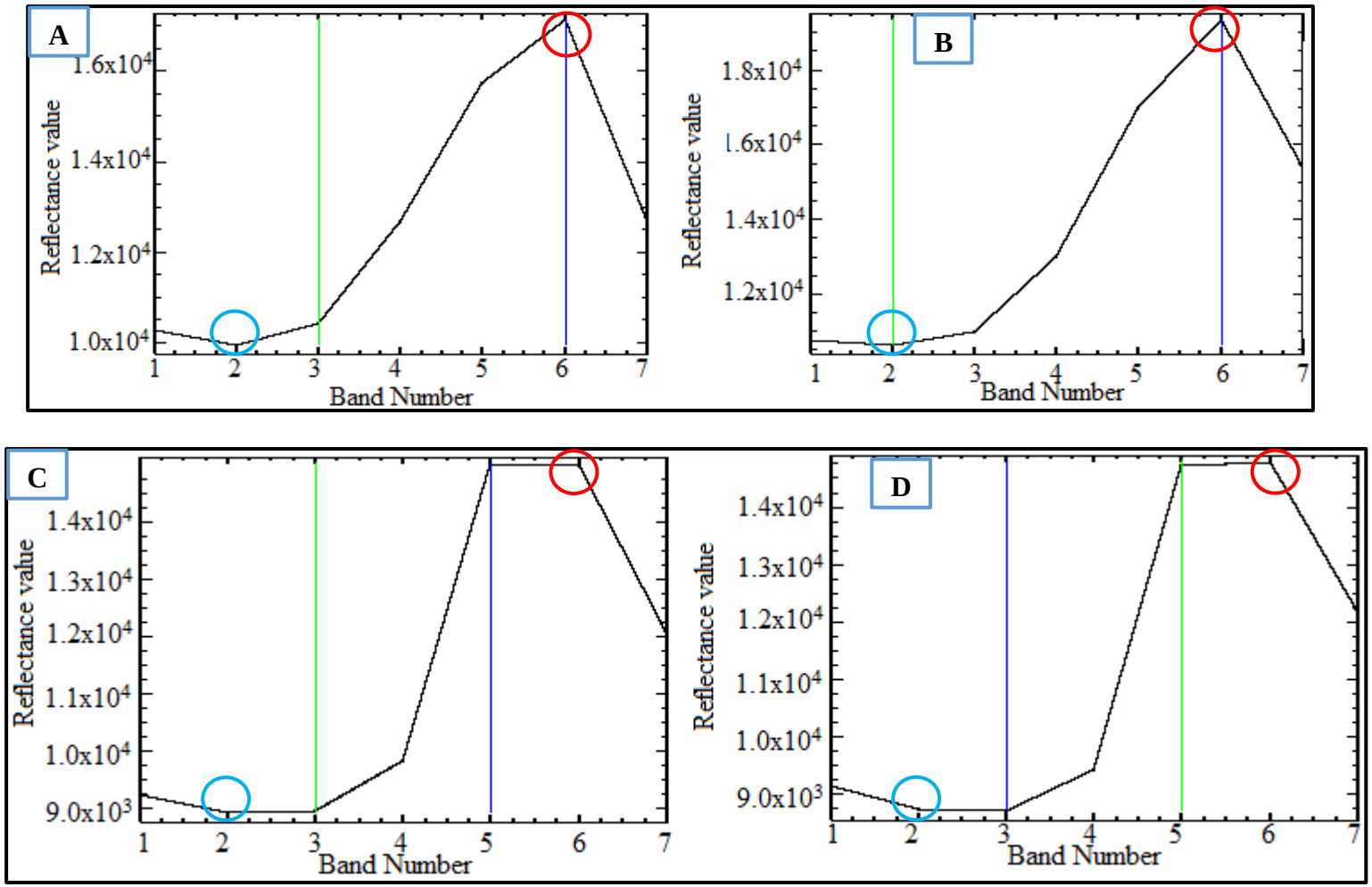

Figure 4.22: *Spectral signature curves. (A) &(B) are for kaolin around lake Koka produced from Landsat ETM+ and (C) & (D) are for Belessa kaolin produced from Landsat 8 OLI.*

CHAPTER FIVE

5. Technological properties and possible fields of applications of Belessa kaolin

5.1. Introduction

To determine the suitability of kaolin deposits for various industrial applications, assessing their technological properties is the key factor. Physical property tests, chemical compositions and crystal morphology are those properties used to assess the quality and commercial viability of kaolin (Murray, 2007). In this study, some available laboratory tests and previous works from Haile Mickael Fentaw (2003) are used to elucidate the possible industrial applications. Furthermore, Belessa kaolin is compared with the known world kaolin deposits, international standards and specifications required by different industries.

5.2. Technological Properties

Belessa kaolin deposits are characterized by different technological properties. Grain size analysis results are taken from the study of Haile Mickael Fentaw (2003). Whereas, density (bulk and specific gravity) and pH are among the available laboratory tests used in the present study. The color is used here by simple observation and comparing it with Munsell Soil Color chart. Moreover, the major oxide, some trace element and crystal morphology results are also used in examining the possible applications. In this sub-section, investigation results of these properties are briefly discussed.

Particle size distributions and color are the critical factors in assessing kaolin for various industrial applications. Thus, along with its color kaolin is commercially more valuable when it is fine particle size. Table 5.1 and figure 5.1 shows the grain size analysis result obtained from Haile Mickale Fentaw (2003). According to these data, the particle size distributions show that the kaolin is rich in terms of clay size fractions (63 % <2 μm), while silt and sand are less abundant. The particle size of Belessa kaolin also contains acceptable critical points (<2 μm, < 10 μm and > 53 μm) which are in agreement to most of the industry specifications. Regarding the qualitative determinations of color, the pure kaolinite sample is characterized by white color and it is comparable with the white color found in the Munsell Soil Color chart. The quartz bearing kaolin samples show gray and pink color. The chemical data revealed that Fe_2O_3 is the primary discoloring agent for quartz bearing kaolin samples.

Table 5.1: *Particle size distributions, Haile Michael Fentaw (2003). A) Weight % of grain size distributions and B) Cumulative weight % of the less than given size fractions [Both samples are from pure kaolinite].*

A

Sieve Size (µm)	Percent Passing (%)		
	Sample A	Sample B	Average
<0.63	49.95	56.14	53.045
0.63-2.0	14.78	5.09	9.935
2.0-6.3	7.69	6.49	7.09
6.3-16	15.28	13.48	14.38
16-40	11.58	16.78	14.18
40-63	0.59	1.89	1.24
>63	0.089	0.095	0.092

B

Sieve Size (µm)	Percent Passing (%)		
	Sample A	Sample B	Average
<0.63	50	56.2	53.1
<2.5	64.8	61.3	63.05
<6.3	72.5	67.8	70.15
<16	87.8	81.3	84.55
<40	99.4	98.1	98.75

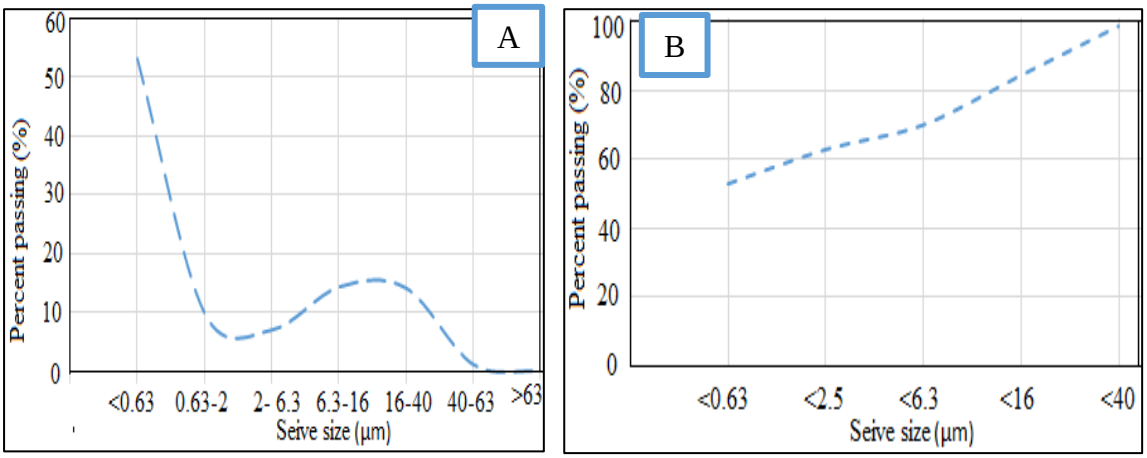

Figure 5.1: *Graphs showing the particle size distributions of Belessa kaolin.*

The shape or morphology of kaolinite crystals is also an important property to explain the possible applications of kaolin. The dominant morphology is characterized by a platy hexagonal kaolinites with regular shape which corresponds to a well crystallized kaolinite particles. This is also confirmed by a sharp diffraction patterns indicating high degree of crystallinity (Chakraborty, 2014).

Suspension yield stresses and viscosities are determined indirectly from the calculation of Hinckley index. Low crystallinity kaolinite is known to have higher suspension yield

stresses and viscosities (Ndlovu, et al., 2014). Thus, the HI calculation result show that Belessa kaolin is characterized by a higher HI (high crystallinity kaolinite) and thus it has lower suspension yield stresses and lower viscosities.

The measured pH values for pure kaolinite BHR-0054 (7.14) and quartz bearing kaolin BHR-0017 (6.65) shows the samples are almost neutral and slightly acidic respectively. The specific gravities (BHR-007C; 2.41, BHR-0053B; 2.66 and BHR-0054; 2.59) are close to the physical constants of kaolin (2.6) Murray (2007) and according to Lambe and Whitman (1979) close to the specific gravity of pure kaolinite (2.62 to 2.66). The bulk density value of 1.44 is also measured for the pure kaolinite sample (BHR-0054).

Based on mineralogical and major element compositions, Belessa kaolin can be divided in to two. The pure kaolinite with higher alumina content and the one with lesser alumina content which is composed of kaolinite and quartz. For pure kaolinite sample, the ratio for SiO2/Al2O3 concentration shows 1.24 which according to Ekosse (2001) is close to ratio of the ideal kaolinite (1.18). Compared to the commercial world kaolin deposits (Georgia, USA and Cornwall, United Kingdom), Belessa kaolin deposit with pure kaolinite has quite comparable chemical compositions having only lower Fe2O3 and MgO and higher P2O5 (see table 5.2). However, kaolin sample (BHR-0017) with less kaolinite shows higher Fe2O3 content (1.84 %) than the maximum allowed limit of 1 % Fe2O3 (Highley, 1984). Moreover, samples with low kaolinite mineral also show low alumina and high Fe2O3 probably due to entrance of Fe in to kaolinite structure and replacement of Al in the octahedral layer (Murray and keller, 1993). Most kaolin samples also show lower concentration of Fe2O3 and TiO2 contents which increases their practical applications. The specifications related to the geochemical data are more important when kaolin is used for industries like ceramic, fiber glass and refractory. The pure kaolinite sample (BHR-0054) shows major oxide values that are acceptable to the most of industry specifications (46.7 % SiO2, 37.5 % Al2O3, 0.14 % Fe2O3, 0.57 % TiO2 and 14.6 % LOI). These data are also quite comparable to the known world kaolin deposits explained in table 5.2.

The physical and chemical properties of Belessa kaolin also showed some notable correlations. This means that, chemical properties have direct bearing on the physical properties of kaolin. This scenario can be observed from properties like grain size and color. For instance, the increase in alumina (Al_2O_3) concentration resulted in more kaolinite content which in turn cause in finer grain size distributions. The higher amount of Fe_2O_3

concentration also showed a significant effect on the color of quartz bearing kaolin samples (BHR-0016B, BHR-0017, BHR-0051 and BHR-0053B) being a major discoloring agent.

5.3. Possible Fields of Applications

The fineness of particle sizes and the acceptable ranges of mineralogical and geochemical compositions make Belessa kaolin useful to various industries. The platy and hexagonal form of kaolinite crystals is also an important characteristic to indicate the deposit in some industrial applications. Chemistry is vital for kaolin to be used in refractories and fiberglass (Pruet, 2016). The low iron, titanium and alkalis concentration could make the pure kaolinite (BHR-0054) and some quartz-bearing kaolin (BHR-0053B) are fit for use in refractory and fiberglass. The pure kaolinite also possesses acceptable properties like chemistry, mineralogy, grain size and color to be used for certain ceramic applications. Also, the halloysite in southern parts of the study area (BHR-0051) could have potential applications in ceramic industry as an additive in the manufacture of high quality dinnerware. Kaolin for pigments and additives require relatively simple specifications containing from nearly pure kaolinite to kaolin having up to 90 % quartz particles (Pruet, 2016). Thus, all Belessa kaolin samples can be used for these two applications. Moreover, the grain size specifications (Murray, 2007) for kaolin used as fillers in paper (40 – 60 % < 2 μm) correlates with the pure kaolinite of Belessa. Because pure kaolinite is relatively white color and free of iron oxides (discoloring impurities), it could have a potential application in paper coatings. The pure kaolinite (BHR-0054) is also suitable for adhesives and sealants for its platy morphology and white color.

In table 5.2, 5.3, 5.4 and 5.5, Belessa kaolin is compared with the specifications of different industries and known world kaolin deposits. Based on available technological properties of Belessa kaolin, the most suited applications are also indicated. The characteristics listed in the tables are not the only ones specified for the industries. But, they are selected based on the available data and laboratory tests of the current study. Therefore, it is understood that with all the limitations of the remaining technological properties, Belessa kaolin could be used in major fields of industries; paper coating, filler (in paper, rubber, plastic and paint), ceramics, pharmaceuticals and cosmetics. However, it should also be noted that this kaolin may require some modifications during processing to meet stringent specifications found in some industries.

Table 5.2: *Chemical and mineralogical composition of Belessa kaolin compared with the world kaolin deposits and specifications of some industries.*

Chemical composition (wt %)	**Ethiopia (This work)**		**World kaolin deposits**					**Industries**			
	Belessa BHR-0053B	Belessa BHR-0054	USA*, (Georgia)	UK*, (Cornwall)	Pakistan*, (Shah Dheri)	Botswana* (Makoro)	Brazil,* (Capim)	Paper* coating ⊕	Paper* filler ⊕	Ceramics * ⊕	Pharmaceuticals and Cosmetics* ⊕
SiO2	64.2	46.7	45.3	46.8	45.3	51.1	44.8	45-49	46-48	48-50	44.6-46.4
TiO2	0.21	0.57	1.4	< L.D.	0.5	1.5	0.55	0.5-1.3	0.5-1.5	0.02-0.1	0-1.4
Al2O3	24.2	37.5	38.4	37.8	36.8	32.0	38.3	36-38	37-38	36-37	38.1-39.5
Fe2O3	0.4	0.14	0.3	0.4	0.8	1.8	0.51	0.5-1	0.5-1	0.6-1	0.1-0.2
CaO	0.02	0.09	0.1	0.1	2.0	0.1	<0.02	-	-	-	0.1-0.2
MgO	< L.D.	0.01	0.3	0.2	0.5	0.2	<0.55	-	-	-	0.1-0.2
Na2O	0.04	< L.D.	0.3	0.2	1.0	0.1	0.13	-	-	-	0-0.1
K2O	0.03	0.01	0.0	1.5	0.2	0.1	<0.02	0.5-1.5	0.5-1.5	1.2-2.7	0-0.2
MnO	< L.D.	< L.D.	< L.D.	< L.D.	< L.D.	0.0	-	-	-	-	-
P2O5	0.01	0.01	< L.D.	< L.D.	< L.D.	0.1	-	-	-	-	-
LOI	9.29	14.6	14.0	13.0	< L.D.	14.8	14.4	-	-	11.2-12.5	13.8-13.9
Mineralogy Kaolinite (%)	59.9	100						93-99	90-95		

**Makoro Kaolin: Ekosse, (2000), Georgia kaolin and Cornwall kaolin: Murray and Keller, (1993), Shah Dheri: Siddiqui, et al (2005), Capim: - Paper coating, paper filler and ceramic standards: Siddiqui et al., 2005 and Pharmaceuticals and Cosmetics: Lopez-Galindo et al., (2007). Possible applications of Belessa (⊕).*

Table 5.3: *Technological properties of Belessa kaolin for utilization as a ceramic raw materials*

Characteristics	**⊕ Ceramic industry**			**Belessa Kaolin (Haile Mickael, 2003)**		**Belessa kaolin (This work)**		
	[a] Grade* I	**[b] Grade* II**	**[c] Grade* III**	**A**	**B**	**BHR-0054**	**BHR-0017**	**BHR-0053B**
Fineness (> 44 µm in %)	0.5 (max)	1 (max)	2 (max)	0.6 (>40 µm) [a]	1.9 (>40 µm) [c]	-	-	-
LOI (wt %)	13 (min)	12 (min)	10.5 (min)	14.74 [a]	13.62 [a]	14.6 [a]	9.66	9.29
Al2O3 (wt %)	37 (min)	34 (min)	32 (min)	37 [a]	36.86 [b]	37.5 [a]	24.1	24.2
Fe2O3 (wt %)	0.8 (max)	1 (max)	1.5 (max)	0.25 [a]	1.03 [c]	0.14 [a]	1.84	0.4 [a]
TiO2 (wt %)	0.7 (max)	0.8 (max)	1 (max)	0.5 [a]	0.71 [b]	0.57 [a]	0.47 [a]	0.21 [a]
Fe2O3 + TiO2 (wt %)	1.5 (max)	1.8 (max)	2.5 (max)	0.75 [a]	1.74 [b]	0.71 [a]	2.31 [c]	0.61 [a]
Grain size dist.(%, max)								
>25 µm	5	7	10	12.26 (> 16 µm)	18.76 (> 16 µm)	-	-	
>10 µm	15	20	25	27.54 (>6.3 µm)	32.24 (>6.3 µm)	-	-	
<2 µm (min)	70	65	60	64.73 [c]	61.23 [c]	-	-	
Color	pink	white	white	white [b &c]	white [b &c]	white [b &c]	gray	pink [a]

****IS: 2840, 1965 in*** *Saikia et al. (2003).* ⊕*: Possible applications of Belessa.*

Table 5.4: *Technological properties of Belessa kaolin for utilization as filler in paper, rubber, plastic and paint industry.*

Characteristics	Filler in paper* ⊕	Filler in rubber, plastic, paint, etc.* ⊕	Belessa Kaolin (Haile Mickael, 2003)		Belessa kaolin (This work)	
			A	**B**	**BHR-0054**	**BHR-0017**
Grain size (%)						
>53 µm (max)	0.8	1	0.679 (>40 µm)	1.985 (>40 µm)	-	-
>10 µm (max)	5	15	27.54 (>6.3 µm)	32.24 (>6.3 µm)	-	-
<10 µm (min)	75	60	87.8 (<16 µm)	81.3 (<16 µm)	-	-
LOI (%, max)	14-15.5	14-15.5	14.74	13.62	14.6	9.66
Fe2O3 (% max)	0.6	0.75	0.25	1.03	0.14	1.84
Whiteness	80-85 %	-	white	white	white	-
PH	4.5-7.5	4.5-7.5	-	-	7.14	6.65
MnO (% max)	0.013	-	0.01	0.01	< D.L.	0.03

Indian standard specifications: IS: 505, 1978: Saikia et al. (2003). <D.L.-Below detection limit.⊕ Possible applications of Belessa.

Table 5.5: *Summary on the chemical and mineralogical composition specifications of industries and possible applications of Belessa kaolin.*

Chemical composition (wt %)	**Belessa kaolin**		**Specifications of Industries**							
			Paper coating		Paper filler		Ceramics		Pharmaceuticals and Cosmetics	
	Belessa BHR-0053B	Belessa BHR-0054		Status		Status		Status		Status
SiO2	64.2	46.7	45-49	•	46-48	•	48-50	x	44.6-46.4	•
TiO2	0.21	0.57	0.5-1.3	•	0.5-1.5	•	0.02-0.1	x	0-1.4	•
Al2O3	24.2	37.5	36-38	•	37-38	•	36-37	•	38.1-39.5	x
Fe2O3	0.4	0.14	0.5-1	x	0.5-1	x	0.6-1	x	0.1-0.2	•
CaO	0.02	0.09	-		-		-	-	0.1-0.2	•
MgO	< L.D.	0.01	-		-		-	-	0.1-0.2	x
Na2O	0.04	< L.D.	-		-		-	-	0-0.1	•
K2O	0.03	0.01	0.5-1.5	x	0.5-1.5	x	1.2-2.7	x	0-0.2	•
MnO	< L.D.	< L.D.	-		-		-	-	-	-
P2O5	0.01	0.01	-		-		-	-	-	-
LOI	9.29	14.6	-		-		11.2-12.5	x	13.8-13.9	x
Mineralogy						x		-	-	-
Kaolinite (%)	59.9	100	93-99		90-95					

- : Suited chemical compositions and x: improvement is required.

CHAPTER SIX

6. Discussion

6.1. Alteration Phenomena

Data from the major element geochemistry (see table 4.2) showed that the rocks in the region have relatively low concentration of the mafic compounds (TiO_2, MgO and Fe_2O_3). On the contrary, they have higher concentration of felsic compounds (SiO_2 and Al_2O_3). Moreover, they have relatively more concentration of Na_2O and K_2O than CaO because of the abundance of alkali-feldspar. As can be seen from section 4.4.1 and table 4.2, the average contents of SiO_2 and Fe_2O_3 decrease going from the hosting rhyolite to the kaolin ores. While, the average contents of Al_2O_3 and LOI increase (see figure 4.11 and figure 4.12). Changes in such chemical composition indicate the effect of alteration by removal of SiO_2 and Fe_2O_3 and concentration of Al_2O_3.Thus, the high SiO_2 content and low Al_2O_3 content in the rhyolite samples is due to low degree of alteration (Fig.4.11). Conversely, the pure kaolinite sample number BHR-0054 shows the lowest SiO_2 and the highest Al_2O_3 content indicating higher degree of alteration. Moreover, the pure kaolinite (BHR-0054) showed a complete leaching of Na_2O and MnO. According to some authors (Eg. Meyer and Hemley, 1967, Meunier et al., 1983), this phenomenon corresponds to the higher mobility of these oxides during kaolinization processes. In addition, the triangular diagrams in section 4.4.1 showed that Belessa kaolin deposits contain lowest Fe2O3, TiO2, MgO and alkali elements. In contrary it shows alumina enrichment. The highest LOI values for all kaolin samples are also possibly due to the later alteration. From triangular diagrams containing SiO_2 –Al_2O_3-Fe_2O_3 in figure 4.12, a clear shift in Fe2O3 is observed in kaolin sample number BHR-0051. The mineralogy of this sample contains halloysite, sanidine and quartz indicating that halloysite and sanidine are not transformed yet to kaolinite. Thus, the Fe shift could be explained by an early stage of alteration.

The type and abundances of clay minerals are significantly affected by the degree of weathering (Duzgoren and Aydin et al., 2002). Thus, the intensity and time interval of weathering and alteration have the ability to dictate the percentage of clay minerals. In the case of Belessa kaolin, the low and high values obtained from CIA and CIW calculation in section 4.4.1 refer to a change from parent rock to a highly altered kaolinized rock .The CIW and CIA result are also consistent with the mineralogical result indicating the condition has favored the formation of kaolinite. Therefore, the chemical index value indicates that Belessa kaolin underwent through intense leaching processes that resulted in

the formation of kaolinite. Moreover, by examining the variation diagrams (Na_2O & K_2O against Al_2O_3) and ternary systems (A-CN-K and A-CNK-F) in figure 4.13 C and 4.14 respectively, it is observed that the mobile elements Ca, Na and K are removed from feldspar increasing the alumina concentration which ultimately results to the formation of clay mineral (kaolinite). In general, the major element data showed that the altered rock is dominated by Si and Al, indicating the high content of kaolinite mineral which is consistent to the mineralogical result. In other way, the loss of alkalis (K_2O+ Na_2O) is attributed to the alteration (kaolinization) of alkali feldspar.

Furthermore, the similar chondrite-normalized REE patterns of the ores and surrounding rhyolite suggest that the latter is parent rock to the kaolinite ore (Fig. 4.15). The kaolin samples show a relative enrichment in the Ce-family or LREE (La, Ce, Pr and Nd) due to their less mobility than other REE. The REE patterns also shows a negative Eu and Ce anomalies and a slightly positive Gd and Lu anomalies. This demonstrates that the kaolin deposit is derived from weathering of acidic source rock (Da costa and Moraes, 1988 cited in Ghadimian and Khodami, 2015). The negative anomaly of Eu in combination with small amounts of Sr, Na2O and K_2O shows the extreme weathering of K-feldspar from the parent rock (Mclennan and Taylor, 1991). In multi element variation diagram (see Fig. 4.17) the depletion of Belessa kaolin ore in Rb, k and Sr reflects their corresponding removal during kaolinization process because of their high mobility. Moreover, the depletion at Ti could be due to the substitution of Cr for tetravalent Ti in TiO_2 (Dill et al., 1997).

6.2. Genesis of Belessa kaolin deposit

This work tried to indicate the genesis of Belessa kaolin by presenting evidences like geological settings, mineralogical, geochemical signatures and morphological studies. These evidences along with the field characteristics and data presented in section 4 strongly support that the supergene (weathering) processes plays the main role to the formation of Belessa kaolin. In addition, this study revealed the absence of hydrothermal activities (quartz veining and high temperature minerals) that are related to the formation of kaolin deposits.

From geological setting it is observed that, the volcanic rocks of the region are not well exposed except by streams and quarries. This is due to the thick soil covers developed by meteoric weathering. The thickness of the soil cover varies from 5 meters to 30 meters. At the kaolin deposit, the soil thickness is minimal probably due to erosion because the area is highly susceptible to erosive activities. This suggests that weathering has played an

important role in the kaolinization process. Also in the field, the absence of quartz veins and the gradual change from partly altered rocks to completely altered kaolinized zone could tell the kaolinization process has no relation to hydrothermal activities.

In the geochemical study, trace elements are used to indicate the origin of kaolinization. The binary diagram containing Ce + Y + La and Ba + Sr suggested by Dill et al. (1997) is used to differentiate the kaolinization processes as supergene and hypogene type. The hypogene type consists of higher Ba + Sr. Conversely, the supergene type kaolin is characterized by having higher Ce + Y + La. Accordingly all Belessa kaolin samples fall in the supergene zone (Fig. 6.1). Moreover, it is also supported by the characteristics of Thorium in the kaolin deposit. Thorium in this study only slightly changed during alteration because it is highly mobile in acidic environment. The enrichment of this element shows that the pH condition during alteration is high; or not too acidic (Ghadimian and Khodami, 2015). Therefore, this scenario also supports the supergene origin of Belessa kaolin. The geochemical study also shows low P and high Cr + Nb concentrations. According to Dill et al. (1997), this implies a condition of supergene origin. Furthermore, the CIA (99.7 %) value stated in section 4.4.1 shows higher values that corresponds to the CIA values (85 - 100 %) of residual clays suggested by McLennan and Taylor (1991).

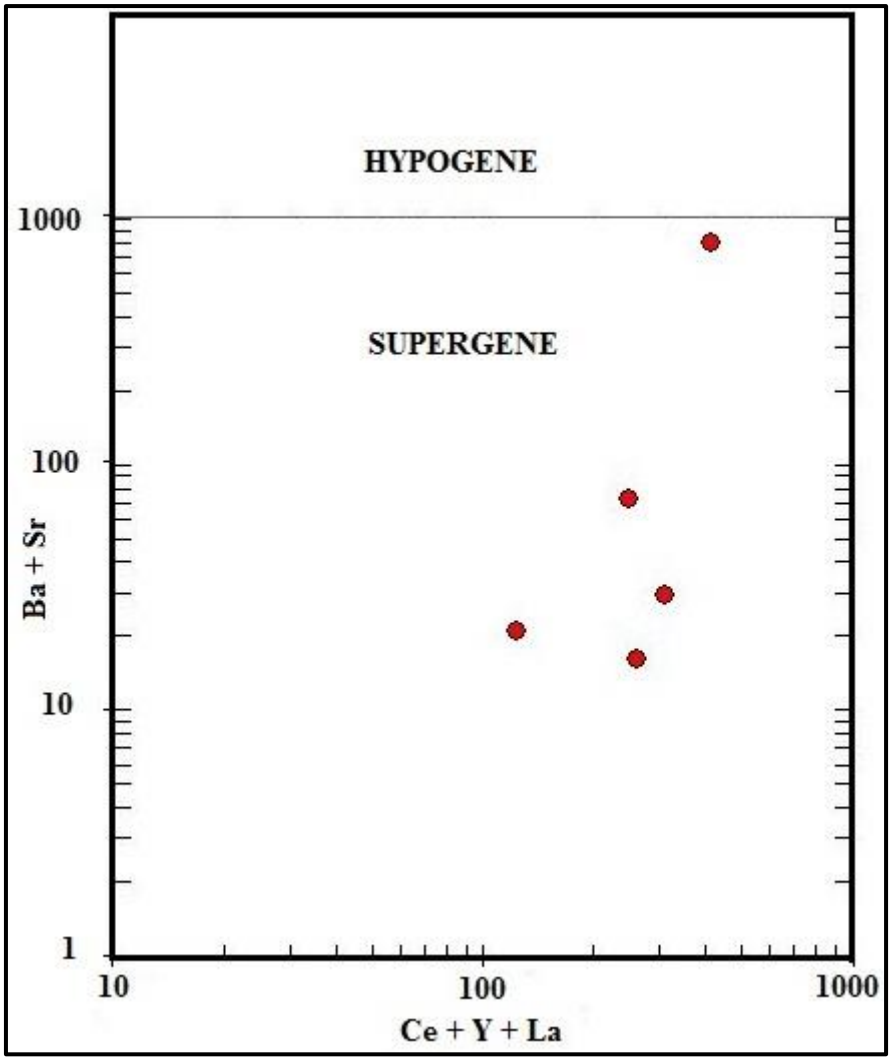

Figure 6.1: *Binary diagram showing the supergene- hypogene zone for kaolin samples: Dill et al. (1997).*

The Mineralogical determinations also agree with the geochemical results. Thus, XRD result identified only kaolinite and quartz minerals as major phases in the mineralogical compositions of the kaolin deposits. According to Nakagawa (2006), the presence of only kaolinite and quartz minerals is indicative to a weathering origin type kaolin deposits. More over the presence of these minerals demonstrate the felsic host rock (Velde, 1995). It is also known that hydrothermal kaolin deposits are usually associated with high temperature alteration minerals like pyrophyllite, diaspor, dickite, nacrite and topaz (e.g. Arribas et al., 1995; Dill et al., 1997). The absence of such diagnostic minerals in Belessa kaolin can be also used as a strong evidence to support a supergene (weathering) origin.

Furthermore, Baumann and Keller (1975) used bulk density of kaolin deposits to show their mode of genesis. According to them, those kaolins originated from weathering process have

low bulk density values (less than 2). In contrast, the hydrothermal origin kaolin show greater bulk density values (greater than 2). In this study, Belessa kaolin shows a bulk density value of 1.4, further suggesting weathering process as a responsible cause for the kaolinization.

6.3. Utility of band ratios, band combinations and spectral curve analysis

In this study, ASTER and Landsat 8 OLI data have been examined to determine the best band ratios and RGB band combinations in identifying the different lithologies, vegetation cover, kaolin host rock, clay minerals and geologic structures found in the study area. Despite the fact that vegetation and soil cover affects some parts of the image products, it is observed that ASTER image is better than the Landsat 8 OLI in standing out the features. Accordingly, ASTER RGB band combination of R: 7, G: 2, B: 1 in figure 4.19 (B) has discriminated the major geologic units (rhyolite, pyroclastic tuff and fluvio-lacustrine sediments) which are in agreement to the field investigations commenced. In this band combination the rhyolite is distinguished by dark brown color. The pyroclastic tuff appeared light gray to brown, while lacustrine sediments are identified by brown color. In figure 4.19 (A), ASTER band ratio of 9/4 were utilized to better discriminate the kaolin host rock (rhyolite) and its tonal color showed cloudy view. Moreover, the vegetation cover is clearly identified using ASTER Band ratios of 5/6, 7/6, 7/5 in RGB (see Fig.4.19 C). ASTER band ratios of (4+6)/5 and 7/5 also depicts kaolinite mineral as white color (Fig. 4.20). Both Chica-Olma's (R: 6/7, G: 6/5 and B: 4/2) and Abraham's ratio (R: 6/7, G: 4/3 and B: 5/6) from Landsat 8 OLI were used to enhance mainly that of clay minerals which are highlighted in the images in red. As can be seen from figure 4.18 (A) and (B), the clay minerals are mostly distributed following the weak zones (major faults: Fonko faults and parts of the Guraghe border fault and lineaments).

Furthermore, spectral reflectance curves of Belessa kaolin are extracted from ASTER and Landsat data. The results are then compared with spectral curves of Koka kaolin from Arsi Zone and kaolinite spectral curves from ENVI 4.7 library (see Fig. 4.21 and 4.22). Consequently, it is observed that Belessa kaolin showed a comparable result that gives spectral curves of kaolinite which could be used as a preliminary model for the kaolin occurrences found in the MER region.

6.4. Critical properties controlling quality and possible industrial applications

Taking into considerations all limitations on the remaining physical property tests and required beneficiation processes, some possible fields of applications could be

recommended. Thus, Belessa kaolin can be used in various industries; such as ceramic, pharmaceuticals, cosmetics, plastic, rubber, paper, sanitary wares, as filler and coatings. Along with the details of industry specifications pointed out in section 5.2, some critical physical, chemical and crystal morphology properties of Belessa kaolin are vital to strengthen the possible applications. In this study the pure white color kaolinite is related to lower concentration of Fe_2O_3 and TiO_2 which shows the probability of having high brightness. So, the kaolin with white color (BHR-0054) can have a potential application in pharmaceutical and paper industry. Belessa kaolin can be also used in refractory because it has lower concentration of alkaline elements and higher concentration of alumina. The kaolin also contains elements like Mn, Fe and Cu not exceeding 5 ppm concentration which allows its function in rubber and plastic industries (Ekosse, 2000). From the aspect of particle shape, the kaolin shows large and small hexagonal crystals, both ordered, platy and highly crystalline. This is also confirmed from HI calculation results in section 4.3. The high HI values show low defect and well crystallized kaolinite particles with smooth platy surface and defined edges. This property can make the kaolin to be used for sanitary wares (De Souza Santos, 1993 cited in Ekosse, 2000). In most cases, the pure and white color kaolinite has low viscosity due to low surface charge, low surface area and low ion exchange (Murray, 2007). Such property could make the pure Belessa kaolinite a prime pigment and extender in paper coating, paints and other applications.

6.5. Major markets and development opportunities

Because most industrial minerals are consumed in bulk, their tonnage can be considered as one of the main factors that could prevent a resource from being converted into a reserve. Depending only on the present information, the tonnage of Belessa kaolin could restrict the resource from its use in industrial applications requiring bulk amount. Thus, from tonnage point of view the major markets could be those industries that require small amount kaolin. These industries are mainly filler (in rubber, paper, paint and plastic), glass and pharmaceuticals.

In Belessa kaolin “modifying factors” (see Fig. 4.4) that are related to mining, processing, environmental and infrastructure can be considered as an opportunity to develop the resource. It is near to Hosaina town and can be accessed by gravel road that runs from Belessa town to the kaolin site. The water required for processing can be also obtained from a Lake called Boyo which is about 8 km from the kaolin site.

CHAPTER SEVEN

7. Conclusion and Recommendation

7.1. Conclusion

The methodologies employed in this work (geological fieldwork, mineralogy, geochemistry, Scanning Electron Microscopy (SEM) and remote sensing), are believed to play important roles in studying the kaolin deposits. These methodologies are thoroughly examined in order to come up with the following important conclusions.

1. Based on the following evidences Belessa kaolin deposit is believed to have formed by supergene alteration (weathering) processes.
    a) The field investigation revealed that the rocks of the region are covered by thick soil covers and vegetation, suggesting that the area is more favorable for meteoric weathering. Also, indicators of hydrothermal activities like quartz veins and hot springs are absent. Moreover, the gradual change from partly altered rocks to completely altered kaolinized zone could be important evidence.
    b) From geochemical data; the higher Th, higher Ce + Y + La compared to Ba + Sr, low P and high Cr + Nb; all corresponds to the supergene type kaolin deposits.
    c) The absence of high temperature minerals (pyrophyllite, diaspor, dickite, nacrite and topaz) which are diagnostic characteristics to the hydrothermal type kaolin deposits.
    d) The CIA (99.7 %) value of Belessa kaolin falls in the ranges of CIA values for residual soils (85 – 100 %).
2. The helpful chemical index (CIA= 99.7 % and CIW=99.7 %) and the triangular diagrams (A-CN-K and A-CNK-F) showed that Belessa kaolin deposit has experienced a higher degree of weathering and alteration processes. This is also confirmed by the completely altered sample showing the largest concentration of Al_2O_3 contents (37.5 wt. %) and highest LOI values (14.6 wt. %) which are in agreement to XRD result indicated as pure kaolinite.
3. During the kaolinization of host rock, significant amounts of Rb, k, Sr and Na are removed due to the breakdown of alkali-feldspars and sodic plagioclase. On the contrary, the completely kaolinized rock is largely dominated by SiO_2 and Al_2O_3,

reflecting the high content of clay mineral (kaolinite) that results in the formation of kaolin.

4. The geological map of Belessa kaolin is produced at a scale 1:25,000. This map can be used to further study the deposit in the upcoming exploration stages.
5. Following the conventional approach (Area, deposit thickness and bulk density) of resource estimation, an amount of 43,218 tons is estimated under indicated mineral resource category.
6. The optimum concentration of Al2O3, Fe2O3 and TiO2 allowed the practical application of Belessa kaolin in various industries. Moreover, the acceptable results of mineralogical and available physical tests like particle size, pH, bulk density and specific gravity revealed its application in industries like paper coating, filler (in paper, rubber, plastic and paint), ceramics, pharmaceuticals and cosmetics.
7. By employing band ratio and band combination techniques on ASTER and Landsat 8 OLI data different maps are produced showing a better result for discriminating the kaolin host rock, kaolinite, lithological units and vegetation.
8. The comparison of Belessa kaolin spectral signature curves with those produced in laboratory and from Lake Koka kaolin showed comparable result. Thus, the spectral curve of Belessa kaolin can be used as a preliminary model for kaolin occurrences in different parts of the Main Ethiopia Rift.

7.2. Recommendations

a) The resource estimation technique followed for this study is conventional and it considers only estimated thickness from field and area from geological map. Thus, further pitting should be carried out to better visualize the occurrence in three dimension and scaling up to a reserve level. Also, detail study should be conducted on the new kaolin occurrences.

b) Firing test, viscosity, brightness and other important technological property tests should be carried out to strengthen the industrial applications listed in this work and to further elucidate and recommend other industrial applications.

c) In this work, the spectral signature curves of kaolin are produced from ASTER and Landsat 8 OLI data. But, to better represent the spectral signature curves of kaolinite and produce a model kaolinite spectral curve accurately, it is advisable to use field spectrometers.

d) Based on Chica-olma and Abrahams ratio images from Landsat 8 OLI data, it was able to identify clay minerals along the major faults of the study area. Some clay showings are also noted during field work but it is not confirmed yet. Thus, further mineralogical studies on these clays are vital.

e) Using remote sensing method in combination with fieldwork has proven in this study to be useful for modeling spectral signature curves and locating kaolin host rock and different lithological units. Hence, such methodology is highly recommended to explore other alteration minerals.

REFERENCES

Abbate, E. and Sagri, M. (1980). Volcanites of Ethiopian and Somali Plateaus and major tectonic lines. Atti Convegni Lincei, **47**:219-227.

Abhary A. and Hassani H. (2016). Mapping hydrothermal mineral deposits using PCA and BR Methods in Baft 1:100000 Geological Sheet, Iran: *International Journal of Advanced Engineering, Management and Science*, **2**: Issue-9, ISSN: 2454-1311.

Abrams, J. M. (1983). Remote sensing for porphyry copper deposits in Southern Arizona. *Economic Geology*, **78**:.591-604 pp.

Acocella, V. and Tesfaye Korme (2002). Holocene extension direction along the Main Ethiopian Rift, East Africa. *Terra Nova*, **14**: 191–197 pp.

Acocella, V., Tesfaye Korme and Salvini, F. (2003). Formation of normal faults along the axial zone of the Ethiopian rift. *Journal of Structural Geology*, **25**:503–513 pp.

Adiri, Z., Harti, A. E., Jellouli, A., Maacha, L. and Bachaoui, E. M. (2016). Lithological mapping using Landsat 8 OLI and Terra ASTER multispectral data in the Bas Drâa inlier, Moroccan Anti Atlas. *Journal of Applied Remote Sensing*, **10(1).**

Agostini, A., Bonini, M., Corti, G., Sani, F. and Mazzarini, F. (2011a). Fault architecture in the Main Ethiopian Rift and comparison with experimental models: Implications for rift evolution and Nubia-Somalia kinematics. *Earth Planet Sci. Lett.*, **301**:479–492 pp.

Al-Ani, T. and Sarapää, O. (2009). Geochemistry and mineralogy of REE in Virtasalmi kaolin deposits, SE Finland. *Geological survey of Finland*.

Aristizabal, E., Roser, B. and Yokota, S. (2005). Tropical chemical weathering of hillslope deposits and bedrock source in the Aburra Valley, northern Colombian Andes. *Engineering Geology*, **81**:389-406 pp.

Arribas, A., Jr., Cunningham, C. G., Rytuba, J. J., Rye, R. O., Kelly, W.C., Podwysocki, M.H., McKee, E. H. and Tosdal, R. M. (1995) Geology, geochronology, fluid inclusions and isotope geochemistry of the Rodalquilar gold alunite deposit, Spain. *Economic Geology*, **90**: 795-822 pp. In: Gilg, H. A., Hulmeyer, S. Miller, H. and Sheppard, M. F. (1995). Supergene origin of the Lastarria kaolin deposit, south-central Chile, and paleo-climatic implications. *Clays and Clay Minerals*, **47 (2)**:201-211 pp.

Baumann, D. and Keller, W.D. (1975).Bulk densities of selected dried natural and fired kaolin clays. *Clay and Clay Minerals*, **23**:424-427.

Bekele Abebe (1993). Studio geologico-strutturale del Rift Etiopico a sud di Asela. Ph. D dissertation, University of Firenze, Firenze, Italy, 153 pp.

Bigazzi, G., Bonadonna, F.P., Di Paola, G.M. and Giuliani, A. (1993). K-Ar and fission-track ages of the last volcano tectonic phase in the Ethiopian Rift Valley (Tullu Moye area). Istituto Agronomico Oltremare, Firenze, Relazioni e Monografie 113 Geology and mineral resources of Somalia and surrounding regions, 311–322 pp.

Bloodworth, A.J., Highley, D.E. and Mitchell, C.J. (1993). Industrial Minerals Laboratory Manual, Kaolin. *British Geological Survey Technical: Report* WG/93/1, 76p. In Ismail, S., Husain V., and Anjum S., (2014). Mineralogy and Genesis of Nagar Parker Kaolin Deposits, Tharparkar District, Sindh, Pakistan. *Int. j. econ. environ. Geol*, **5(1):** 33-40 pp.

Boccaletti, M. and Peccerillo, A. (1999). Foreword to the Ethiopian Rift System. In: Boccaletti, M. and Peccerillo, A. (Eds.), *Acta Vulcanologica*, **11**: V–VII pp.

Boccaletti, M., Bonini, M., Mazzuoli, R., Bekele Abebe, Piccardi, L. and Tortorici, L. (1998).Quaternary oblique extensional tectonics in the Ethiopian Rift (Horn of Africa). *Tectonophysics,* **287(1)**: 97–116 pp.

Boccaletti, M., Getaneh Assefa and Tortorici, L. (1992). The Main Ethiopian Rift: an example of oblique rifting. *Annales Tectonicae,* **6**: 20–25 pp.

Boccaletti, M., Mazzuoli, R., Bonini, M., Trua, T. and Bekele Abebe. (1999 a). Plio-Quaternary volcano-tectonic activity in the northern sector of the Main Ethiopian Rift (MER): relationships with oblique rifting. *Journal of African Earth Sciences,* **29**: 679–698 pp.

Bonini, M., Corti, G., Innocenti, F., Manetti, P., Mazzarini, F., Tsegaye Abebe and Pecskay, Z. (2005). Evolution of the Main Ethiopian Rift in the frame of Afar and Kenya rifts propagation. *Tectonics,* **24**:TC1007.

Bonini, M., Souriot, T., Boccaletti, M. and Brun, J. P. (1997). Successive orthogonal and oblique extension episodes in a rift zone: laboratory experiments with application to the Ethiopian Rift. *Tectonics*, **16**: 347–362 pp.

Bottrill, R. S. (1998). A Corundum-Quartz Assemblage in Altered Volcanic Rocks, Bond Range, Tasmania. *Mineralogical Magazine*, **62(3)**: 325–332pp. In: Yuan Y., Shi G., Yang M., Wu Y., Zhang Z., Huang A.Z and hang J. (2014). Formation of a Hydrothermal Kaolinite Deposit from Rhyolitic Tuff in Jiangxi, China. *Journal of Earth Science,* **25(3)**: 495–505 pp.

Boynton, W. (1984). Cosmochemistry of the rare earth elements. *Elsevier*.

Braile, L.W., Keller, G.R., Wendlandt, R.F., Morgan, P. and Khan, M.A. (1995). The East African Rift System. In: Olsen, K.H. (Ed.), Continental Rifts: Evolution, Structure, Tectonics. *Developments in Geotectonics*, **25**: 213–231 pp.

Bramao, L., Cady, J. G., Hendricks, S. B. and Swerlow, M. (1952). Criteria for the characterization of kaolinite, halloysite, and a related mineral in clays and soils. *Soil Sci.*, **73**:272-287 pp.

Bundy, W. M. and Conley, R. F. (1962). French Patent, 1287683.

Caliani, J. C. F., Galán, E., Aparicio, P., Miras, A. and Márquez, M.G. (2010). Origin and geochemical evolution of the Nuevo Montecastelo kaolin deposit (Galicia, NW Spain). *Applied Clay Science*, **49**:91–97 pp.

Chakraborty, A.K. (2014). Phase Transformation of Kaolinite Clay.

Chorowicz, J. (2005). The East African Rift System. *Journal of African Earth Sciences*, **43**: 379–410 pp.

Chorowicz, J., Collet, B., Bonavia, F. and Tesfaye Korme (1994). Northwest to North–Northwest extension direction in the Ethiopian rift deduced from the orientation of extension structures and fault-slip analysis. *Geological Society of America Bulletin*, **105**: 1560–1570 pp.

Corti, G. (2009). Continental rift evolution: from rift initiation to incipient break-up in the Main Ethiopian Rift, East Africa. *Earth-Science Reviews*, **96(1)**: 1-53 pp.

Cravero F., Domınguez E. and Iglesias C. (2001). Genesis and applications of the Cerro Rubio kaolin deposit, Patagonia (Argentina). *Applied Clay Science*, **18**:157–172 pp.

Crosta, A., De Souza Filho, C., Azevedo, F. and Brodie, C. (2003).Targeting key alteration minerals in epithermal deposits in Patagonia, Argentina, using ASTER imagery and principal component analysis. *Int. J. Remote Sensing*, **24**:4233–4240 pp. In: Pournamdari M., Hashim M. and Pour A. B. (2014). Spectral transformation of ASTER and Landsat TM bands for lithological mapping of Soghan ophiolite complex, south Iran. *Advances in Space Research*, **54**:694–709 pp.

Da Costa, M. L. and Moraes, E. L. (1998). Mineralogy, geochemistry and genesis of kaolins from the Amazon region: *J Mineralium Deposita*, **33**: 283–297 pp. In: Ghadimian, A. and Khodami, M. (2015). Mineralogy, geochemistry, and genesis of the Garak Baghi kaolin deposit in the northwest of Saveh, Iran. *Arab J Geosci*, **8**:3019–3030 pp.

De Souza Santos, P. (1993). The use of clay particle morphology studies to characterize industrial clay deposits: examples from Brazil. *Clay Mineral*, **28**: 539–553 pp.

Di Paola, G.M. (1976). Geological Map of the Tullu Moje` Volcanic Area (Arusi: Ethiopian Rift valley). 1:75,000 Scale. Laboratorio di Geocronologia e Geochimica isotopica, CNR, Pisa, Italy.

Dill, H. G. (2016). Kaolin: Soil, rock and ore from the mineral to the magmatic, sedimentary and metamorphic environments. *Earth-Science Reviews*, **161**:16–129 pp.

Dill, H. G., Bosse, H. R., Henning, H., Fricke, A. and Ahrendt, H. (1997). Mineralogical and chemical variations in hypogene and supergene kaolin deposits in a mobile fold belt in the Central Andes of northwestern Peru. *Mineralium Deposit*, **32**:149–163 pp.

Dominguez, E., Iglesias, C. and Dondi, M. (2008). The geology and mineralogy of a range of kaolins from the Santa Cruz and Chubut provinces, Patagonia (Argentina). *J Clay Sci.* **40**:124–142 pp.

Dominguez, E., Iglesias C. and Dondi, M. (2010). Genesis of the La Espingarda kaolin deposit. Implications for epithermal deposit exploration in Patagonia. *J Clay Sci.*, **47**:290–302 pp.

Duddy, I.R. (1980). Redistribution and fractionation of rare-earth and other elements in a weathering profile. *Chem. Geol*., **30**:363–381 pp.

Duzgoren-Aydin, N. S., Aydin, A. and Malpas, J. (2002). Distribution of clay minerals along a weathered pyroclastic profile, Hong Kong. *Catena*, **50**:17-41 pp.

Ebinger, C. (2005). Continental breakup: the East African perspective. *Astronomy and Geophysics*, **46**:2.16–2.21 pp.

Ebinger, C., J. and Casey, M. (2001). Continental breakup in magmatic provinces: an Ethiopian example. *Geology*, **29**:527–530 pp.

Ebinger, C. J., Tilahun Yemane, Gidey Wolde Gabriel, Aronson, J. L. and Walter, R.C. (1993). Late Eocene recent volcanism and faulting in the Southern Main Ethiopian rift. *Journal of the Geological Society of London*, **150**:99–108 pp.

Ekosse, G. (2000). The Makoro kaolin deposit, Southeastern Botswana: its genesis and possible industrial applications. *Applied Clay Science,* **16**:301–320 pp.

Ekosse, G. (2001). Provenance of the Kgwakgwe kaolin deposit in south eastern Botswana and its possible utilization. *Applied Clay Science*, **20**:137–152 pp.

Fernandes, R. M. S., Ambrosius, B. A. C., Noomen, R., Bastos, L., Combinck, L., Miranda, J. M. and Spakman, W. (2004). Angular velocities of Nubia and Somalia from

continuous GPS data: implications on present-day relative kinematics. *Earth and Planetary Science Letters*, **222**:197–208 pp.

Fernández-Caliani, J. C., Galán, E., Aparicio, P., Miras, A. and Márquez, M.G. (2010). Origin and geochemical evolution of the Nuevo Montecastelo kaolin deposit (Galicia, NW Spain). *Applied Clay Science*, **49**:91–97 pp.

Fiore, S., Huertas, F. J., Huertas, F. and Linares, J. (1995). Morphology of Kaolinite crystals synthesized under hydrothermal conditions. *Clays and Clay Minerals,* **43 (3)**: 353-360 pp.

Ghadimian A. and Khodami M. (2015). Mineralogy, geochemistry, and genesis of the Garak Baghi kaolin deposit in the northwest of Saveh, Iran. *Arab J Geosci.*, **8**:3019–3030 pp.

Gibson, I.L. (1969). The structure and volcanic geology of an axial portion of the Main Ethiopian Rift. *Tectonophysics,* **8**:561–565 pp.

Gibson, I.L. and Tazieff, H. (1970). The structure of the Afar and the northern part of the Ethiopian Rift. Philosophical Transactions. *Royal Society of London*, **267**:331–338 pp.

Gidey WoldeGabriel, Aronson, J. L. and Walter, R. C. (1990). Geology, geochronology, and rift basin development in the central sector of the Main Ethiopia Rift. *Geological Society of America Bulletin,* **102**:439–458 pp.

Gilg, H. A., Hulmeyer, S., Miller, H. and Sheppard S. M. E. (1999). Supergene origin of the Lastarria kaolin deposit, south-central Chile and paleo climatic implications. *Clay and Clay Minerals*, **47**:201-211 pp.

Grant, J.A. (1986). The isocon diagram. A simple solution the Gresens' equation for metasomatic alteration. *Econ. Geol.* **81**:1976–1982 pp.

Grim, R.E. (1953). Clay Mineralogy. New York, *McGraw-Hill*.

Haile Michael Fentaw (1995). Comparison between Kombelcha and Bombowha Kaolin Deposits, Ethiopia: *EIGS*.

Haile Michael Fentaw (2003). Evaluation of the Belesa kaolin, Hadiya Zone, SNNPRG, Ethiopia: *GSE*.

Haile Mickael Fentaw and Tibebu Mengistu (1998). Comparison of Kombolcha and Bombowha Kaolins of Ethiopia. *Applied Clay Science,* **13**:149-164 pp.

Han, T. and Nelson, J. (2015). Mapping hydrothermally altered rocks with Landsat 8 imagery: A case study in the KSM and Snowfield zones, northwestern British

Columbia. In: Geological Fieldwork 2014, British Columbia Ministry of Energy and Mines, British Columbia Geological Survey Paper, **1**:103-112 pp.

Harnois, L. (1988). The CIW index: a new chemical index of weathering. *Sediment. Geol*. **55**:319–322 pp.

Hayward, N. J. and Ebinger, C. J. (1996). Variations in the along-axis segmentation of the Afar Rift system. *Tectonics,* **15**:244–257 pp.

Hemley, J. J. and Jones, W. R. (1964). Chemical Aspects of Hydrothermal Alteration with Emphasis on Hydrogen Metasomatism. *Economic Geology*, **59(4)**: 538–569 pp. In: Yuan, Y., Shi, G., Yang, M., Wu, Y., Zhang, Z., Huang, A. and Zhang, J. (2014). Formation of a Hydrothermal Kaolinite Deposit from Rhyolitic Tuff in Jiangxi, China. *Journal of Earth Science*, **25 (3)**:495–505 pp.

Highley, D. E. (1984). China clay mineral dossier. British Geological Survey, UK, **26**.

Hinckley, D. N. (1963). Variability in "crystallinity" values among the kaolin deposits of the coastal plain of Georgia and South Carolina. *Clays Clay Miner.,* **11**:229-235 pp.

Hofmann, C. (1997). Datation $^{40}Ar/^{39}Ar$ etpale´omagnetisme des trapps d'Ethiopie, du Deccan et de Sibe´rie. Unpublished Doctoral dissertation, University of Paris VI-IPGP.

http://www.bestbridge.org/communities/hadiya-zone-hossana/ accessed on 17.12.2016.

http://www.georgiamining.org/GMA-georgia-kaolin-mining.php accessed on 19/04/2017.

https://en.climate-data.org/location/3664/ accessed on 17.12.2016.

https://www3.epa.gov/ttnchie1/ap42/ch11/final/c11s25.pdf accessed on 18/04/2017.

Ismail, S., Husain, V., and Anjum, S. (2014). Mineralogy and Genesis of Nagar Parker Kaolin Deposits, Tharparkar District, Sindh, Pakistan. *Int. j. econ. environ. geol*., **5(1)**:33-40 pp.

Jeong Gi, Y. (1998). Formation of vermicular kaolinite from halloysite aggregates in the weathering of plagioclase. *Clays Clay Miner.,* **46 (3)**:270–279 pp. In: Cravero, F., Domınguez, E. and Iglesias C. (2001). Genesis and applications of the Cerro Rubio kaolin deposit, Patagonia (Argentina). *Applied Clay Science*, **18**:157–172 pp.

Kalinowski, A. and Oliver, S. (2004). ASTER Mineral Index Processing Manual. *Remote Sensing Applications Geoscience, Australia*.

Kazmin, V., Seife Mickael Berhe, Nicoletti, M. and Pertucciani, C. (1980). Evolution of the northern part of the Ethiopian rift. *Atti Convegni Lincei*, **47**: 275 – 292 pp.

Keller, W. D. (1969). Classification and problems of hydrothermal refractory clay deposits in Mexico. In: Ismail, S., Husain, V. and Anjum, S. (2014). Mineralogy and Genesis

of Nagar Parker Kaolin Deposits, Tharparkar District, Sindh, Pakistan. *Int. j. econ. environ. Geol.*, **5(1)**:33-40 pp.

Keller, W. D. (1976a). Scanning electron micrographs of kaolins collected from diverse environments of origin-I. *Clays Clay Miner.*, **24**:107-113 pp.

Keller, W. D. (1978). Classification of kaolins exemplified by their textures in scanning electron micrograph. *Clays Clay Miner*., **26(1)**:1–20 pp.

Keller, W.D. (1989). Scanning electron micrographs of clay minerals formed by weathering and other genetic processes. Pp. 29-47

Kitagawa, R. and Koster, H. M. (1991). Genesis of the Tirschenreuth kaolin deposit in Germany compared with the Kohdachi kaolin deposit in Japan. *Clay Minerals*, **26**:61-79pp.

Kogel, J. E. (2014). Mining and processing kaolin. *Elements, an international magazine of mineralogy, geochemistry and petrology*, **10**: ISSN 1811-5209.

Kogel, J. E., Pickering, S. M., Shelobolina, E., Chowns, T., Yuan, J. and Avant Jr, D. M. (2009). The Georgia kaolins geology and utilization. *Society for mining, metallurgy, and exploration.*

Kurz, T., Gloaguen, R., Ebinger, C., Casey, M., Bekele Abebe. (2007). Deformation distribution and type in the Main Ethiopian Rift (MER): A remote sensing study. *Journal of African Earth Sciences*, **48**: 100–114 pp.

Lambe, T. W., and Whitman, R. V. (1979). Soil mechanics, SI version, New York, Wiley. In: Ismail, S., Husain, V., Hamid, G. and Bilal, M. (2015). Physico-chemical characteristics of Nagar Parkar kaolin deposits, Thar Parkar district, Sindh, Pakistan. ***J**ournal of Himalayan Earth Sciences*, **48(1)**:50-58 pp.

Le Bas, M. J., Le Maitre, R., Streckeisen, A. and Zanettin, B. (1986). A chemical classification of volcanic rocks based on the total alkali-silica diagram. *Journal of Petrology*, **27(3)**:745-750 pp.

Levitte, D., Columba, J. and Mohr, P. (1974). Reconnaissance geology of the Amaro horst, southern Ethiopian rift. *Geological Society of America Bulletin*, **85**:417–422 pp.

Lohva, J. and Lehtimäki, J. (2005). Geophysical investigation of kaolin and ilmenite deposits in Finland. *Geological Survey of Finland, Special Paper*, **39**:147–154 pp.

Lopez-Galindo, A., Viseras, C. and Cerezo, P. (2007). Compositional, technical and safety specifications of clays to be used as pharmaceutical and cosmetic products. *Applied Clay Science*, **36**:51–63 pp.

Mazzarini, F., Rooney, T. and Isola, I. (2013). The intimate relationship between strain and magmatism: A numerical treatment of clustered monogenetic fields in the Main Ethiopian Rift. *Tectonics,* **32**:49–64 pp.

McDonough, W. F. and Sun, S. S. (1995). The composition of the Earth. *Chemical Geology* **120 (3)**: 223-253 pp.

McLennan, S. M. and Taylor, S. R. (1991). Sedimentary rocks and crustal evolution: tectonic setting and secular trends. *J Geol.,* **99**:1–21 pp.

Meunier, A., Velde, B., Dudoignon, P. and Beaufort, D. (1983). Identification of weathering and hydrothermal alteration in acidic rocks: petrography and mineralogy of clay minerals. *Sci. Géol. Mém.,* **72**:93–99 pp.

Meyer, C. and Hemley, J. J. (1967). Wall rock alteration. In: Njoya, A., Nkoumbou, C., Grosbois, C., Njopwouo, D., Njoya, D., Courtin-Nomade, A., Yvon, J. and Martin, F. (2006). Genesis of Mayouom kaolin deposit (western Cameroon). *Applied Clay Science,* **32**:125–140 pp.

Meyer, W., Pilger, A., Rosier, A., and Stets, J. (1975). Tectonic evolution of the northern part of the Main Ethiopian Rift.

Middelburg, J. J., Van der Weijden, C. H. and Woittiez, J. R. W. (1988). Chemical processes affecting the mobility of major, minor and trace elements during weathering of granitic rocks. *Chem. Geol.*, **68**:253–273 pp.

Mohr, P. (1962). The Ethiopian Rift System. *Bulletin of the Geophysical Observatory of Addis Ababa,* **5**:33–62 pp.

Mohr, P. (1967). The Ethiopian Rift System. *Bulletin of the Geophysical Observatory of Addis Ababa,* **11**:1–65 pp.

Mohr, P. (1983). Volcano tectonic aspects of the Ethiopian Rift evolution. *Bulletin Centre Recherches Elf Aquitaine Exploration Production,* **7**:175–189 pp.

Mohr, P. (1987). Patterns of faulting in the Ethiopian Rift Valley. *Tectonophysics,* **143**: 169–179 pp.

Mohr, P. A. and Wood, C. A. (1976). Volcano spacing and lithospheric attenuation in the Eastern Rift of Africa. *Earth and Planetary Science Letters,* **33**:126–144 pp.

MOME, (1994): Mineral Investment Opportunities in Ethiopia. *Geology and mining, **2**.*

Murray, H. H. (1988). Kaolin minerals: Their genesis and occurrences. 67-89 pp. In: Hydrous Phyllosilicates (Exclusive of Micas): Reviews in Mineralogy. *Min. Soc. Am., Washington*, DC., **19**.

Murray, H. H. (2007). Occurrences, processing and application of Kaolins, Bentonites, Palygorskite-Sepiolite, and Common Clays. *Elsevier B.V.,* 9 pp.

Murray, H. H. and Keller, W. D. (1993). Kaolin, kaolin and kaolin. In: Ismail, S., Husain, V. and Anjum, S. (2014). Mineralogy and Genesis of Nagar Parker Kaolin Deposits, Thar parkar District, Sindh, Pakistan. *Int. j. econ. environ. gel.*, **5(1)**:33-40 pp.

Mwaniki, M. W., Moeller, M. S. and Schellmann, G. (2015). A comparison of Landsat 8 (OLI) and Landsat 7 (ETM+) in mapping geology and visualizing lineaments: A case study of central region Kenya. The International Archives of the Photogrammetry, Remote Sensing and Spatial Information Sciences,VolumeXL-7/W3, 36th International Symposium on Remote Sensing of Environment, 11–15 May 2015, Berlin, Germany.

Nakagawa, K., Santosh, M., Yoshikura, S., Miura, M., Fakuda, T. and Harada, A. (2006). Kaolin deposits at Melthaonnakkal and Pallipuram with in Trivandrum block, southern India. *Gondwana Research*, 530-538 pp.

Ndlovu, B., Farrokhpay, S., Forbes, E. and Bradshaw, D. (2014). Characterization of kaolinite colloidal and flow behavior using its crystallinity measurements, *Powder Technology.* doi: 10.1016/j.powtec.2014.09.029.

Nesbitt, H. W. (1979). Mobility and fractionation of rare earth elements during weathering of a granodiorite. *Nature*, **279**:206–210 pp.

Nesbitt, H. W. and Young, G. M. (1982). Early Proterozoic climates and past plate motions inferred from major element chemistry of lutites. *Nature,* **299**:715–717 pp.

Nesbitt, H. W. and Young, G. M. (1989). Formation and diagenesis of weathering profiles. *Journal of Geology*, **97**:129-147 pp.

Nesbit, H. W. and Young, G. M. (1996). Petrogenesis of sediments in the absence of chemical weathering: effect of abrasion and sorting on bulk composition and mineralogy. *Sedimentology,* **43**:341–358 pp.

Njoya, A., Nkoumbou, C., Grosbois, C., Njopwouo, D., Njoya, D., Courtin-Nomade, A., Yvon, J. and Martin, F. (2006). Genesis of Mayouom kaolin deposit (western Cameroon). *Applied Clay Science,* **32**:125–140 pp.

Parham, W. E. (1976). Clay mineralogy and geology of Minnesota's kaolin clays. *Minnesota geological survey*.

Pik, R., Deniel, C., Coulon, C., Gezahegn Yirgu, Hofmann, C. and Dereje Ayalew (1998). The north western Ethiopian Plateau flood basalts: classification and spatial distribution of magma types. *J. Volc. Geoth. Res.,* **81**: 91–111 pp.

Pizzi, A., Coltorti, M., Bekele Abebe, Disperati, L., Sacchi, G. and Salvini, R. (2006). The Wonji fault belt (Main Ethiopian Rift): structural and geomorphological constraints and GPS monitoring.

Pour, A. B. and Hashim, M. (2011). Identification of hydrothermal alteration minerals for exploring of porphyry copper deposit using ASTER data, SE Iran. *J. Asian Earth Sci.*, **42**:1309–1323 pp.

Pour, A. B. and Hashim, M. (2014). Hydrothermal alteration mapping from Landsat-8 data, Sar Cheshmeh copper mining district, south-eastern Islamic Republic of Iran. *Journal of Taibah University for Science*, **9**:155–166 pp.

Pournamdari, M., Hashim, M. and Pour, A. B. (2014). Spectral transformation of ASTER and Landsat TM bands for lithological mapping of Soghan ophiolite complex, south Iran. *Advances in Space Research*, **54**:694–709 pp.

Prudencio, M. I. and Gouveia, M. A. (1995). REE distribution in present-day and ancient surface environments of Basaltic Rocks (Central Portugal). *Clay Miner.,* **30**:239–248 pp.

Pruett, R. J. (2016). Kaolin deposits and their uses: Northern Brazil and Georgia, USA. *Applied Clay Science*, **131**:3–13 pp.

Pruett, R.J. and Pickering, S. M. (2006). Kaolin.

Rollinson, H. R. (1993). Using geochemical data: evaluation, presentation, interpretation. *Routledge*.

Rosendahl, B. L. (1987). Architecture of continental rifts with special reference to east Africa. *Annual Reviews of Earth and Planetary Sciences*, **15**:445**–**503 pp.

Ross, C. S. and Kerr, P. F. (1931). The kaolin minerals. *U.S. Geological Survey*. Professional Paper 156 E. Reston, VA: USGS, 151–175 pp.

Rowan, L. and Mars, J. (2002). Lithological mapping in the Mountain Pass, California area using Advanced Space borne Thermal Emission and Reflection Radiometer (ASTER) data. *Remote Sensing of Environment*, **84**: 350-366 pp.

Rowan, L. C., Mars, J. C. and Simpson, C. J. (2005). Lithologic mapping of the Mordor N.T, Australia ultramafic complex by using the Advanced Space borne Thermal Emission and Reflection Radiometer (ASTER). *Remote sensing of Environment*, **99**:105-126 pp.

Sabov Y.V., Said Mohammed, Tesfaye Esuyawkal and Haileyesus Wale (1985). Bombowoha Kaolin and Kenticha Feldspar-Quartz deposits, Sidamo Administrative Region. *MOM, EIGS*.

Sabov Y.V., Tibebu Mengistu and Endale Debela (1986). Report on recalculation of kaolin reserves of the Bombowoha-I deposit, Sidamo Administrative Region. *MOM, EIGS.*

Said Mohammed and Sentayew Zewdie (2000). Report on the Evaluation of Bombowoha Kaolin Deposits. *GSE*.

Said Mohammed and Solomon Engidayehu (1993). Progress report on recalculation of Bombowoha I kaolin deposits. *EIGS*.

Saikia, N. J., Bharali, D. J., Sengupta, P., Bordoloi, D., Goswamee, R. L., Saikia, P.C. and Borthakur, P. C. (2003). Characterization, beneficiation and utilization of a kaolinite clay from Assam, India. *Applied Clay Science*, **24**: 93– 103 pp.

Salter, T. and Murray, H. H. (1993). SEM investigation of a lateritic weathering profile, Saline County, Arkansas. In: Cravero, F., Domınguez, E. and Iglesias, C. (2001). Genesis and applications of the Cerro Rubio kaolin deposit, Patagonia (Argentina). *Applied Clay Science,* **18**:157–172 pp.

Samuel Getachew, Abate Assen, Ayenew Kindie, Metasebiya Mitiku and Abate Amsalu (2015). Exploration and Evaluation of Kaolin Deposits around Lake Koka, Arsi Zone Oromiya Regional State. *MOM, GSE*.

Santos, M. C., Varajão, A. F. D. C. and Yvon, J. (2004). Genesis of clayey bodies in Quadrilàtero Ferrífero, Minas Gerais, Brazil. *Catena,* **55**:277–291 pp.

Schroeder, P. A. and Erickson, G. (2014). Kaolin: From ancient porcelains to nanocomposites. *Elements, an international magazine of mineralogy, geochemistry and petrology*, **10**: ISSN 1811-5209.

Searle, A. B. and Grimshaw, R. W. (1959). The chemistry and physics of clays: Interscience Publishers, Inc., New York, 942 p.

Seife Mickael Berhe (1978). Geological map (1:250,000) sheet NC37-15 (Nazret): Ethiopian institute of geological sciences, ministry of mines, energy and water resources.

Sella, G., Dixon, T. H. and Mao, A. (2002). REVEL: a model for recent plate velocities from space geodesy. *Journal of Geophysical Research,* **107**.

Siddiqui, M. A., Ahmed, Z. and Saleemi, A. A. (2005). Evaluation of Swat kaolin deposits of Pakistan for industrial uses. *Applied Clay Science*, **29**:57–72 pp.

Solomon Tadesse (2009). Mineral Resources Potential of Ethiopia. *Addis Ababa University Press.*

Solomon Tadesse, Jean-Pierre, M. and Yves, D. (2003). Geology and mineral potential of Ethiopia: a note on geology and mineral map of Ethiopia. *Journal of African Earth Sciences* **36**: 273–313 pp.

Stock, L. and Sikora, W. (1976). Transformations of Micas in the process of kaolinization of granites and gneisses. *Clays Clay Miner.,* **24 (4)**:156–162 pp.

Suresh G. J. R., Sreenivas K. and Sivasamy R. (2014). Hyperspectral analysis of clay minerals. The International Archives of the Photogrammetry, Remote Sensing and Spatial Information Sciences, Volume XL-8: ISPRS Technical Commission VIII Symposium, 09 – 12 December 2014, Hyderabad, India.

Tadiwos Chernet, Hart, W. K., Aronson, J. L. and Walter, R. C. (1998). New age constraints on the timing of volcanism and tectonism in the northern Main Ethiopian Rift-southern Afar transition zone (Ethiopia). *J. Volcanol. Geotherm. Res.,* **80**:267 – 280 pp.

Tesfaye Kidane, Otofuji, Y., Komatsu, Y., Shibasaki, H. and Rowland, J., (2009). Paleomagnetism of the Fentale-magmatic segment, main Ethiopian Rift: New evidence for counterclockwise block rotation linked to trans-tensional deformation. *Physics of the Earth and Planetary Interiors,* **176**:109–123 pp.

Tesfaye Korme, Chorowicz, J., Collet, B. and Bonavia, F. F. (1997). Volcanic vents rooted on extension fractures and their geodynamic implications in the Ethiopian Rift. *Journal of Volcanology and Geothermal Research,* **79**:205–222 pp.

Tibebu Mengistu and Haile Mickael Fentaw (1993). Kaolin Resources of Weathered Granites near Kombolcha, Eastern Hararghe. *EIGS.*

Tibebu Mengistu and Haile Mickael Fentaw (2000). The industrial mineral and rock resource potential of Ethiopia. *Chron. Rech. Min.* **540**: 33- 40 pp.

Tigistu Melka, Sofiya Abdulkadir and Habtamu Kebede (2011). Report on Exploration of kaolin Occurrences of Ansho and the Surroundig areas. *MOM, GSE*.

Tsegaye Abebe, Manetti, P., Bonini, M., Corti, G., Innocenti, F., Mazzarini, F., and Pecskay, Z. (2005).Geological map (scale 1:200000) of the northern main Ethiopian rift and its implication for the volcano-tectonic evolution of the rift. *Geological Society of America, Boulder Colorado, USA, Maps and Charts series*, MCH094.

Tsegaye Abebe, Balestrieri M.L. and Bigazzi G. (2010). The Central Main Ethiopian Rift is younger than 8 Ma: confirmation through apatite fission-track thermo-chronology. *Terra Nova,* **22**: 470–476 pp.

Ukstins, I. A., Renne, P. R., Wolfenden, E., Baker, J., Dereje Ayalew and Menzies, M. (2002). Matching conjugate volcanic rifted margins: 40Ar⁄39Ar chrono-stratigraphy of pre- and syn-rift bimodal flood volcanism in Ethiopia and Yemen. *Earth Planet. Sci. Lett.*, **198**: 289–306 pp.

Velde, B. (1995). Origin and mineralogy of clays. *Springer, Berlin*, 271 pp.

Williams, F. M., Williams, M. A. J. and Aumento, F. (2004). Tensional fissures and crustal extension rates in the northern part of the Main Ethiopian Rift. *Journal of African Earth Sciences*, **38**:183–197 pp.

Wolfenden, E., Ebinger, C., Gezahegn Yirgu, Deino, A. and Dereje Ayalew (2004). Evolution of the northern Main Ethiopian rift: birth of a triple junction. *Earth and Planetary Science Letters*, **224**:213–228 pp.

Yuan, Y., Shi, G., Yang, M., Wu, Y., Zhang, Z., Huang, A. and Zhang, J. (2014). Formation of a Hydrothermal Kaolinite Deposit from Rhyolitic Tuff in Jiangxi, China: *Journal of Earth Science*, **25 (3)**:495–505 pp.

Zanettin, B., Justin-Visentin, E., Nicoletti, M. and Petrucciani, C. (1978). Evolution of the Chencha escarpment and the Ganjiuli graben (Lake Abaya) in the southern Ethiopian rift. *Neues Jahrbuch fur Geologie und Palaontologie*, Monatshefte, **8**:473–490 pp.

Appendix I

Geochemical Data: Major elements in elemental form (%)

Sample Name	BHR-0006	BHR-0012	BHR-0016A	BHR-0016B	BHR-0017	BHR-0051	BHR-0053B	BHR-0054
Si	35.175	34.291	37.909	36.255	33.156	27.546	33.679	25.672
Al	8.775	6.303	9.394	11.241	13.919	13.66	14.375	23.34
Fe	3.161	3.273	0.629	0.643	1.406	5.239	0.315	0.112
Ca	0.129	0.157	0.021	0.021	0.036	0.429	0.014	0.079
Mg	0.054	0.048	0.006	0.012	0.018	0.084	_	0.006
Na	1.128	3.205	_	_	0.022	2.411	0.03	_
K	1.353	4.084	_	_	0.058	2.316	0.025	0.008
Ti	0.126	0.216	0.114	0.138	0.306	0.42	0.144	0.402
Mn	0.008	0.062	_	_	0.023	0.155	_	_
P	_	0.009	0.004	_	0.009	0.004	0.004	0.004
Ba	_	0.027	_	_	0.009	0.081	_	_
O	50.081	48.304	51.911	51.689	51.028	47.665	51.414	50.367

Appendix II

Properties, application and Laboratory tests of kaolin

A) Important properties of kaolin (Murray, 2007).	
1.	White or near-white in color
2.	Chemically inert over a wide PH range (4-9)
3.	Fine in particle size
4.	Soft and non-abrasive
5.	Platy with the plate surface dimensions relatively large compared to the thickness
6.	Hydrophilic and disperses readily in water
7.	Because of its shape, it has good covering and hiding power when used as a pigment or extender in coatings.
8.	Plastic, refractory and fires to a white or near-white color
9.	Low conductivity of both heat and electricity
10.	A very low charge on the lattice
11	A low surface area as compared with other clay minerals
12	Some kaolins have a low viscosity and flow readily at 70% solids
13	Relatively low in cost

B) Physical constants of kaolinite (Murray, 2007)	
Specific gravity	2.62
Index of refraction	1.57
Hardness (Mohs' scale)	1.5-2.0
Fusion temperature	1850
Einlehner abrasion number	4-10
Dry brightness at 457 nm (%)	75-93
Crystal system	Triclinic

C) **Commonly used tests and procedures for evaluating kaolin samples (Murray, 2007).**	
1	Crude clay X-ray diffraction
2.	Crude clay moisture
3.	Percent grit (+325 mesh) (screen residue test)
4.	Degritted X-ray diffraction
5.	Crude clay pH
6.	Crude clay brightness
7.	Degritted clay brightness
8.	Crude clay particle size
9.	Crude clay Brookfield viscosity
10.	Crude clay settling procedure
11.	Leaching and brightness test
12.	Magnetic separation
13.	High shear (Hercules) viscosity
14.	Processed clay Brookfield viscosity
15.	Processed clay particle size
16.	Processed clay brightness
17.	Conductivity measurement

D) Chemical and physical properties that are important for kaolin applications (Pruet, 2016).

	Refractory	Fiberglass	Ceramic	Rubber	Plastic	Pigment, coating	Pigment, filling
Chemistry, major oxide	x	x	x				
White or near white			x			x	x
Refractive index						x	x
Particle size, fineness & range			x	x	x	x	x
Particle shape , platy or delaminated					x	x	x
Surface area (5 to 25 m^2/g)				x		x	x

Abrasivity, soft					x	x
Hydrophilic, readily make-down		x			x	x
Insoluble, wide pH range					x	x
Surface charge, low (meq/g)		x	x		x	x
Low viscosity, clay-water slurry					x	x
Plasticity		x				
Conductivity, low (heat, electrical)	x			x		
Refractory, high melting temperature	x	x				
Stability, form (heat and chemical)		x			x	x
Calcined/sintered mineral content	x	x	x	x	x	x